

**Investigations of Bacteria Viability on Surfaces Using ω -functionalized Alkanethiol
Self-Assembled Monolayers**

Joshua R. Uzarski

Thesis submitted to the faculty of the Virginia Polytechnic Institute and State University
in partial fulfillment of the requirements for the degree of

MASTER OF SCIENCE
in
Chemistry

John R. Morris, Chair
Mark R. Anderson
Richard D. Gandour

June 19, 2006
Blacksburg, Virginia

Keywords: self-assembled monolayers, antibacterial surface, silver carboxylate SAM,
Escherichia coli

Copyright 2006, Joshua R. Uzarski

Investigations of Bacteria Viability on Surfaces Using ω -functionalized Alkanethiol Self-Assembled Monolayers

Joshua R. Uzarski

ABSTRACT

The structure/function relationship between bacteria and biocidal molecules in the vapor or solution phase is well-understood. However, the fundamental structure/function relationship between covalently-bound biocidal surface molecules and bacteria is not. While a number of antibacterial surfaces have been reported, detailed analysis of the molecular scale surface structure has not been performed. The lack of structural knowledge makes it difficult to determine how alterations to the surface affect the viability of the bacteria. Most of the antibacterial surfaces reported to date are composed of polymer systems. Controlling the properties of large surface-bound molecules like polymers is difficult.

Self-assembled monolayers, or SAMs, of alkanethiols on gold have been used extensively in the past 20 years as model surfaces for investigation of a large breadth of surface phenomena. SAMs allow for control of the molecular scale surface structure and are amenable to a great number of characterization techniques. The primary objective of the work in this study is to establish the use of SAMs as a tool to investigate the fundamental relationship between surface structure and bacteria viability.

The surfaces were characterized before interaction with bacteria by reflection-absorption infrared spectroscopy (RAIRS) and X-ray photoelectron spectroscopy (XPS). Determination of the viability of *Escherichia coli* on the surfaces was performed via the antibacterial assay. In the assay, a culture of *E. coli* was sprayed onto the surfaces using a chromatography sprayer. After addition of growth agar and overnight incubation, the number of colony forming units on the surface were counted. Statistical analyses were performed to compare the number of colony forming units on different surfaces. Surfaces were characterized after the assay by RAIRS. The RAIR spectra indicated that no significant change to the well-ordered alkane chain configuration was evident. The

structural stability shown by the SAMs will allow for their use in future studies to determine fundamental relationship between surface structure and bacteria viability.

Acknowledgements

I would like to thank my advisor, Dr. John R. Morris, for helping me develop and grow as a scientist over the past 3 years. I'd also like to thank him for recruiting me from Aquinas College back home in Michigan. If it wasn't for him, I would have never thought to attend Virginia Tech. I am also grateful to him for wanting and allowing me to continue my studies towards a hopeful Ph. D. I am also thankful to my committee members, Dr. Gandour and Dr. Anderson for their help and guidance. Dr. Popham, a microbiology professor, along with his group members also deserve special recognition for allowing me to use their laboratory in addition to their help and advice.

I would like to acknowledge current and past Morris group members that I have had the pleasure of working with. They have always made coming to lab an enjoyable experience and make being a graduate student not such an arduous task. Mr. Frank Cromer deserves appreciation for his assistance and expertise in using the XPS.

I would like to thank my family and friends for their support and understanding: my mom and dad, Krys and Bob Uzarski, and my sisters Nicki and Sarah, and my friends in Virginia and back home in Michigan. I especially want to thank my girlfriend, Stephanie Hooper, for her endless care and understanding.

TABLE OF CONENTS

<u>Chapter 1: Introduction, Motivation, and Review of Bacteria</u>	1
1.1 Introduction.....	1
1.2 Classification and Physical Characteristics of Bacteria.....	3
1.3 Chemistry of the Cell Surface.....	4
1.3.1 The Gram-positive Cell.....	4
1.3.2 The Gram-negative Cell.....	9
1.4 Previous Bacterial Adhesion Studies.....	11
1.4.1 Bacterial Adhesion Process.....	12
1.4.2 Factors Influencing Bacterial Adhesion.....	12
1.4.2.1 Environmental Factors.....	12
1.4.2.2 Bacterial Surface Properties.....	13
1.4.2.3 Substratum Surface Properties.....	14
1.5 Previous Antibacterial Surface Studies.....	15
1.5.1 Bulk Phase Antibacterial Molecules.....	15
1.5.2 Surface-bound Antibacterial Quaternary Ammonium Compounds.....	17
1.5.2.1 Antibacterial Surface Composed of Poly(4-vinyl- <i>N</i> -alkylpyridinium bromide).....	18
1.5.2.2 Antibacterial Surface Composed of 3-(trimethoxysilyl)-propyldimethyloctadecyl ammonium chloride.....	20
1.5.3 Remaining Questions About Antimicrobial Surfaces.....	20
<u>Chapter 2: Self-Assembled Monolayers as Model Surfaces: Motivation and Background</u>	22
2.1 Introduction.....	22
2.2 Formation of Alkanethiol SAMs.....	24
2.3 Structure of Alkanethiol SAMs.....	25
2.4 Stability of Alkanethiol SAMs.....	27
2.5 Modification of Alkanethiol SAMs.....	29
2.6 Concluding Remarks.....	30
<u>Chapter 3: Experimental Approach and Antibacterial Assay Method Development</u>	31
3.1 Introduction.....	31
3.2 Reflection-Absorption Infrared Spectroscopy (RAIRS).....	31
3.3 X-Ray Photoelectron Spectroscopy (XPS).....	36
3.4 The Antibacterial Assay.....	39
3.4.1 Details of the Antibacterial Assay.....	39
3.4.1.1 Materials.....	39
3.4.1.2 Preparation of Self-Assembled Monolayers.....	40
3.4.1.3 Preparation of Bacteria.....	40
3.5 Antibacterial Assay Method Development.....	41
3.5.1 Initial Assays.....	41
3.6 Analysis of Variance Tests (ANOVA).....	49
3.7 Discussion.....	56
<u>Chapter 4: Antibacterial Silver Carboxylate Self-Assembled Monolayers</u>	59
4.1 Introduction.....	59
4.2 Experimental Details.....	60

4.2.1	Materials	60
4.2.2	Preparation of Self-Assembled Monolayers	61
4.2.3	Preparation of Silver Carboxylate Self-Assembled Monolayers	61
4.2.4	Reflection-Absorption Infrared Spectroscopy	61
4.2.5	X-ray Photoelectron Spectroscopy	62
4.2.6	Antibacterial Assays	62
4.2.7	Cleaning of Surfaces After Antibacterial Assay	63
4.3	Results and Discussion	63
4.3.1	Characterization of Self-Assembled Monolayers Before Antibacterial Assay	63
4.3.1.1	Reflection-Absorption Infrared Spectra	63
4.3.1.2	X-ray Photoelectron Spectra	66
4.3.2	Antibacterial Assays	69
4.3.3	Stability of a Silver Carboxylate SAM	71
4.3.4	Regeneration of a Silver Carboxylate SAM	73
4.3.5	Antibacterial Assay of Other Metal Carboxylate SAMs	75
4.3.6	Discussion of the Antibacterial Activity of a Silver Carboxylate SAM	77
4.4	Conclusions	78
<u>Chapter 5: Conclusions and Future Work</u>		80
5.1	Conclusions	80
5.2	Future Work	81
<u>References</u>		85

LIST OF FIGURES

Figure 1: Diagram of the structure of a Gram-positive bacterium.	5
Figure 2: Structures of (A) N-acetylglucosamine (NG) and (B) N-acetylmuramic acid (NM).	6
Figure 3: General bonding of the cell wall peptidoglycan in Gram-positive bacteria.....	7
Figure 4: Structure of glycerol teichoic acids.....	8
Figure 5: Diagram of the structure of a Gram-negative bacterium.....	9
Figure 6: General structure of bacterial phospholipids.....	10
Figure 7: Structure of a quaternary ammonium compound.	16
Figure 8: Structure of cetyl trimethylammonium bromide (CTAB) and cetyl pyridinium chloride.	16
Figure 9: Structure of poly (4-vinyl- <i>N</i> -alkylpyridinium bromide).	19
Figure 10: Structure of Si-QAC.....	20
Figure 11: General structure of an alkanethiol SAM on gold.....	23
Figure 12: Lattice structure of an adsorbed alkanethiol monolayer on an Au(111) substrate.	26
Figure 13: Orientation of alkanethiol on Au(111)..	27
Figure 14: Components of light impinging on a surface.	32
Figure 15: Schematic of the Bruker IFS66v/S infrared spectrometer.....	34
Figure 16: Example energy diagram for the photoelectric effect in XPS.....	37
Figure 17: Initial antibacterial assay images.....	43
Figure 18: Layout of SAMs in a Petri dish using one square centimeter sized gold slides	45
Figure 19: Graphical representation of the data in Table 5.	49
Figure 20: One-way ANOVA table.....	50

LIST OF FIGURES (CONTINUED)

Figure 21: Two-way ANOVA setup.....	54
Figure 22: RAIR spectra of a 16-C CH ₃ -T SAM pre- and post-immersion in silver nitrate.	64
Figure 23: RAIR spectra of a 16-C COOH-T SAM pre- and post-immersion in silver nitrate.	65
Figure 24: Reaction diagram for complexation reaction of a metal salt with a carboxylic acid group.....	66
Figure 25: XP spectra of the Ag 3d multiplex for a 16-C CH ₃ -T SAM pre-and post-immersion in silver nitrate solution.	67
Figure 26: XP spectra of the Ag 3d multiplex for a 16-C COOH-T SAM before and after immersion in silver nitrate solution.	68
Figure 27: Atomic percent composition of a silver carboxylate terminated SAM.	69
Figure 28: Antibacterial assay images for a 16-C COOH-T SAM before and after and a 16-C CH ₃ -T SAM before and after immersion in a silver nitrate solution.....	70
Figure 29: Antibacterial assay images for a silver carboxylate SAM.	71
Figure 30: RAIR spectra of a 16-C COOH-T SAM before reaction with silver nitrate, after reaction, and after an antibacterial assay.	72
Figure 31: Antibacterial assay images demonstrating the regeneration of the antibacterial silver carboxylate SAM.	74
Figure 32: RAIR spectra of 16-C COOH-T SAMs after complexation reactions with different metal salts.....	75
Figure 33: Images from the antibacterial assay of a series of metal carboxylate SAMs.. ..	76
Figure 34: Antibacterial assay image of a silver carboxylate SAM.	77
Figure 35: Synthetic route for the total synthesis of a quaternary ammonium containing thiol.....	82

LIST OF FIGURES (CONTINUED)

Figure 36: Synthetic route of quaternary ammonium SAMs via modification of an initial carboxylic acid terminated SAM. 83

LIST OF EQUATIONS

(1) Oxidative addition of alkanethiol to gold.....	25
(2) Intensity of an infrared absorption.....	33
(3) Angular dependence of IR intensity on dipole moment orientation.....	33
(4) Kinetic energy of an X-ray photon.....	36
(5) Sensitivity factor of XPS.....	37
(6) Rearrangement of equation (5).....	38
(7) XPS atomic percent concentration ratio.....	38
(8) ANOVA total sum of squares.....	50
(9) ANOVA treatment sum of squares.....	50
(10) ANOVA error sum of squares.....	50
(11) One-way ANOVA F-test.....	51
(12) ANOVA block sum of squares.....	54
(13) Two-way ANOVA error sum of squares.....	54
(14) Two-way ANOVA between treatment F-test.....	54
(15) Two-way ANOVA between block F-test.....	55
(16) Confidence limits for a population mean.....	56

LIST OF TABLES

Table 1: Viable colony counts from the initial antibacterial assays.	44
Table 2: Assay results for COOH-T and CH ₃ -T SAMs which were placed in the same Petri dish.	45
Table 3: Assay data testing COOH-T, OH-T, and CF ₃ -T SAMs.....	47
Table 4: Variation statistics for data from Table 3.	47
Table 5: Mean percent difference of average SAM colony counts from clean gold colony counts.....	48
Table 6: 16-C CH ₃ -T ANOVA results.....	51
Table 7: 16-C COOH-T ANOVA results	52
Table 8: 16-C OH-T ANOVA results.....	52
Table 9: 10-C CF ₃ -T ANOVA results	53
Table 10: Summary of F-test values for one-way ANOVA.	53
Table 11: Two-way ANOVA data.....	55
Table 12: Two-way ANOVA calculations	56
Table 13: 95% confidence limits for four SAMs tested via the antibacterial assay..	57

Chapter 1: Introduction, Motivation, and Review of Bacteria

1.1 Introduction

Since the beginning of human existence, man has been in constant battle with harmful microorganisms. One classification of microorganisms is bacteria. Bacteria cause a large number of problems for human populations including spoilage of food, disease, illness, and even death. Before the development of technology capable of recognizing and identifying microorganisms, the battle against harmful bacteria was entirely one sided. Dying from infections stemming from simple injuries was commonplace as the knowledge of sterilization was not yet obtained. Communicable diseases like bubonic plague spread easily. However, not all bacteria are harmful to humans. In fact, some bacteria are essential to our survival. Without bacteria, events such as digestion and decomposition of deceased organisms would not be possible.

The battle against harmful bacteria essentially began with their discovery. Microorganisms were first observed in 1674 by Antony van Leeuwenhoek. Leeuwenhoek used his crude microscope to observe bacteria, protozoa, yeasts, spermatozoa, red blood cells, and muscle cells. He suggested a possible link between the observed microorganisms and fermentation, decay, and disease. However, at the time the suggestion was based merely on postulation without the benefit of experimental evidence.

In 1862, Louis Pasteur demonstrated that all putrefactions are caused by microorganisms. His work helped change microbiology from a speculative to experimental science. Pasteur's work at that time also helped develop the sterilization process that bears his name, Pasteurization. The process of Pasteurization involves heating a food material to a temperature high enough to kill microorganisms followed by cooling. Pasteurization is still used universally to preserve milk and other food products.

Credit for the discovery that bacteria cause and transmit a large number of diseases goes to Robert Koch. In 1876, Koch demonstrated that anthrax is transmitted through bacterial spores. Koch also formulated a set of postulates that laid down the conditions needed to be fulfilled if the microbial basis of a disease was to be established.

The postulates were: (i) the organism must be present in the lesions of the disease, (ii) it must be possible to culture the organisms in pure form outside of the host body, (iii) the pure cultures should be able to produce typical symptoms of the disease, and (iv) the same organism should be present in the disease caused by the inoculum.

Efforts to control the occurrence and spread bacterial disease began around the same time as the discoveries of Koch. The concept of vaccination for prevention of bacterial disease was developed around this time. A Glasgow surgeon named Joseph Lister, taking a clue from Pasteur's work, suggested using phenol-soaked bandages to overcome post-surgery infections. Lister also stressed the use of sterilized instruments and conduct of surgery under a spray of disinfectants to prevent the access of microorganisms to wounds. Such methods, although highly refined, are still in use in operating rooms today.

Continuing advancements in the fields of microbiology and chemistry have led to development of a large number of antibacterial compounds. One such advancement is the development of surfaces containing antibacterial compounds. The use of antibacterial surfaces can eliminate the need for manual application of solution or aerosol based antibacterial compounds to an environment. Antibacterial surfaces have been developed for use on such things as kitchen utensils and toilet seats. However, there is a lack of fundamental understanding of the influence of molecular scale surface structure on antibacterial activity. Such fundamental knowledge could some day lead to the development of better, more effective antibacterial surfaces that do not suffer the caveats of many current antibacterial surfaces.

The objective of the research presented here was to establish the use of self-assembled monolayers (SAMs) of alkanethiols on gold as a tool to investigate the fundamental relationships between molecular scale surface structure and the viability of bacteria. SAMs were chosen because they allow for control of surface structure and they can be characterized by a large number of techniques. A SAM composed of silver complexed carboxylic acid terminal groups showed antibacterial activity, and the structure of the underlying alkyl chains proved to be robust. The antibacterial activity and structural stability of the alkyl chain organization demonstrated that functionalized alkanethiol SAMs can be used for fundamental studies into the influence of molecular

scale surface properties on the viability of bacteria. Specifically, SAMs afford control over surface roughness, chemical functionality, and chemical density of a surface.

The remaining manuscript is organized as follows. The next part of chapter 1 discusses general features of bacteria and the physiology of their outmost parts, the cell wall. Subsequently, a brief review of the process of bacterial adhesion to surfaces is presented, followed by a discussion of previous antibacterial surfaces. The discussion of previous antibacterial surfaces is closed by presenting questions remaining from those studies. The remaining questions serve as the motivation to use SAMs as model surfaces.

In chapter 2, a brief review of previous SAM work is presented that helps to justify the selection of SAMs as model surfaces. In chapter 3, the experimental techniques utilized for characterization of the surfaces and for assessment of antibacterial activity are explained. Preliminary work in development of the antibacterial assay and the statistical techniques used to analyze the data are also explained. In chapter 4, the experimental results are presented and discussed, followed by chapter 5, which offers a summary and discussion of future work.

1.2 Classification and Physical Characteristics of Bacteria

It is estimated that bacteria have been in existence on Earth for at least 3.5 billion years, making them one of the oldest living organisms.¹ Bacteria are ubiquitous in nature, surviving in extreme environments that would kill most other organisms. Bacteria are considered the simplest life forms, but this does not mean they are without complexity. Their ability to adapt to environmental stress is truly remarkable, however, like all organisms; they can and do succumb to the environmental conditions.

Bacteria are classified as prokaryotes, which signifies that they lack membrane bound organelles and that their genetic material is not contained within a nucleus. Prokaryotes differ from eukaryotes, such as animal cells, which are more complex and contain well-defined organelles such as a nucleus. A typical prokaryotic cell consists of the following major structures: cell wall, cytoplasmic membrane, ribosomes, some inclusions, and nucleoid. The average size of a bacterial cell is 0.5-1.0 μm in diameter and 1.0-3.0 μm in length. Using the bacteria size dimensions, the number of non-overlapping bacteria that can fit onto a one square centimeter surface is between 3.33×10^{11} and 2.00×10^{12} . About a trillion bacteria (10^9) can fit into a one milliliter pipette.

The majority of bacteria can be divided into two main groups, the Gram positive cell and the Gram negative cell. The two types are named as such based upon their response to a staining procedure developed by Hans Christian Gram in 1884.² In a Gram staining procedure, bacteria are stained with a basic dye like, crystal violet, followed by treatment with iodine and 95% alcohol. The addition of alcohol differentiates the bacteria into two broad groups; those that retain the dye and those that are decolorized by the alcohol. The former group is called Gram-positive and the latter are called Gram-negative.

The different response to the staining procedure is caused by differences in the structure and composition of the cell walls. The cell wall of the Gram-negative bacteria is thinner and has higher lipid content. The alcohol causes the cell walls to distort and disorganize and leads to an increase in permeability and release of the dye molecules. In turn, the alcohol causes the cell wall of Gram-positive bacteria to dehydrate and tighten. The tightening of the cell wall decreases the permeability and retains the dye molecules.

1.3 Chemistry of the Cell Surface

The distinction between Gram-positive and Gram-negative bacteria is the structure and composition of the outmost cell wall. The cell wall is the first site of interaction between a bacterium and its environment, including a surface such as a self-assembled monolayer. For a surface molecule to cause a disruption in the cell surface, it must have a favorable interaction with the cell wall molecules. This section will describe the chemical composition and structure of the cell wall of the two types of bacteria. Understanding of the complex cell wall systems will help facilitate design of antibacterial surfaces and help recognition of important structure/function relationships.

1.3.1 The Gram-positive Cell

The general structure of the Gram-positive cell is shown in Figure 1.

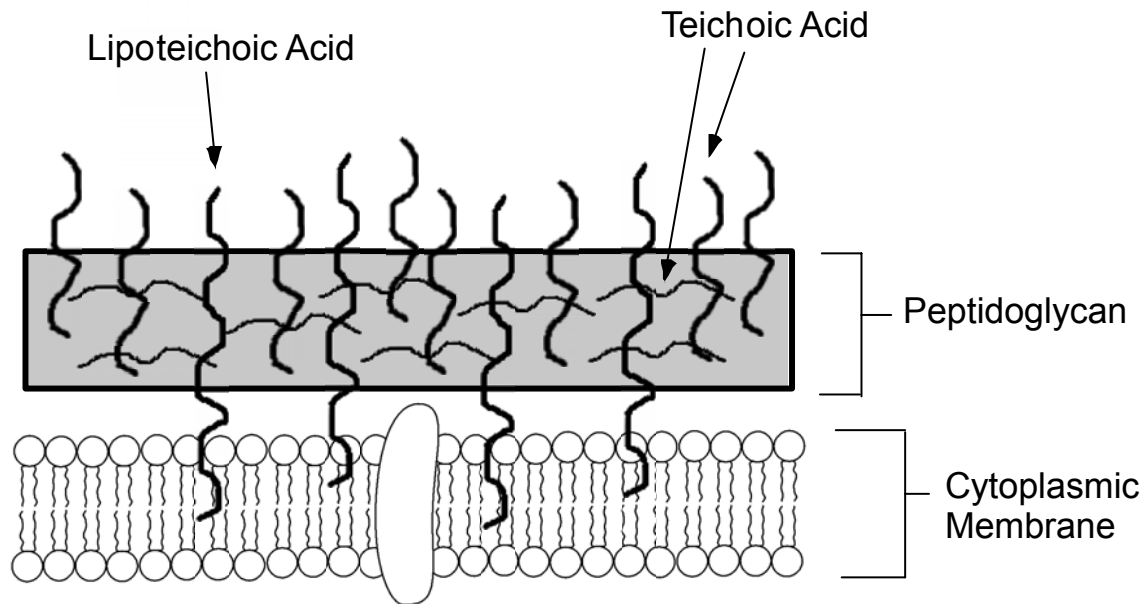


Figure 1: Diagram of the structure of a Gram-positive bacterium. The identifying structure is the large cell wall composed primarily of peptidoglycan

The Gram-positive cell wall contains a massive peptidoglycan layer, comprising approximately 90% of the wall. The average thickness of the wall is 15-20 nm, which corresponds to approximately 1% of the total thickness and 20-30% of the cell's dry weight. The peptidoglycan layer is a glycopeptide that is composed of two polymers. One polymer consists of saccharide subunits and the other consists of amino acid subunits. The saccharide component of peptidoglycan comprises alternating repeat units of two amino sugars related to glucose, *N*-acetylglucosamine (NG) and *N*-acetylmuramic acid (NM). The alternating units of NM and NG are linked together by a glycosidic bond (β -1,4 linkage) which contributes to the stability of the cell wall. Figure 2 shows the structure of NM and NG.

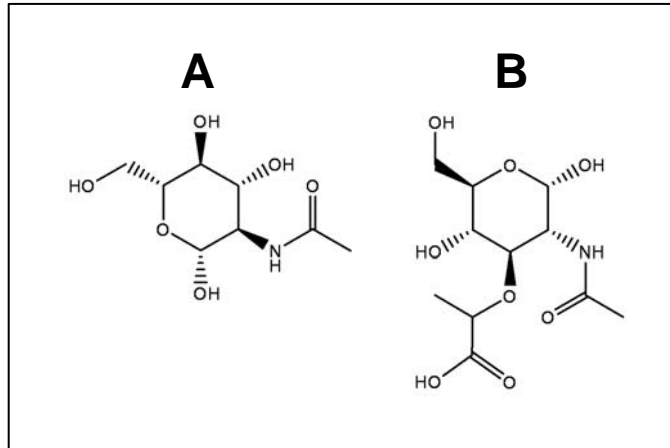


Figure 2: Structures of (A) N-acetylglucosamine (NG) and (B) N-acetylmuramic acid (NM). These two molecules are the primary constituents of cell wall peptidoglycan.

Small peptides attached to the NM help provide additional rigidity to the cell wall. In the Gram-positive cell, the small peptides are composed of four amino acids; *L*-alanine, *D*-glutamic acid, *L*-lysine, and *D*-alanine. The peptide chains are cross-linked through a pentaglycine bridge formed between the terminal *D*-alanine of one peptide chain and the third amino acid of the other. The general bonding structure of the peptidoglycan is shown in Figure 3.

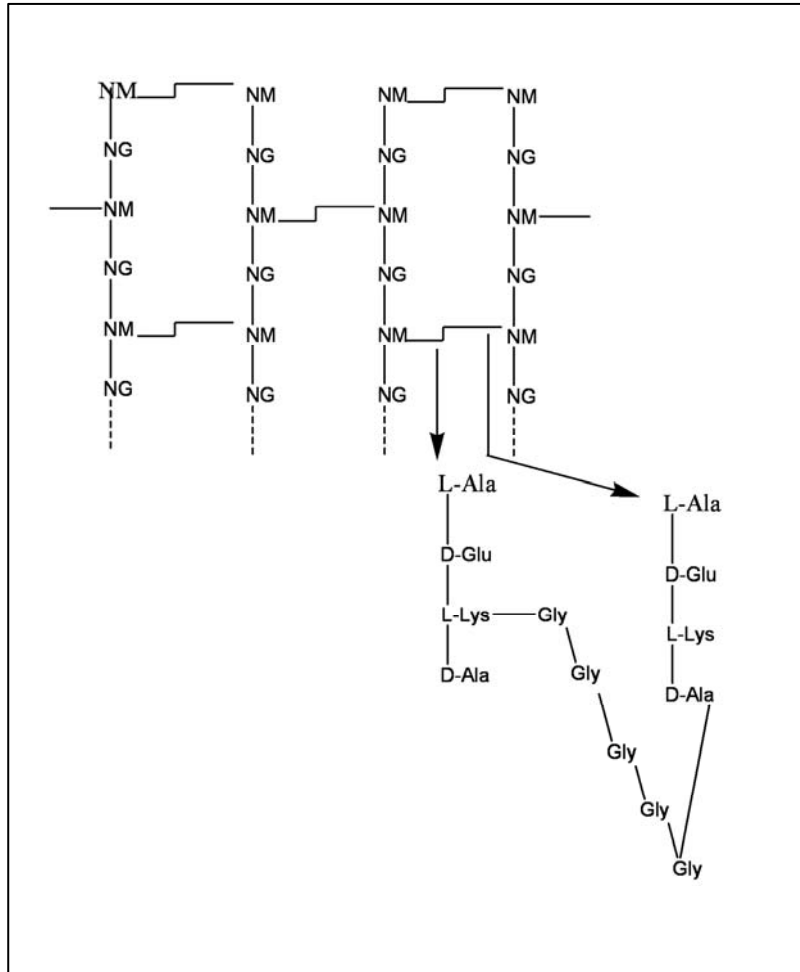


Figure 3: General bonding of the cell wall peptidoglycan in Gram-positive bacteria.²
 NG=N-acetylglucosamine; NM=N-acetylmuramic acid; L-Ala=L-Alanine; D-Ala=D-Alanine;
 D-Glu=glutamate; L-Lys=Lysine; L-Gly=Glycine.

Throughout the peptidoglycan layers are covalently bonded acid polysaccharides known as teichoic acid. Teichoic acid structures differ among different species of bacteria, but all are composed of carbohydrate, such as glucose, an alcohol, such as glycerol or ribitol, and phosphate. The function of teichoic acid is to bind protons and maintain the cell wall at a relatively low pH. The structure of glycerol teichoic acid is shown in Figure 4.

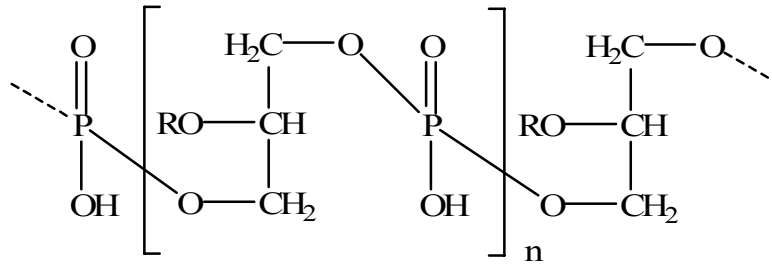


Figure 4: Structure of glycerol teichoic acids. The presence of the phosphate group contributes to the negative charge of the cell wall.

The functional groups found in both the peptidoglycan and teichoic acids give rise to an overall negative charge associated with the cell wall. As far as it is known, all walls of Gram-positive bacteria are negatively charged in media capable of supporting growth.³⁻⁶ The negative charge arises from anionic sites in the cell wall including carboxylate from the peptidoglycan and phosphate from the teichoic acids. Numerous studies have concluded that the more electronegative sites in Gram-positive cell walls are on the outer surface, that is the surface exposed to the environment, and not on the inner surface.⁷⁻¹² As a result of the negative charge, it is possible to postulate that Gram-positive bacteria would be attracted to surfaces presenting a positive charge.

1.3.2 The Gram-negative Cell

The basic structure of the Gram-negative cell is shown in Figure 5

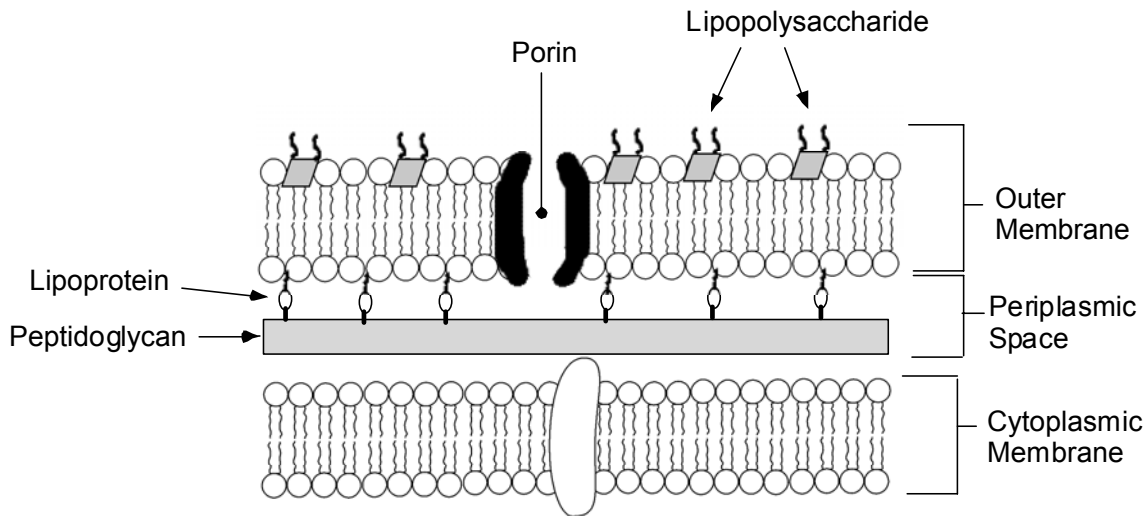


Figure 5: Diagram of the structure of a Gram-negative bacterium. The key identifying structure is the outer membrane which is composed primarily of phospholipids.

The Gram-negative cell wall is more complex than the Gram-positive cell wall. The primary difference between the two is the size and location of the peptidoglycan layer. In the Gram-positive cell, the peptidoglycan layer comprises approximately 90% of the cell wall, but in the Gram-negative cell the peptidoglycan layer comprises only 10%. There are no teichoic acid molecules found in the Gram-negative cell wall. The teichoic acid molecules are replaced by lipoproteins. The outside of the peptidoglycan is surrounded by an outer membrane composed of lipopolysaccharides (LPS), phospholipids, and proteins. The multilayered outer membrane structure is generally referred to as the cell envelope of the Gram-negative cell wall.

While the composition may vary among different species, the outer membrane usually contains between 20 and 25% phospholipids, 30% LPS, and 45-50% protein by weight.¹³ The principal phospholipids are phosphatidylethanolamine, phosphatidylglycerol, and diphosphatidylglycerol.¹⁴ In *Escherichia coli*, the predominant phospholipid is usually phosphatidylethanolamine, which can account for 75-95% of the total phospholipids content of the membrane.¹⁵ The structure of some phospholipids is shown in Figure 6.

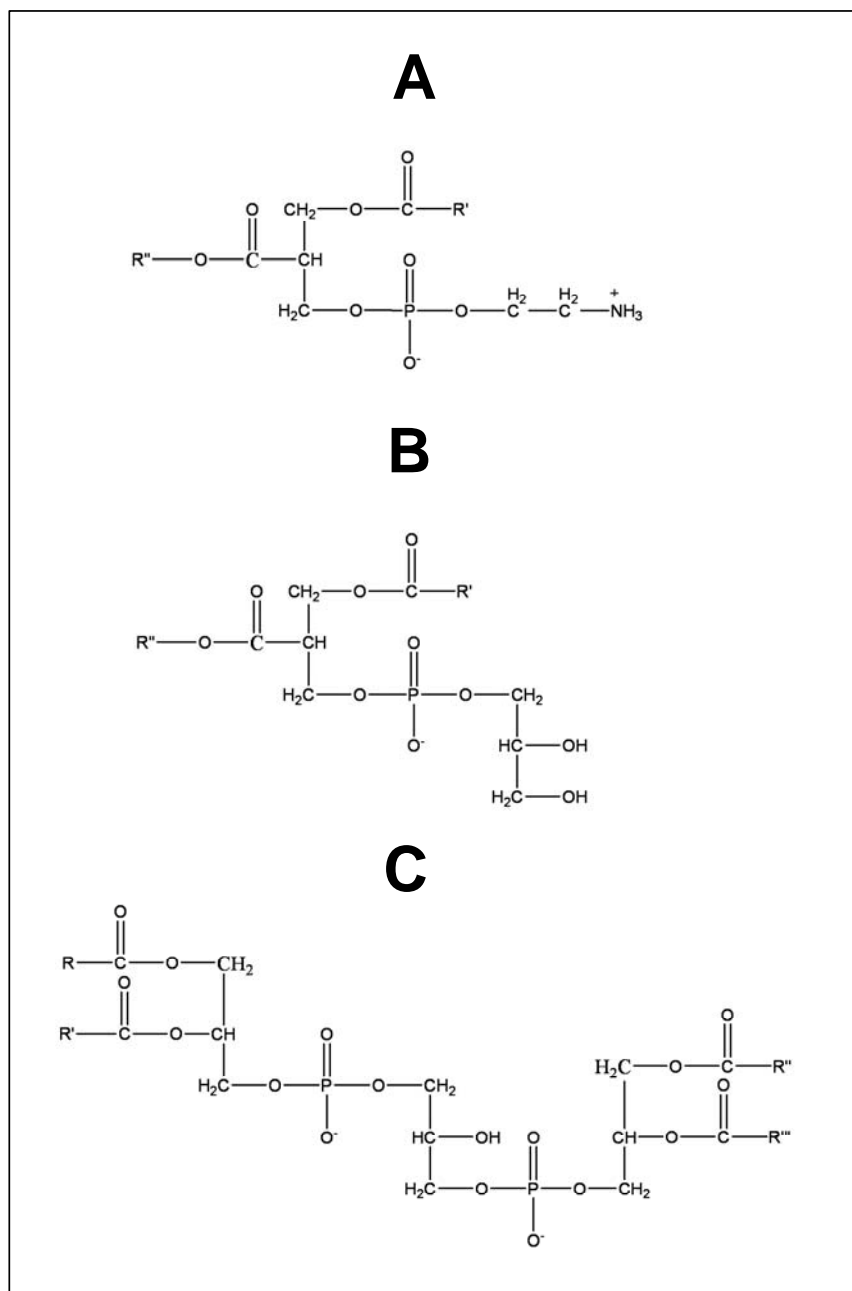


Figure 6: General structure of bacterial phospholipids. The R groups are unsaturated or saturated alkane chains that depend on the specific phospholipid. A) Phosphatidylethanolamine, B) Phosphatidylglycerol, C) Diphosphatidylglycerol

The outer membrane is essentially held together by non-covalent forces caused by the amphiphilic nature of the lipid molecules. By adopting a bilayer structure in aqueous milieu, the lipid molecules minimize their free energy by orienting their hydrophilic and

hydrophobic ends towards and away from the external environments respectively.¹⁶ As a result of the bilayer orientation, the hydrophilic polar head groups of the lipid molecules, which contain anionic phosphoryl and carboxyl groups, remain exposed to the external environment and effectively determine the reactivity of the cell surface.^{13,17}

In addition to the phospholipids, the outer membrane contains proteins and lipopolysaccharides (LPS). The LPS are made up of three distinct regions: lipid A, R core region, and the O side chain. Lipid A is composed of fatty acids linked to a disaccharide, N-actylglucosamine phosphate. On the outer side of the membrane, the LPS are associated with a number of proteins. On the inner side, a lipoprotein complex consisting of small proteins anchors the outer membrane to the peptidoclycan layer. The toxicity of some Gram-negative bacteria such as *Escherichia coli*, *Salmonella*, and *Shigella* is attributed to the LPS, which is often referred to as endotoxin.

The outer membrane of the cell envelope is relatively permeable to small hydrophilic and hydrophobic molecules. The permeability is attributed to the presence of proteins called porins that form membrane channels. The porins are both specific and non-specific to exchange of molecules with the environment. Between the outer and cytoplasmic membranes is the periplasm, also known as the periplasmic space. The periplasm has a gel-like consistency and contains the peptidoglycan layer. In *E. coli*, the periplasm measures approximately 12 to 15 nm across. There are three protein types found in this region: hydrolyzing enzymes for initial digestion of food molecules, binding proteins that help transport various substances, and chemoreceptors involved in various chemoactive responses. The defined periplasmic space and LPS layer is found only in the Gram-negative bacteria.

The interaction between bacteria and surfaces is controlled both by the chemistry of the outer surfaces of the bacteria and chemistry of the external surface. The process of bacterial adhesion is one example of interaction between bacteria and surfaces and is reviewed in the next section.

1.4 Previous Bacterial Adhesion Studies

A large number of studies of bacteria on surfaces have investigated bacterial adhesion. Bacterial adhesion is the process in which a bacterium physically or chemically bonds to a surface. Adhesion is the initial step in the process of biofouling or

biofilm formation. Biofouling leads to many undesirable consequences, such as infection of medical implants or decay of important structural materials.¹⁸ The adhesion of bacteria to surfaces has been found to exist in two primary phases, the initial and secondary phases.^{19, 20}

1.4.1 Bacterial Adhesion Process

Bacteria prefer to grow on available surfaces rather than in the surrounding aqueous phase.²¹ The initial interaction involves physiochemical interactions with the surface, both of the long and short range variety. The long range forces facilitate the movement of bacteria to a material surface through and by the effects of physical forces such as van der Waals attraction forces, gravitational forces, and hydrophobic interactions. Some long range forces between the cells and material surfaces are non-specific and occur at distances greater than 150 nm. They are described by mutual forces and are a function of distance and free energy. Short range interactions occur at distances less than 3 nm and can be separated into chemical bonds, such as hydrogen bonding, ionic and dipole interactions, and hydrophobic interactions. The initial interaction of bacteria to material surfaces is the initial step of adhesion, which makes the molecular or cellular phase of adhesion possible.

In the second phase of adhesion, molecular reactions between the bacterial surface structures and substratum surfaces become predominant. The molecular reactions produce a firmer adhesion of bacteria to a surface through the bridging function of bacteria surface polymeric structures. The polymeric structures include capsules, fimbriae or pili, and slime, and are responsible for the irreversible adhesion of bacteria after the initial phase.

1.4.2 Factors Influencing Bacterial Adhesion

A large number of studies have found that a variety of factors can influence the extent of bacterial adhesion to a surface. The factors include environmental conditions, characteristics of the bacteria surface, and properties of the material surface. This section will discuss how the different factors influence bacterial adhesion.

1.4.2.1 Environmental Factors

The adhesion of bacteria has been found to be effected by numerous environmental factors including temperature, time of exposure, bacterial concentration,

and concentration of electrolytes in the culture medium. Adhesion of *Streptococcus faecium* to glass was found to increase with increasing temperature (up to 50°C), time of exposure, and bacterial concentration. Equilibrium of bacteria on the surface was not reached after eight hours of incubation or a cell concentration of 3×10^{10} cells/mL.²² The effect of temperature has also been found by other researchers.²³ Fletcher and Marshall²³ and Satou²⁴ et al. found that the number of bacteria adhering to a substrata surface increased with time until a saturation level was reached. The saturation level was specific for each type of surface.

The amount of various chemical species in the culture medium has been found to effect adhesion. Concentrations of electrolytes (potassium chloride, sodium chloride),^{22, 25} carbon dioxide,²⁶ and pH^{22, 27, 28} have all been found to vary the extent of adhesion. All of the environmental factors may influence bacterial adhesion by either changing the physical interactions in the initial phase of adhesion or by changing the characteristics of the bacteria or the substratum surfaces.¹⁸

1.4.2.2 Bacterial Surface Properties

The properties of the surface of a bacterium affect its adhesion to material surfaces. The surface properties vary among species and even strains of particular organisms. In general, bacteria prefer to adhere to substratum surfaces that more closely match the hydrophobicity of their own surface. Hydrophilic bacteria prefer hydrophilic surfaces, and likewise, hydrophobic bacteria prefer hydrophobic surfaces.^{24, 29} The hydrophobic bacteria adhere to a greater extent than the hydrophilic bacteria.³⁰ Altering the hydrophobicity of a bacterium has been found to change its adhesion properties. Treatment of *Staphylococcus epidermidis* with pepsin or extraction with aqueous phenol yielded cells with decreased hydrophobicity and resulted in decreased adhesion to FEP.²⁹

The charge of the bacterial surface has also been found to effect the adhesion properties.^{31, 32} The surface charge attracts ions of opposite charge in the medium and results in the formation of an electric double layer. Bacteria in solution have been found to be always negatively charged.³² A higher surface charge is accompanied by a more hydrophilic character of the bacteria; however, hydrophobic bacteria may still have a high surface charge.³² The surface charge of bacteria varies according to bacterial species and is influenced by growth media, bacteria age, and bacterial surface structure.³¹

1.4.2.3 Substratum Surface Properties

Many properties of the substratum surface influence bacterial adhesion including the chemical composition of the surface,^{33, 34} the charge of the surface,³² the surface hydrophobicity,^{35, 36} and the surface roughness and physical configuration.^{37, 38} The surface energy, empty binding sites, and hydrophobic and hydrophilic characteristics can quickly be altered by the adsorption or binding of serum proteins and formation of biofilms.^{39, 40}

Chu and Williams⁴¹ compared the adhesion of both *E. coli* and *S. aureus* to polydioxanone and Dexon sutures, among other surfaces. They found that both organisms exhibited the highest adherence affinity for Dexon and the lowest for polydioxanone. Gristina⁴⁰ et al. showed that *S. epidermidis* preferentially adheres to polymers, whereas *S. aureus* preferentially adheres to metals. Various researchers have found that bacterial adhesion can be discouraged by chemically modifying the surface with antimicrobial peptides,⁴² pluronic surfactant coating,⁴³ nonsteroidal anti-inflammatory drug coating,⁴⁴ a solid surface with adsorbed cations,⁴⁵ or amine-containing organosilicon surfaces.⁴⁵

Surface roughness has been found to influence bacterial adhesion. In general, increasing the surface roughness increases bacterial adhesion.¹⁸ McAllister et al.⁴⁶ found that irregularities of polymeric surfaces promoted bacterial adhesion, biofilm deposition, and accumulation of biliary sludge and ultrasmooth surfaces do not allow bacterial adhesion or biofilm deposition. Baker and Greenham⁴⁷ discovered that roughening the surface of either glass or polystyrene with a grindstone greatly increased the rate of bacterial colonization in a river environment. The causes of surface roughness phenomena may include the fact that a rough surface has a greater surface area and the depressions in the roughened surfaces provide more favorable sites for colonization.⁴⁷

The configuration of a surface can affect bacterial adhesion. The surface configuration is a morphological description of the pattern of a material surface, such as a monofilament surface, a braided surface, a porous surface, or a grid-like surface and is a three-dimensional parameter. Merritt et al.⁴⁸ found that implant site infection rates were different between porous and dense materials with porous materials having a much higher rate, which implies that bacteria adhere and colonize porous surfaces preferentially.

Additionally, braided suture materials have increased bacterial adherence compared to non braided ones,⁴⁹ which is probably due to the increased surface area of the braided surfaces.

The wetting properties of a surface, or more specifically the surface free energy, influence bacterial adhesion. Hydrophobicity of both the bacteria and substratum surface effect the overall adhesion.^{24, 29, 50} In general, hydrophilic materials are more resistant to bacterial adhesion than hydrophobic material.^{29, 51} Fletcher and Loeb⁵⁰ studied the attachment of marine *Pseudomonas sp.* to a variety of surfaces. They found that more bacteria attached to hydrophobic plastics with little or no surface charge (Teflon, polyethylene (PE), polystyrene, and polyethylene terphthalate); moderate numbers attached to hydrophilic metals with positive or neutral surface charge; very few attached to hydrophilic, negatively charged substrata (glass, mica, oxidized plastics). Modifying surfaces by coating with proteins, such as bovine serum albumin (BSA), bovine glycoprotein, or fatty-acid free BSA decreased the surface hydrophobicity and led to an inhibition of bacterial adhesion to the surfaces.⁵²

Despite the detailed information known about bacterial cell structure, chemical nature, and adhesion to surfaces, little is known about the fundamental processes involved in the interaction of bacteria with antibacterial surfaces. A few of the prior studies in this area are presented in the next section.

1.5 Previous Antibacterial Surface Studies

This section briefly introduces early antibacterial studies and discusses two important surface-bound antibacterial molecules; alkylated pyridinium polymers on glass and organosilicon bound quaternary ammonium chloride on glass. Quaternary ammonium compounds are one of the very few known antibacterial molecules that retain their bactericidal properties when covalently bound to a surface.

1.5.1 Bulk Phase Antibacterial Molecules

Amphiphilic quaternary ammonium compounds (QACs) are considered surface active due to their increased concentration at the liquid-gas interface in aqueous environment. Because of their surface active properties, many amphiphilic QACs are used as detergents, wetting agents, and emulsifying agents. QACs are organically

substituted ammonium compounds in which the nitrogen atom has a valency of five. They have the general formula shown in Figure 7 where the X is usually a halogen.

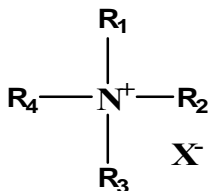


Figure 7: Structure of a quaternary ammonium compound.

For the QAC to be active on a monolayer surface, one of the alkyl substituents must be sufficiently long. The surface active properties are a result of the amphiphilic structure of the molecule. The long alkyl chain of the surfactant molecule orients away from the liquid/air interface and the head group, usually polar or charged, orients at the interface. As a consequence of their surface activity, some QAC are also antibacterial. It is thought that the antibacterial surfactants embed their long alkyl chains into the outer cell membrane, which effectively disrupts the membrane structure and functionality.⁵³ The most widely used antibacterial QAC compound is cetyltrimethylammonium bromide (CTAB).⁵⁴ Another example of an antibacterial QAC has the quaternary ammonium placed in a ring structure, like pyridine. Cetylpyridinium chloride is an example of such a QAC and its structure along with CTAB is shown in Figure 8.

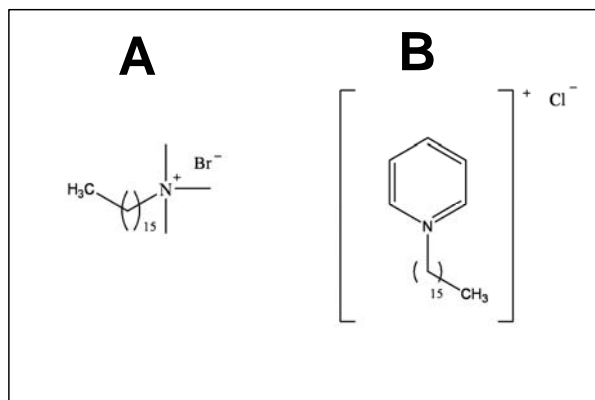


Figure 8: Structure of A) cetyl trimethylammonium bromide (CTAB) and B) cetyl pyridinium chloride, which are well known solution based antibacterial compounds.

The antibacterial action of surface active cations was reported in 1928 by Hartmann and Käig.⁵⁵ In 1940, Kuhn and Bielig suggested that quaternary ammonium

cation (QAC) detergents might act on the bacterial membrane.⁵⁶ The end result of the interaction between bacteria and a QAC is the leakage of intracellular components due to disruption of the membrane functionality. Hotchkiss proved this in 1944 when he detected the leakage of nitrogen and phosphate containing compounds from *Staphylococcus aureus* upon treatment with a wide range of agents.⁵⁷ Further studies using a variety of methods proved the hypothesis.⁵⁸

In 1968, Salton proposed the following sequence of events with microorganisms exposed to cationic agents.⁵⁹ First, the agent is adsorbed and penetrates into the cell wall due to the electrostatic interaction between the surface-bound cations and the anions in the cell wall. The agent then reacts with the cytoplasmic membrane, which is followed by membrane disorganization. Leakage of intracellular low molecular weight material follows. Next, the proteins and nucleic acids begin to degrade followed by the final event; wall lysis caused by autolytic enzymes.

Studies of antibacterial quaternary ammonium compounds in solution are extensive and their mode of action is well documented. However, surface-bound antibacterial quaternary ammonium compounds are not as well studied. It is not unreasonable to think that the mode of action of surface-bound QAC's is different from the bulk phase analogs due to the different physical and chemical environments experienced by the two systems. The next section will outline two studies of surface-bound antibacterial QAC's and the remaining questions they present.

1.5.2 Surface-bound Antibacterial Quaternary Ammonium Compounds

Bulk phase antibacterial compounds are effective against liquid borne bacteria; however it is difficult to test them against airborne bacteria. To be effective against airborne, and possibly liquid borne bacteria as well, the antibacterial molecules need to be present at the solid-air interface. The chemistry at an interface is different than the bulk phase; therefore it is not unreasonable to expect different modes of antibacterial action for the two systems. Surfaces that can repel the adhesion of bacteria and in turn, stop their growth have been developed. Surfaces resistant to bacterial adhesion usually present poly(ethylene glycol) or certain other synthetic polymers.^{43, 60-64} The surfaces do not kill the bacteria, however. The resistance is made possible by presenting a surface that is unfavorable for the bacteria adhesion. There are also materials that can be

impregnated with antimicrobial agents, such as antibiotics, silver ions, iodide ions, and quaternary ammonium ions. The method of action of the impregnated materials is based upon slow release of the active agent into the surrounding solution.^{63, 65-67} The impregnated antimicrobial surfaces present two problems: (1) the need of a liquid medium for the release of the antimicrobial agent and (2) the eventual exhaustion of the antimicrobial agent due leaching. In the review of two studies, antibacterial surfaces were created that were both non-leaching and active against airborne bacteria.

1.5.2.1 Antibacterial Surface Composed of Poly(4-vinyl-*N*-alkylpyridinium bromide)

The antibacterial surface composed of the surface-bound polymer poly(4-vinyl-*N*-alkylpyridinium bromide) was developed in the Klivanov group at MIT.⁶⁸⁻⁷⁰ The idea to use such a molecule as a surface antimicrobial came from a study by Kawabata and Nishiguchi,⁷¹ who found that both cross-linked poly(*N*-benzyl-4-vinylpyridinium halide) and linear poly(*N*-benzyl-4-pyridinium salt) exhibited antibacterial activity in solution. The antibacterial activity of the cationic, polymeric disinfectant was considerably greater than that of the corresponding monomeric compound and was approximately equal to that of conventional disinfectants such as benzalkonium chloride and chlorhexidine. In their study, Klivanov *et al.* used a similar polymer bound to a surface.

The procedure used to bind the polymers to the surface was done as follows. First, an NH₂ glass slide was acylated with acryloyl chloride followed by copolymerization with 4-vinylpyridine. Following removal of non-bonded reactants, the slide was placed in a 10% solution of alkyl bromide. The final step alkylates the nitrogen on the pyridine to give a quaternary ammonium, with the alkyl chain ranging in size from propyl to hexadecyl. The general structure of polymers is shown in Figure 9. Bacteria were prepared and sprayed on to the surfaces using a commercial chromatography sprayer. Using a viable count method, the antimicrobial activity was determined for each surface.

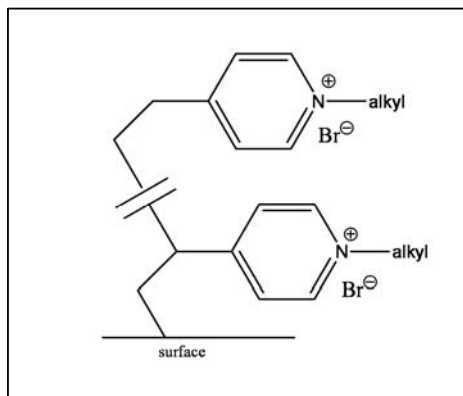


Figure 9: Structure of poly (4-vinyl-*N*-alkylpyridinium bromide). The alkyl chain length was varied from propyl to hexadecyl.

The viable counts from polymer surfaces with different alkyl chain lengths were compared. Lower viable counts were the result of greater antibacterial activity of the polymer surfaces. The largest antibacterial activity was found for propyl, butyl, and hexylated polymers. The longer alkyl chain polymers (decyl, docecyl, and hexadecyl) showed viable counts similar to those of non-alkylated polymers. The reason that the shorter alkyl chains are more effective is most likely due to the weaker van der Waals interactions relative to the longer chain systems. The hydrophobic van der Waals interactions of the longer chains might overcome the electrostatic repulsion of the cationic quaternary ammonium groups. The diminished electrostatic repulsion could lead to a charge separation too small to interact favorably with the cell wall of a bacterium. In the shorter chain molecules, the electrostatic repulsion probably dominates over the hydrophobic attraction and might provide the correct charge separation needed to interact favorably with the bacteria.

The possibility of the antimicrobial agent leaching from the surface was also investigated. If leaching does occur, there will be a zone of inhibition where no bacterial growth occurs surrounding the surface.⁷² To test for leaching, the bottom surface of a Petri dish was sprayed with bacteria in addition to spraying of the antibacterial surface. The results showed that approximately 60 colonies/cm² grew on the dish, even in the immediate proximity of the antibacterial surface, but only 3 colonies/cm² grew on the antibacterial surface. The viable colony counts only provided indirect evidence that leaching did not occur.

The Klibanov study showed that surface-bound polycationic polymers were effective antimicrobials. In the next study presented, a monomeric surface is shown to be antimicrobial.

1.5.2.2 Antibacterial Surface Composed of 3-(trimethoxysilyl)-propyldimethyloctadecyl ammonium chloride

Antibacterial surfaces composed of 3-(trimethoxysilyl)-propyldimethyloctadecyl ammonium chloride were developed by Isquith et al. at Dow Corning Corporation (Figure 10).⁷³ The antimicrobial surface, from here on referred to as Si-QAC, were bound to a number of surfaces including siliceous surfaces, natural fibers, man-made fibers, and metals via hydrolysis and condensation with reactive surface functional groups. Si-QAC showed antimicrobial activity only when bound to a surface, not in free solution. The surface-bound Si-QAC showed no evidence of leaching and remained 95% effective after 50-four minute washings.

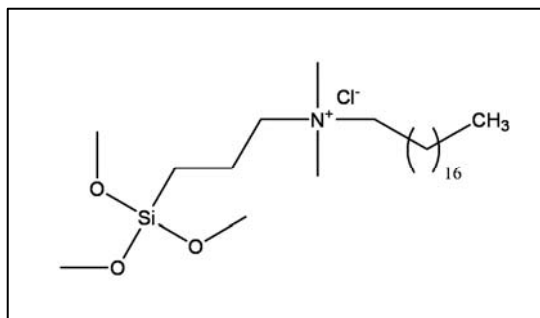


Figure 10: Structure of Si-QAC.⁷³ Si-QAC demonstrated high antibacterial activity when bound to a variety of surfaces.

The basic explanation of the mode of action for the antimicrobial effect of Si-QAC is a disruption of membrane phenomenon such as membrane lysis, membrane enzyme inactivation, or interference with ion transport.⁷⁴ It is most likely that the site of action occurs at the cell wall and not inside the cytoplasm.

1.5.3 Remaining Questions About Antimicrobial Surfaces

The two antimicrobial surfaces discussed in section 1.5.2 left some important remaining questions. Most antibacterial surfaces have not been carefully characterized. The lack of detailed characterization presents fundamental questions about the relationship between the surface structure and antibacterial activity. How does the order

of the surface molecules effect activity? Does a crystalline-like arrangement of surface molecules promote or inhibit bactericidal activity? How important is the surface concentration of the bactericidal molecules? Does the surface density of the bactericidal molecules play a role in the antibacterial mechanism? Is there a limit to how close together or how far apart the surface-bound bactericidal molecules need to be to maximize antibacterial activity? Is the counter ion of the quaternary ammonium cations important? Most of the previous studies utilized bromine or chlorine, but did not investigate larger ions, such as iodine, or molecular anions, such as triflate.

To gain insight to these fundamental questions, self-assembled monolayers (SAMs) of alkanethiols on gold will be used. SAMs on gold are used to create ideal interfaces where the surface properties can be systematically changed. Properties such as molecular order, surface coverage, density, and concentration can be altered using self-assembly techniques. By fully characterizing the SAMs, followed by determination of the viability of bacteria on the SAMs, insights into the fundamental relationships between surface structure and antibacterial activity can be achieved. In the following chapter, the motivation for using SAMs will be explained in more detail, in addition to a concise literature review of previous SAM work.

Chapter 2: Self-Assembled Monolayers as Model Surfaces: Motivation and Background

2.1 Introduction

Studies of the chemical and physical processes that occur at interfaces often require careful control of the structure and properties of the surface. Ideally, study of natural surfaces would be straightforward and require little effort to control experimental variables. Unfortunately, the heterogeneity of natural surfaces makes it extremely difficult to isolate the chemical and physical processes that occur. Natural surfaces commonly undergo reactions with environmental contaminants, such as oxidation by atmospheric gases, which can further complicate isolation of chemical and physical processes occurring on surfaces. To help isolate and identify the chemical and physical processes, model surfaces are commonly used. Model surfaces enable control over surface structure and can diminish heterogeneity and reduce environmental contamination issues. Model surfaces also enable systematic studies into the role of structural order, chain lengths, and functional group density on bacteria viability. One such model system that allows for systematic studies are self-assembled monolayers of alkanethiols on gold.

Self-assembled monolayers are composed of surfactant like molecules that self-assemble into well-ordered structures when exposed to an appropriate substrate. Examples of self-assembled monolayers include fatty acids adsorbed on metal oxide⁷⁵⁻⁷⁷ and silver substrates,⁷⁸ organosilicons adsorbed on hydroxylated surfaces,^{63, 79-95} and organosulfur compounds adsorbed on metals.⁹⁶ The most studied and versatile of these systems are the organosulfur compounds adsorbed to metals, specifically alkanethiols adsorbed to gold.

The primary goal of this research project is to understand the fundamental relationship between surface structure and the viability of bacteria. Systematic alteration of surface structure followed by assessment of bacteria viability will help develop understanding of the fundamental relationship. Systematic alteration will encompass changing the ordering of the monolayer, varying the length of alkyl chains, and adjusting

the density and surface concentration of specific functional groups. Self-assembled monolayers (SAMs) of alkanethiols on gold are ideal for such studies because they allow for easy control and modification of the aforementioned variables.

SAMs composed of alkanethiols adsorbed to gold have been used extensively as model surfaces. Alkanethiol SAMs have also been used for applications including non-linear optics,⁹⁷ chemical sensors,⁹⁸⁻¹⁰⁰ and coating technologies.¹⁰¹ The versatility of SAMs allows for control of many surface properties including wetting,¹⁰²⁻¹⁰⁶ electron transfer,¹⁰⁷ and corrosion resistance.¹⁰⁸ The fact that SAMs can be used for such a wide assortment of research areas stems from the fact that surface properties are primarily controlled by the functional groups present at the solid/air interface of the monolayer.

Figure 11 shows the general structure of an alkanethiol SAM adsorbed to gold.

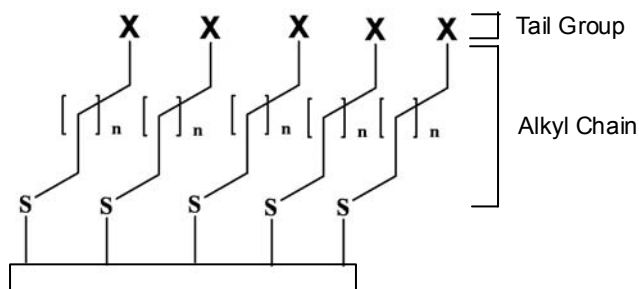


Figure 11: General structure of an alkanethiol SAM on gold. The tail group (X) can be a wide range of functional groups compatible with thiol groups.

The sulfur, known as the head group, is chemically bonded to the gold substrate. The alkyl chains assemble in an all trans configuration, leading to the tail group being exposed at the interface. The tail group can be any functional group that is compatible with the thiol head group, which includes methyl, hydroxyl, carboxylic acid, ester, ketone, aldehyde, amine, amide, sulfate, alkene, and many more.⁹⁶

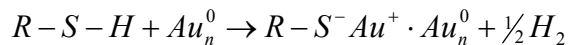
Alkanethiol SAMs on gold are amenable to a large number of characterization techniques, including reflection-absorption infrared spectroscopy (RAIRS), x-ray photoelectron spectroscopy (XPS), ellipsometry, surface plasmon resonance (SPR), contact angle goniometry, force microscopy, many types of electrochemistry, and more. Such detailed knowledge of surface structure can help provide information about chemical processes occurring at interfaces.

2.2 Formation of Alkanethiol SAMs

The primary driving force behind the formation of alkanethiol SAMs is the strong affinity of sulfur for transition metal surfaces,¹⁰⁹⁻¹¹³ which results from the ability of sulfur to form multiple bonds with surface metal clusters.¹¹⁴ Alkanethiol SAMs have been formed on many different metal surfaces, but the most widely used system employs gold. Gold is used extensively because it does not form a stable oxide surface,¹¹⁵ which limits atmospheric contamination.

Whitesides *et al.* investigated the chemisorption of thiols onto gold in dilute (~1mM) solutions. They found that the adsorption of alkanethiols on Au(111) occurs in two distinct phases.¹¹⁶ The first phase is very fast, occurring within a few minutes. Within this short time frame, the contact angles reach limiting values and the monolayer thickness reaches 80-90% of the final value. The first phase is strongly dependent on thiol concentration; the higher the concentration the less time the first stage takes to complete. The second phase is a slow step that occurs over several hours and can be described as a surface crystallization process. The kinetics of the second phase are related to chain disorder, components of chain-chain interaction, and the surface mobility of the chains. The two step mechanism has been confirmed by second-harmonic generation,¹¹⁷ X-ray photoelectron spectroscopy measurements,¹¹⁸ and near-edge X-ray adsorption fine structure.¹¹⁹

The chemical reaction of an alkanethiol with gold is a formal oxidative addition of the S-H bond to the gold surface followed by elimination of the hydrogen, shown in Equation 1. The protons released combine to form H₂ molecules, which stems from the fact that monolayers have been formed in the absence of oxygen.¹²⁰⁻¹²² Work using XPS,^{104, 123-125} FTIR,¹²⁶ Fourier transform mass spectroscopy,¹⁰³ electrochemistry,¹²⁷ and Raman spectroscopy^{128, 129} all confirm that the thiolate is the adsorbing species. The bonding of the thiolate to gold is very strong, approximately 40 kcal/mol.¹¹⁰ Using individual bond energies of the entire thiol molecule, a rough estimate for the net energy of adsorption is -5 kcal/mol, which is confirmed by electrochemical data that gives -5.5 kcal/mol.¹³⁰ The adsorption energy values show that the lowering of enthalpy is the primary driving force for the spontaneous adsorption of alkanethiols on gold.



Oxidative addition of alkanethiol to gold. (1)

2.3 Structure of Alkanethiol SAMs

The structure of alkanethiols adsorbed to Au(111) has been investigated using a large number of methods. The spatial orientation of the monolayers with respect to the underlying gold lattice was studied by Strong and Whitesides¹³¹ and by Dubois.¹³² Using high energy electron diffraction, they determined that the symmetry of the adsorbing sulfur atoms is hexagonal with an inter-atomic spacing of 4.97 Å and a calculated area per molecule of 21.4 Å².

Sellers *et al.* have shown using *ab initio* calculations that alkanethiolates on Au(111) have two binding modes.¹¹⁴ One mode was found to have a bend angle around the sulfur of 180° (*sp* hybridization) and the other mode has a 104° angle (*sp*³ hybridization). The latter structure was found to be more stable by 0.41 kcal/mol. The energy barrier between the two modes is very small; only 2.5 kcal/mol. The small barrier suggests that the thiolate may easily cross from one of the two energy minima to the other.

The overlaying structure of alkanethiols on Au(111) is primarily ($\sqrt{3} \times \sqrt{3}$)R30°, ^{110, 132-134} which is shown in Figure 12. The overlaying structure has also been shown to adopt a secondary organization of the chains corresponding to a c(4 x 2) superlattice.¹³⁵ Work performed via experiment and theory¹³⁶ have found that thiolates bind to both the 3-fold hollow and 2-fold bridge sites of the Au(111) lattice.

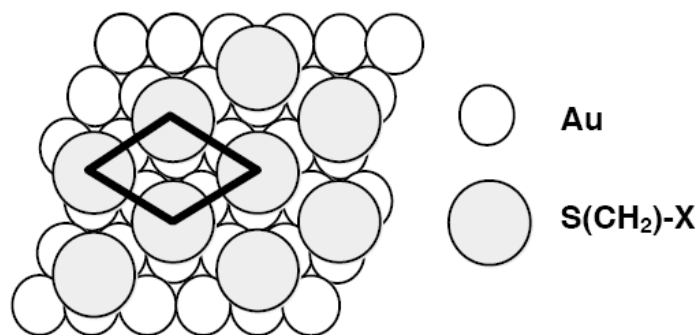


Figure 12: Lattice structure of an adsorbed alkanethiol monolayer on an Au(111) substrate.¹³⁷ The lattice has dimensions $\sqrt{3} \times \sqrt{3}$ and is rotated 30° relative to the substrate lattice.

The structure of the alkane chains is driven by the lowest energy configuration whereby the van der Waal interactions of adjacent chains are maximized. To accomplish maximum van der Waal's interaction, the chains adopt an all-trans, or zigzag configuration. For a monolayer with all chains perpendicular to the substrate, the chain-chain distance is 4.6 \AA .¹³⁰ However, the chain-chain spacing of alkanethiols on Au(111) is 4.97 \AA . Because of the increased chain-chain distance, maximization of van der Waal's interactions cannot occur if the chains are in a perpendicular conformation. To maximize the van der Waal's interactions, the chains tilt away from the surface normal. Nuzzo and coworkers studied a number of SAMs with different terminal groups, including CH_3 , CH_2OH , COOH , COOCH_3 , and CONH_2 .¹⁰³ They determined that, regardless of terminal group, the chains are usually tilted approximately $26\text{-}28^\circ$ from the surface normal and show an approximately $52\text{-}55^\circ$ rotation about the molecular axis. Figure 13 shows tilt and rotation angles.

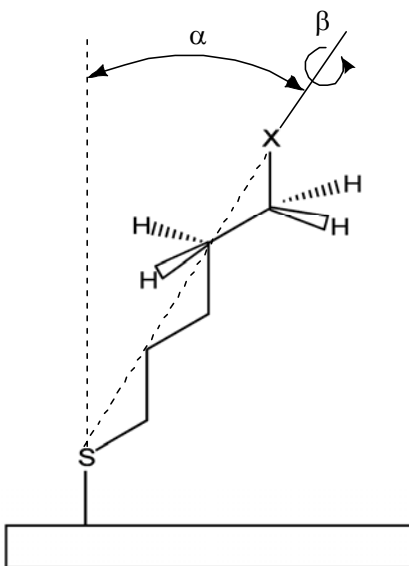


Figure 13: Orientation of alkanethiol on Au(111). The tilt angle (α) is $\sim 26\text{-}28^\circ$ and the twist angle (β) is $52\text{-}55^\circ$ ¹⁰³.

2.4 Stability of Alkanethiol SAMs

The stability of alkanethiol SAMs is an important aspect of the study of bacteria viability on surfaces. The monolayers must remain stable under the experimental conditions encountered. Three important conditions of stability are thermal stability, solution stability, and stability in biological media. This section will report on previous research to establish the stability of SAMs

Hickman *et al.* studied the thermal stability of alkanethiols on gold and found that hexadecanethiol desorbed from gold over the temperature range of $170\text{-}230^\circ\text{C}$.¹³⁶ Nuzzo *et al.* used temperature programmed desorption of methanethiol and found a maximum desorption temperature at approximately 220°C .¹²⁶ The two studies indicate that both long (sixteen carbons) and short (one carbon) alkanethiols have desorption temperatures much higher than standard room temperature. Because the maximum desorption temperatures were much higher than the temperatures found in the natural environments of most bacteria, alkanethiol SAMs should be thermally stable enough to be used as model surfaces in the study of bacteria viability.

Schlenoff *et al.* investigated the stability of octadecanethiol SAMs on gold in various solvents including tetrahydrofuran, hexane, water, and ethanol.¹³⁸ In the study, they used radio labeled sulfur atoms to investigate desorption kinetics. Their results

demonstrated that desorption rate is strongly dependent on solvent properties. In THF, they observed almost quantitative desorption, however in water they observed 90% less octadecanethiol desorption. They explained their observations based on the differences in polarity between water and THF. Because octadecanethiol molecules are non-polar, the molecules will have a greater affinity for a non-polar solvent. THF is much less polar than water, hence the octadecanethiol molecules are more likely to desorb in THF than they are in water.

Most relevant to the work in this thesis is the stability of alkanethiol SAMs in biological media. Flynn *et al.* studied the stability of SAMs upon long term exposure to biological media.¹³⁹ They determined that the structure of monolayers composed undecanethiol and tri(ethylene glycol)-terminated undecanethiol was significantly altered during the latter stages of a 35 day exposure to both phosphate-buffered serum and calf serum. The structural change was the result of oxidation of the sulfur moieties followed by subsequent desorption from the surface into the surrounding liquid medium. Surface properties such as contact angles were monitored periodically during the 35 days. Considerable changes to the surface properties did not occur until approximately 15-20 days. The integrity of the SAM structure did not appear to be compromised upon short term exposure.

Alkanethiol SAMs with different functional end groups have been found to undergo structural reorganizations. Monolayers of 11-hydroxyundecanethiol on Au(111) undergo surface reorganization by exposure to ambient atmosphere for a few hours.¹⁴⁰ Using molecular dynamics simulations, Klein *et al.* showed that the driving for the reorganization is the formation of surface-correlated hydrogen bonds.^{141, 142} Surface structure instability has also been found for mixed monolayers comprised of hydroxyl- and methyl-terminated chains. A lower surface free energy is reached if the methyl groups are exposed at the interface, as opposed the hydroxyl groups. The reorganization can be offset by strong intermolecular interactions and studies of long chain alkanethiols show that surface reorganization is a function of monolayer melting point. The final equilibrium structure of a surface monolayer is a result of the balancing of numerous factors; temperature, relative humidity, and adsorption at the monolayer interface.¹³⁰

2.5 Modification of Alkanethiol SAMs

One very useful aspect of SAMs is the ability to modify the surface structure after the original monolayer is formed. This is accomplished using relatively simple reactions where the SAM is placed into to a vapor or a solution of the reactant molecules. Modifying a SAM after formation can simplify the synthesis of complicated surface molecules whose total synthesis prior to SAM formation is extremely laborious or even impossible. The gold-sulfur bond also protects the sulfur moiety from unwanted side reactions that are commonly encountered during synthesis of complicated thiols.

A large number of surface modifications involve initial SAMs with reactive terminal groups, commonly –OH and –COOH. Duevel and Corn produced amide and ester terminated SAMs by reacting a carboxylic acid terminated SAM with gas phase thionyl chloride.¹⁴³ The resulting acid chloride terminated SAM was further reacted with gas phase amine to create the amide. Yan *et al.* reacted carboxylic acid terminated SAMs with trifluoroacetic anhydride to form carboxylic anhydride terminated SAMs.¹⁴⁴ The anhydride terminated SAMs were then reacted with alkyl amines to form a 1:1 mixed monolayer composed of carboxylic acid and amide terminal groups. Amide groups have also been formed by the aqueous solution reaction of carboxylic acid terminal groups with amines, catalyzed by 1-ethyl-3-[3-(dimethylamino)propyl]carbodiimide (EDC).^{145,}
146

Suter and coworkers developed a fairly simple and versatile procedure to modify a hydroxyl terminated SAM.¹⁴⁷ They reacted hydroxyl terminated SAMs with 1,4-phenylene diisocyanate, which results in a reactive carbamate group at the interface. This group can be further reacted with a variety of functional groups including water, alcohols, and amines to form new interfaces. They found that reaction of the hydroxyl groups with the diisocyanate offered near 100% conversion. McPherson *et al.* utilized Suter's procedure to create SAMs with urethane, or carbamate terminal groups.¹³⁷ The position of the carbamate group was systematically varied to determine the role of buried hydrogen bonding groups on monolayer structure.

2.6 Concluding Remarks

Self-assembled monolayers of alkanethiols on gold have been shown to be ideal systems for studying fundamental interfacial chemistry. The structure and chemical functionality of alkanethiol SAMs can be carefully controlled, SAMs are amenable to a large number of characterization techniques, and SAMs can be modified after formation of the original surface. SAMs have also been shown to be stable upon short-term exposure to biological media. The versatility and stability shown by SAMs make them excellent model surfaces and will allow for systematic studies of bacteria viability on surfaces.

Chapter 3: Experimental Approach and Antibacterial Assay Method Development

3.1 Introduction

The data for the study of bacteria viability on surfaces can be divided into two parts: surface characterization and assessment of bacteria viability on the surfaces. As explained in Chapter 2, the primary motivation for using self-assembled monolayers (SAMs) is the fact that they form well ordered surfaces that can be characterized and systematically varied with a number of well established techniques. Three of the most important surface characteristics in this study are the surface composition, the structural ordering, and surface concentration of specific species. Reflection-absorption infrared spectroscopy (RAIRS) and X-ray photoelectron spectroscopy (XPS) are the primary tools used to acquire this information.

Once the surface is characterized, the next step is to assess the viability of the bacteria on the SAM. The first step of this process is to introduce the bacteria to the surface followed by measuring their subsequent response. The surface is characterized again and compared to the original data to learn about any changes to the surface structure that may be occurring as a result of reacting with the bacteria.

3.2 Reflection-Absorption Infrared Spectroscopy (RAIRS)

Reflection infrared spectroscopy is a well established tool to study surface-bound species and reactions.^{148, 149} The use of gold as the substrate for the SAMs permits the use of reflectance methods due to its highly reflective nature. The impinging infrared photons cause the chemical bonds of the surface molecules to vibrate. By measuring the frequency and intensity of the absorbed photons due to the chemical bond vibrations, information such as chemical environment, structure, and functional group identity can be elucidated.

In a typical RAIRS experiment, a beam of infrared radiation is directed towards a surface where it interacts with the surface-bound molecules and reflects towards a set of mirrors that send the reflected beam to a detector. Fourier transform, which is an algorithm that deconvolutes individual cosine waves that are collected by the

interferometer, is then used to turn the raw signal into spectra. The resulting output is the familiar plot of absorption intensity versus wavelength, frequency, or wavenumber.

The basis for using reflection infrared instead of conventional transmission infrared were developed by Greenler in the 1960's.^{148, 149} He investigated both the effects of the polarization of the light and the angle of incidence in which the light strikes the surface. Figure 14 outlines the effects of polarization.

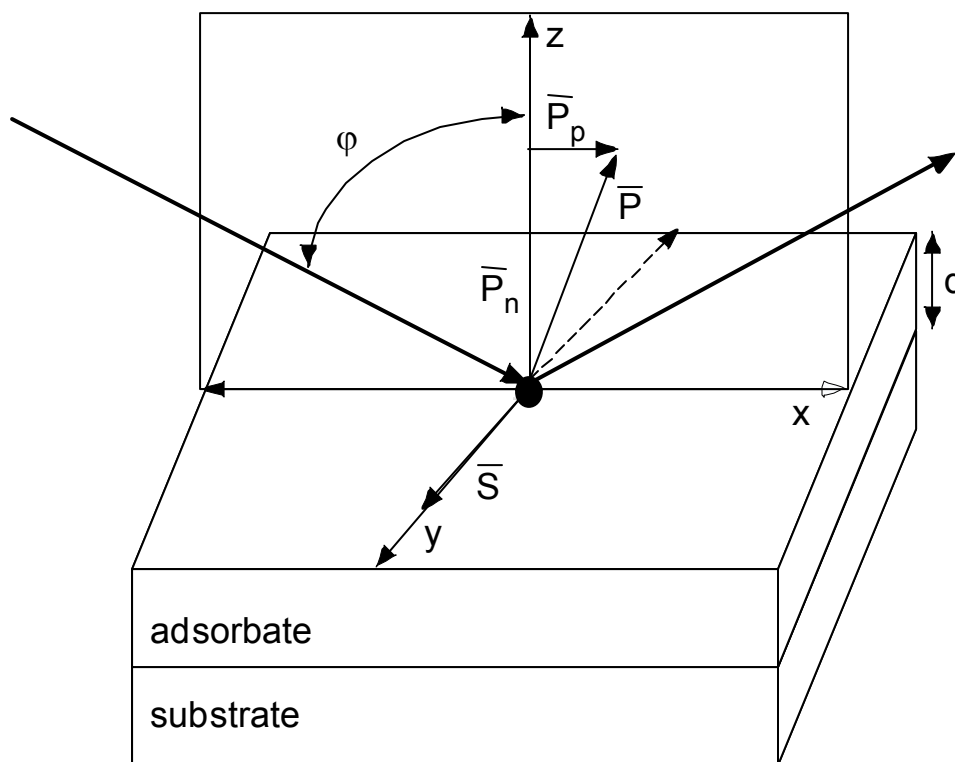


Figure 14: Components of light impinging on a surface. The light can be divided into two perpendicular oscillations. P_n oscillates perpendicularly to the plane of the surface, P_p oscillates parallel to the plane of the surface.

Incoming light that is linearly polarized can be separated into two different polarizations, S and P. The S polarization is parallel to the surface in the y direction and perpendicular to the plane of incidence, while P represents the polarization component in the plane of the surface normal and the propagation direction of the incident light. When the S polarized light reflects from the surface, it suffers a 180° phase shift that results in a near total cancellation of amplitude. The P polarized light undergoes a 90° phase shift that results in an amplitude addition. By using a polarizer, only P-polarized light is allowed to impinge on the surface.

Greenler also found, by using Maxwell's equations, that the amplitude of the p-polarized light reaches a maximum at grazing angles of incidence (ϕ). Using mathematical calculations, he established that the absorption factor increases by a factor of 10^7 for 89° incidence compared to normal incidence.¹⁴⁸ By using the same approach, the critical angle of RAIRS experiments using gold substrates is found to be 86° , which is the approximate angle of incidence of all of the RAIRS experiments performed for this project.

A consequence of the use of p-polarized light is the surface selection rule. This rule states that only adsorption modes that have a component of their dipole moment that is perpendicular to the surface will be excited. Modes that are completely parallel to the surface normal do not interact with p-polarized light and are not detected. Mathematically, the surface selection rule is expressed by Equation 2, where I is the intensity of the absorption mode, E is the scalar product of the electric field, and μ is the transition dipole moment relative to the surface normal. The transition dipole moment is dependent on the spatial orientation of the vibrating molecule. Mathematically, this is expressed in equation 3, where z is the surface normal vector and θ is the angle between μ and z . If $\theta=90^\circ$, $\cos \theta=0$ and the intensity of the absorption mode becomes zero.

$$I = \left| \vec{E} \cdot \vec{\mu} \right|^2 \quad (2)$$

$$\left| \vec{\mu} \cdot \vec{z} \right|^2 \propto \cos^2 \theta \quad (3)$$

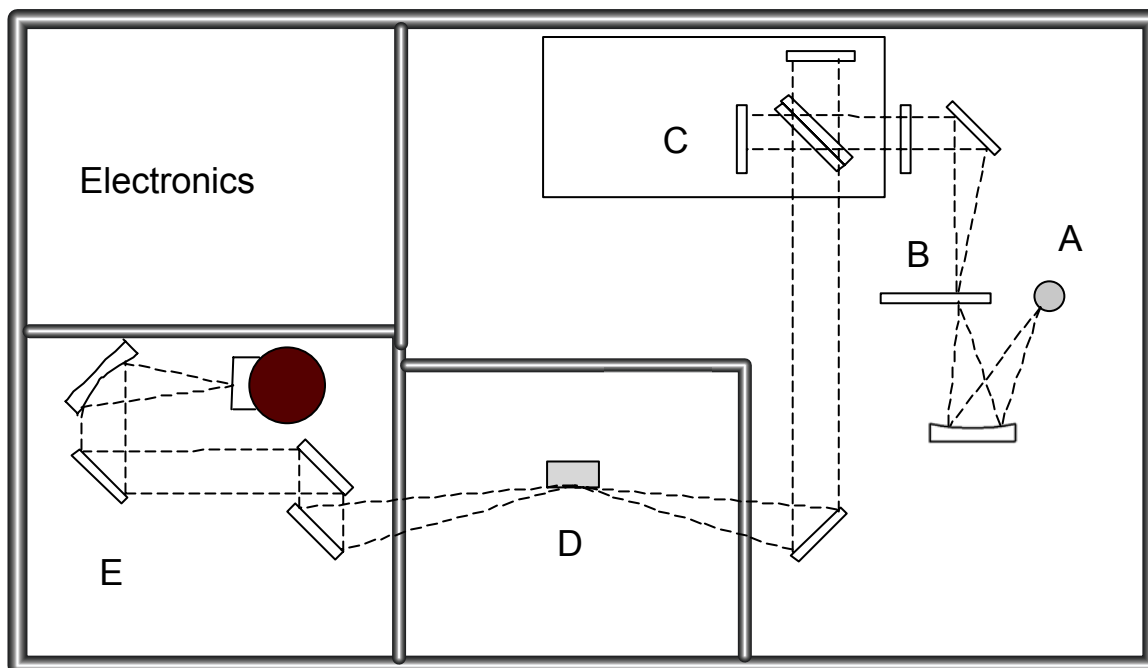


Figure 15: Schematic of the Bruker IFS66v/S infrared spectrometer: (A) SiC glowbar MIR source, (B) aperture wheel, (C) interferometer (beam splitter, moving mirror, polarizer), (D) sample chamber, (E) MCT detector chamber

All of the RAIRS work was performed using a Bruker IFS 66v/S spectrometer, as shown in Figure 15. The IR light, generated by a SiC glowbar MIR source (A), is passed through a polarizer, and sent to the surface at an incident angle of 86° . After reflection from the surface, the radiation is collected by a liquid N_2 cooled MCT (mercury-cadmium-telluride) detector (E). To enhance the signal-to-noise ratio, the light is passed through a wire grid polarizer. The polarizer allows use of only P polarized light, whose amplitude is augmented upon reflection. All spectra are generated in comparison to a background reference, which for these experiments is a clean gold substrate. The spectra were collected using a resolution of 2 cm^{-1} and are the average of 100 scans.

To avoid contamination by atmospheric molecules such as water or carbon dioxide, the RAIRS experiments are performed under vacuum conditions. The sample chamber and interferometer housings are kept at a pressure of 18 mbar by a Vacuubrand diaphragm pump (MD4, pumping speed 1.04 L/s) when nitrogen is flowing. The IR radiation from the glowbar source is reflected from a gold coated parabolic mirror (focal length 180 mm) and through an aperture that spatially filters the IR beam so that the detector element is not saturated with light. The collimated beam the passes through a

Zn-Se wire-grid polarizer that selects the p-polarized component of the IR radiation. The p-polarized IR radiation is then directed through the interferometer and sent into the sample chamber through a KBr window.

The sample compartment is housed separately from the optics and the detector and is connected to them by two KBr windows. The isolation of the sample compartment allows for ease of sample introduction and helps protect the sensitive optical equipment. Samples are placed on an aluminum block that is affixed to an optical mount with the use of forceps. The final focal mirror in the source chamber (focal length 250 mm) directs the IR beam towards the sample at grazing incidence of $\sim 86^\circ$. Upon reflection from the sample surface, the radiation is passed through the second KBr window and into the detector chamber. Here, the IR beam is reflected from a series of flat, gold coated mirrors onto a final parabolic mirror (focal length 43 mm) which sends the beam to the MCT detector.

To ensure the proper performance and function of the spectrophotometer, great care must be given daily. Routine maintenance and careful optic and sample alignments are necessary to ensure the quality of the spectra. If the sample is not properly aligned so that the surface is perpendicular to the incident IR beam, artifacts such as a sine-wave containing baseline may result.¹⁵⁰ This problem can be avoided by assuring that both the background and sample slide are positioned properly. If sine-wave containing baselines occur, they can be corrected by using the baseline correction function of the OPUS software. However, one must be careful not to accidentally eliminate important spectral peaks when using the baseline correction feature.

The quality of the spectra can also be affected by the condition of the MCT detector. The detector is a semiconductor and operates on the process of electron production from valence bands to conduction bands when infrared photons are absorbed. The electrons in the conduction band respond to an applied voltage by producing an electric current. The current is a measure of the number of promoted electrons and is directly proportional to the number of infrared photons striking the detector. The spectral response and signal-to-noise ratio (S/N) of the detector change with temperature. The number of background photons striking the detector increases with increasing temperature as a result of heat given off by the detector. The response of the spectra to

this phenomenon is a shift to shorter wavelengths. To help eliminate the problem of background photons, the MCT detector is equipped with a vacuum jacketed liquid nitrogen dewar that helps to maintain a cold shield surrounding the photoconductive detector. Over time, the vacuum is lost and must be re-obtained to avoid “icing” issues. The loss of vacuum causes the partial pressure of water in the shield to increase and can cause large spectral artifacts in the region of 3000-3600 cm^{-1} . To control icing issues, the detector jacket needs to be re-evacuated about every six months. Evacuation is completed by using an adapter valve (InfraRed Associates) to connect the detector jacket to a turbomolecular pump (Varian Model 969-9008, pumping speed 250 L/s). Pumping on the vacuum jacket for a few days can bring the pressure to approximately 10^{-6} or 10^{-7} Torr. After evacuation, the detector will remain in optimal condition for several months.

In work to be discussed in Chapter 4, RAIR spectra provide information about the ordering of the surface molecules and the identity of surface-bound functional groups. The RAIR spectra also provide evidence of surface chemical reactions and alteration of surface properties after interaction the bacteria.

3.3 X-Ray Photoelectron Spectroscopy (XPS)

X-ray photoelectron spectroscopy, also known as electron spectroscopy for chemical analysis (ESCA), is a powerful analytical tool that allows analysis of the surface atomic composition, formal oxidation state of the atoms, and the local physical and chemical environment. In an x-ray photoelectron experiment, the samples are placed in a vacuum environment and irradiated with photons in the energy range of 0 to 2000 eV. The basis of the technique relies on the exchange of energy between the incoming photons and the core energy level electrons of the surface atoms. X-ray photons have sufficient energy to cause core level electrons to be ejected from the atom, as shown in Figure 16. The kinetic energy (E_k) of the escaping electrons can be calculated, as shown in Equation 4, where ($h\nu$) is the x-ray photoelectron energy, (E_b) is the electron binding energy, and (E_w) is the work function of spectrometer.

$$E_k = h\nu - E_b - E_w \quad (4)$$

Each core level electron from a different atom has a different binding energy. The identity and atomic composition of the surface can be determined from the different

binding energies. Different chemical environments of the core electrons cause small changes in the binding energies. The small binding energy shifts allow for the determination of specific oxidation states of the atoms.

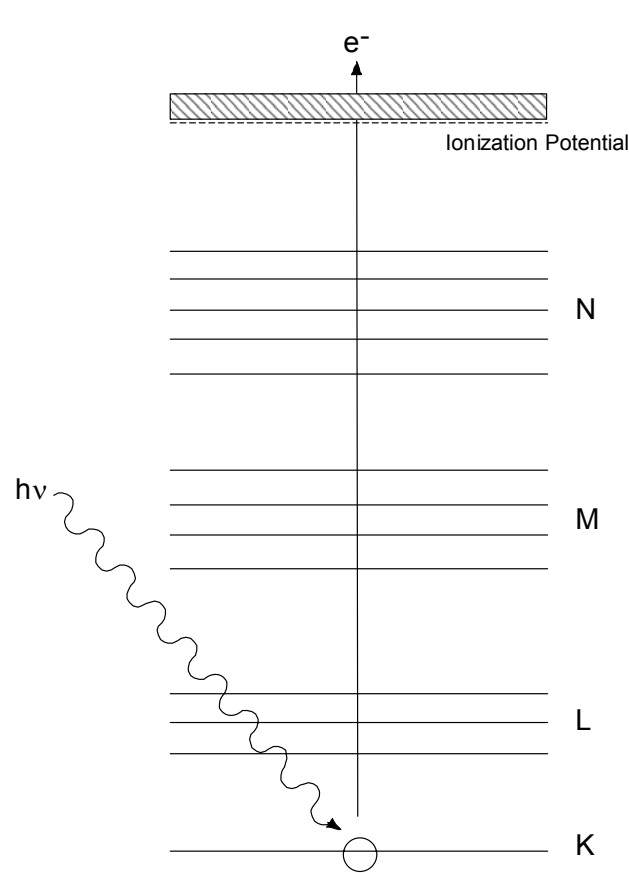


Figure 16: Example energy diagram for the photoelectric effect in XPS. X-ray photons cause core level electrons to be ejected from the atom.

XPS can also be used to determine the relative concentrations of the constituents of interest. Relative concentration determination is based on the following relationship:¹⁵¹

For a homogeneous sample, the number of photoelectrons per second in a specific spectra peak is given by:

$$I = nf\sigma\phi\lambda AT \quad (5)$$

where n is the number of atoms of the element per cm^3 of the sample, f is the x-ray flux in photons/ cm^2/sec , σ is the photoelectric cross-section for the atomic orbital of interest in cm^2 , ϕ is an angular efficiency factor for the instrumental arrangement based on the angle

between the photon path and detected electron, y is the efficiency in the photoelectric process for formation of photoelectrons of the normal photoelectron energy, λ is the mean free path of the photoelectrons in the sample, A is the area of the sample from which the photoelectrons are detected, and T is the detection efficiency for electrons emitted from the sample.

Rearranging Equation 5 to solve for the number of atoms of the element in question gives:

$$n = \frac{I}{f\sigma\theta y\lambda AT} \quad (6)$$

The denominator of equation 6 can be defined as the atomic sensitivity factor, S , and can be determined for every element and is specific to each spectrometer system. The percent concentration of a specific atom can then be determined using the following ratio:

$$C_x = \frac{n_x}{\sum n_i} = \frac{I_x / S_x}{\sum I_x / S_x} \quad (7)$$

To ensure accurate results using this technique, it is important to check the spectrometer operation frequently to ensure that the analyzer response is constant and optimum.

XPS work was performed on a Perkin Elmer 5400 X-ray Photoelectron Spectrometer equipped with a monochromatized Mg(K α) radiation source (1253.6 eV) and a positron sensitive, multi-channel plate detector. The measurements were taken at a pressure of less than 5×10^{-7} Torr and a take-off angle of 15° with respect to the surface normal. Binding energies are referenced to the Au 4f^{7/2} peak at 83.9 eV. Unless otherwise noted, survey spectra were recorded with a pass energy of 89.45 eV for ten minutes on a 1mm x 3.5 mm spot size and 250 W electron beam power. High resolution multiplex scans were taken with varying parameters that will be given in later experimental discussions.

The XP spectra that will be discussed in Chapter 4 provide both qualitative and quantitative information about the composition of the self-assembled monolayers. Specific chemical species and their respective oxidation states are identified based upon measurement of the electron binding energies. Calculation of peak areas and intensities provide data to determine the atomic percent composition of the surfaces. Comparison of

the calculated atomic percent composition to predicted composition help determine the extent of surface chemical reactions and the resulting approximate surface concentration of specific chemical species.

3.4 The Antibacterial Assay

After surface characterization, the viability of bacteria upon the surfaces is assessed. The most common method of determining the ability of a surface to kill airborne bacteria involves spraying an aerosolized bacteria suspension on to the surfaces, adding a growth media, incubating overnight, and counting the number of resulting colonies that have grown on the surface. The viable count method was employed in the Klibanov pyridinium polymer studies mentioned in the Chapter 1.⁷⁰ A variation of the viable count method is used in this study to determine the viability of bacteria on the self-assembled monolayers.

3.4.1 Details of the Antibacterial Assay

3.4.1.1 Materials

Absolute ethanol was obtained from Aaeper Alcohol and Chemical Co. 16-mercaptohexadecanoic acid (90%), 1-hexadecanethiol (92%), and 11-mercapto-1-undecanol (97%), were purchased from Sigma-Aldrich and used as received. 1H, 1H, 2H, 2H-perfluorodecanethiol was purchased from Oakwood Products, Inc. and used as received.

Escherichia coli (strain JM109) was purchased from New England Bio Labs. Tryptone and yeast extract were purchased from Difco. Sodium chloride, sodium dodecyl sulfate (99%), ammonium sulfate, potassium hydrogen phosphate, potassium dihydrogen phosphate, and sodium citrate dihydrate were purchased from Fisher Scientific and used as received. Media used in the preparation of bacteria had the following compositions:

2XYT: 16 g tryptone, 10 g yeast extract, 5 g NaCl in 1 L of deionized H₂O

LB: 10 g tryptone, 5 g yeast extract, 10 g NaCl in 1 L of deionized H₂O
Spizizen Mineral Salts: 2 g NH₄SO₄, 14 g K₂HPO₄, 6 g KH₂PO₄, 1 g Na₃CH₃CH₂COO · 2H₂O in 1L of deionized water.

3.4.1.2 Preparation of Self-Assembled Monolayers

Gold substrates were purchased from EMF Corporation (Ithaca, NY). The substrates were prepared by evaporation of a 5 nm titanium or chromium adhesion layer onto a silica substrate, 1" x 1" x 0.62" or 1 cm x 1 cm x 1 mm, followed by coating with 100 nm of gold. The substrates were cleaned in "piranha solution", a 7:3 mixture of H₂SO₄ (concentrated) / H₂O₂ (30%) ("*piranha solution*" is an oxidizing mixture that can be explosive) for one hour at room temperature. The substrates were removed from piranha, rinsed with copious amounts of deionized water (Millipore Purification Systems, 18.2 MΩ), dried with ultra-high pure nitrogen, and placed in a 1 mM ethanolic solution of the desired thiol for 18-24 hours. Prior to analysis, the gold slides were removed from the thiol solution, rinsed with absolute ethanol and deionized water, and finally dried in a stream of ultra-pure nitrogen.

3.4.1.3 Preparation of Bacteria

One of the most important procedures employed in the antibacterial assay experiments, or any bacteria experiment, is the use of aseptic techniques. All glassware used is autoclaved prior to use to kill any unwanted bacteria. All chemicals that come into contact with the bacteria, including growth media, buffers, and water, are autoclaved prior to use. Chemical and bacteria transfers are done under an open flame which causes an updraft that prevents airborne bacteria from entering open containers.

All of the bacteria used in the viability studies are *Escherichia coli* (Strain JM109). Until needed, the bacteria are stored frozen at -80° C. The bacteria are revived by incubating at 37° C overnight on a plate of LB growth agar. For each assay, bacteria from the LB agar plate are transferred by a wire ring to 5 mL of 2XYT growth media. The bacteria are then incubated at 37° C and mechanically stirred at 300 RPM for at least 3 hours. After incubation, the concentration of the bacteria is measured by optical density at 600 nm on a Spectronic Genesis 5 UV-Vis spectrometer. The culture is then adjusted so that the optical density is 0.1, where it is assumed that an optical density of 0.1 at 600 nm is equal to a concentration of 1 x 10⁸ cells/mL.¹⁵² The bacteria is then

further diluted to 1×10^5 cells/mL by taking 10.0 μ L of the bacteria and adding it to 10.0 mL of SMS buffer (Spizizen Mineral Salts containing 2g $(\text{NH}_4)_2\text{SO}_4$, 14g K_2HPO_4 , 6g KH_2PO_4 , 1g $\text{Na}_3\text{CH}_2\text{CH}_2\text{COOH} \cdot 2\text{H}_2\text{O}$ in 1L H_2O).

The bacteria are sprayed onto the surfaces using a 50 mL chromatography sprayer from VWR. The sprayer is hooked up to an airline that is filtered through a 0.2 μm filter that prevents any bacteria in the airline from reaching the sprayer. When the air is turned on, the aerosol spray is produced when the air exit hole of the sprayer is covered. The flow rate of the spray is controlled by changing the flow rate of the air. Before the bacteria are sprayed, the sprayer is first sterilized by spraying pure ethanol for a minimum of 30 seconds. Sterile deionized water is sprayed next to remove the ethanol, followed by the bacteria solution. Before spraying onto the surfaces, the bacteria solution is sprayed into a waste container for 10 to 15 seconds to ensure only the bacteria solution is exiting the sprayer and not any water left over from the rinsing step.

The antibacterial assays are performed in a standard fume hood. The surfaces are first removed from their thiol solution, rinsed with pure ethanol, dried with air, and placed into sterile Petri dishes that are then covered until ready for spraying. The arrangement of the surfaces in the dishes was varied for different experiments.

3.5 Antibacterial Assay Method Development

The lack of a literature precedent in using the modified viable count method resulted in trial and error to develop and understand the experimental factors that affect the results. The following experimental details and results discuss the progress in developing this method.

3.5.1 Initial Assays

The initial assays investigated self assembled monolayers of 16-mercaptohexadecanoic acid and 1-hexadecanethiol, which are examples of hydrophilic and hydrophobic surfaces, respectively. For the rest of the manuscript, the SAMs used will be abbreviated in the following way: ##-C XXXX-T, where ##-C refers to the number of carbons in the alkyl chain and XXXX-T refers to the functional group at the terminal end of the molecule. With this labeling, 16-mercaptohexadecanoic acid would be 16-C COOH-T and 1-hexadecanethiol would be 16-C CH_3 -T. In the first assays, a one

square inch surface sample was placed into a 2.75 cm radius Petri dish. The bacteria were sprayed on the surface by passing the sprayer over the surface twice so that a complete coverage was visually evident. 10 mL of melted LB agar (5 g tryptone, 2.5 g yeast extract, 5 g NaCl, 3.75 g agar in 500 mL H₂O) was immediately poured into the dish, but not directly on the surfaces. After pouring, the agar completely covered the bottom of the dish, including the surface. The Petri dishes were then re-covered and the agar was allowed to cool and solidify. The dishes were then incubated at 37°C overnight.

Bacteria that remain viable on the surface multiply and form colonies. Each colony is known as a “colony forming unit”, or CFU. The colonies grow until the available nutrients are extinguished. Each colony forms a whitish, circular spot on the surface that can be seen with the naked eye. After incubating, the bacteria colonies were counted using the *AlphaImager Imaging System* from Alpha Innotech. The system is equipped with the *AlphaEase* image analysis software. This program contains a colony counting feature that counts the visible colonies based on the contrast between the colonies and the surface. The Petri dish is placed into a light box and an image of the surface is taken by a digital camera, followed by manual software processing.

The results of the first assay are shown in Table 1 along with the images taken using the AlphaImager software, shown in Figure 17. The experiment was repeated three times for a total of four trials. Each experiment tested three acid terminated and two methyl terminated SAMs. Because of the variations in experimental conditions from day to day, such as temperature, humidity, flow rate of the bacteria spray, amount of spray that covers the surface, and exact starting concentration of the bacteria solution, the counts from assay experiments performed on different days cannot not be directly compared. To be able to compare the values, the percent difference between the acid terminated surface count and the average of the methyl terminated counts are reported. A positive percent difference indicates more colonies on the COOH-T SAM, whereas a negative percent difference indicates fewer colonies on the COOH-T SAM.

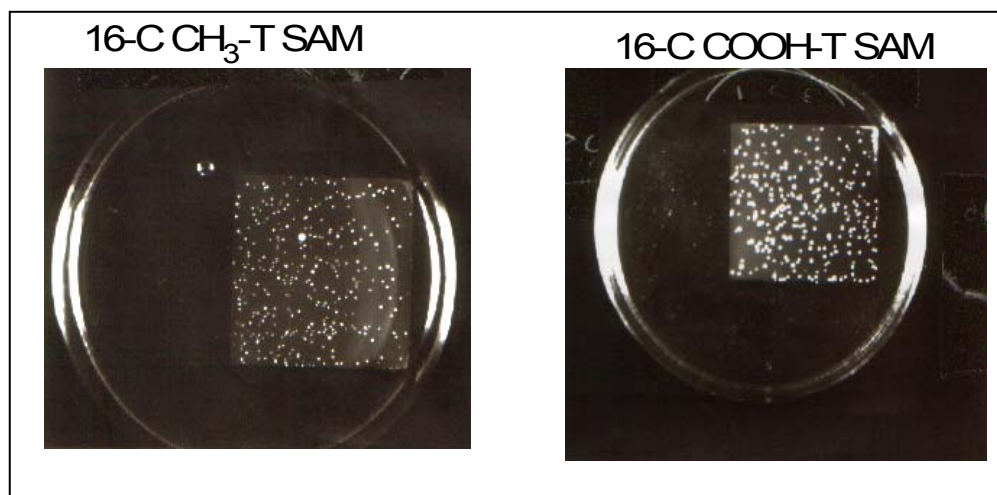


Figure 17: Initial antibacterial assay images. Each bright spot is a colony-forming-unit (CFU). One CFU is representative of a viable bacterium.

Assay #: 1			Assay #: 2		
Surface	Count	% Diff	Surface	Count	% Diff
COOH-T #1	306	67%	COOH-T #1	31	-79%
COOH-T #2	236	29%	COOH-T #2	78	-48%
COOH-T #3	220	20%	COOH-T #3	98	-34%
CH ₃ -T #1	183		CH ₃ -T #1	132	
CH ₃ -T #2	x		CH ₃ -T #2	167	
Avg CH ₃	183		Avg CH ₃	150	
Avg COOH	254	39%	Avg COOH	69	-54%
St. Dev COOH	46	25%	St. Dev COOH	34	23%

Assay #: 3			Assay #: 4		
Surface	Count	% Diff	Surface	Count	% Diff
COOH-T #1	417	116%	COOH-T #1	344	-34%
COOH-T #2	376	95%	COOH-T #2	498	-4%
COOH-T #3	346	79%	COOH-T #3	387	-26%
CH ₃ -T #1	152		CH ₃ -T #1	520	
CH ₃ -T #2	234		CH ₃ -T #2	x	
Avg CH ₃	193		Avg CH ₃	520	
Avg COOH	380	97%	Avg COOH	410	-21%
St. Dev COOH	36	18%	St. Dev COOH	79	15%

Table 1: Viable colony counts from the initial antibacterial assays. The %Diff values are the percent difference between the average counts of the COOH-T SAMs and the average count of the CH₃-T SAMs.

The data exhibits a very large variation from experiment to experiment. The average of all of the percent differences is 15% with a pooled standard deviation of 21%. The resulting relative standard deviation (RSD) is 1400 parts per thousand! The large RSD is a clear indication that the initial assays had a random errors too large to provide reproducible results. To try to eliminate some of the factors that could be causing the errors, a new set of assays were performed using one square centimeter surfaces that were

all placed in the same Petri dish. The placement of the surfaces in the same Petri dish would help eliminate differences in the amount of bacteria sprayed and spray rates encountered when using separate dishes for each surface. The surfaces were setup in the dish as displayed in Figure 18.

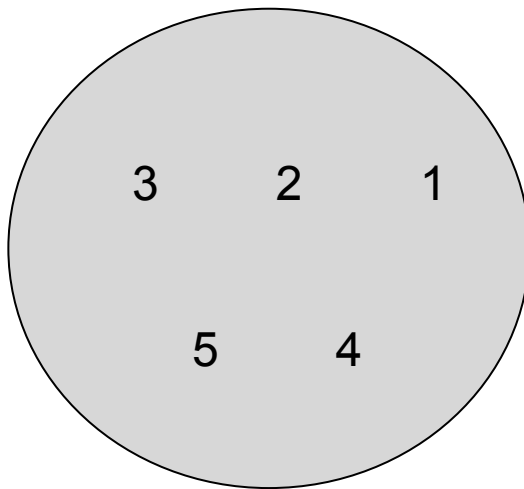


Figure 18: Layout of SAMs in a Petri dish using one square centimeter sized gold slides. Positions 1, 2, and 3 were 16-C COOH-T SAMs and positions 4 and 5 were 16-C CH₃-T SAMs. The surfaces in the same dish were all sprayed before the agar was added. Table 2 shows the results of the second set of assays

Assay #:	1	
Surface	Count	% Diff
COOH-T #1	46	-56%
COOH-T #2	53	-50%
COOH-T #3	41	-61%
CH ₃ -T #1	105	
CH ₃ -T #2	x	
Avg CH ₃ -T	105	
Assay #:	2	
Surface	Count	% Diff
COOH-T #1	56	-57%
COOH-T #2	49	-62%
COOH-T #3	45	-65%
CH ₃ -T #1	122	
CH ₃ -T #2	138	
Avg CH ₃ -T	130	

Table 2: Assay results for COOH-T and CH₃-T SAMs which were placed in the same Petri dish.

The second set of assays had less variation than the first. The mean percent difference of the second set of assays was -59% with a pooled standard deviation of 5%. The relative standard deviation is 86 ppt, which is 1528% less than the RSD of the first tests. By placing the surfaces in the same Petri dish, it appears some of the variation has been reduced.

The next set of assay experiments investigated two new surfaces in addition to the 16-C CH₃-T and 16-C COOH-T SAMs; 16-mercaptohexadecanol (16-C OH-T) and 1H, 1H, 2H, 2H-perfluorodecanethiol (10-C CF₃-T). The two new SAMs introduce two new variables. The perfluorinated SAMs have a tilt angle (α) closer to the surface normal than alkylated SAMs because of the increased volume of the fluorinated groups.¹⁵³ The different tilt angle of the perfluorinated SAM might demonstrate if surface molecular orientation has an effect on bacteria viability. The hydroxyl terminated SAM is an example of a known solution antimicrobial agent, ethanol, being covalently tethered to a surface. The antibacterial assay will determine if covalently tethering a hydroxy group to a surface alters the antibacterial activity.

The surfaces were arranged in the same manner as shown in Figure 18 with positions 1, 2, and 3 all being either the COOH, OH, or CF₃-T surfaces and positions 4 and 5 being the CH₃-T surfaces. Percent differences were again taken in reference to the average CH₃-T counts from each dish. Table 3 shows the data for the third set of antibacterial assays.

Assay #: 1								
Dish 1	Count	% Diff	Dish 2	Count	% Diff	Dish 3	Count	% Diff
COOH-T #1	53	-40%	OH-T #1	57	-44%	CF3-T #1	38	-8%
COOH-T #2	89	0%	OH-T #2	64	-38%	CF3-T #2	59	42%
COOH-T #3	123	38%	OH-T #3	76	-26%	CF3-T #3	65	57%
Avg COOH-T	88	-1%	Avg OH-T	66	-36%	Avg CF3-T	54	30%
St.Dev. COOH-T	35	39%	St.Dev. OH-T	10	9%	St.Dev. CF3-T	14	34%
CH3-T #1	88		CH3-T #3	118		CH3-T #5	58	
CH3-T #2	90		CH3-T #4	87		CH3-T #6	25	
Avg CH3-T	89		Avg CH3-T	103		Avg CH3-T	42	
Assay #: 2								
Dish 1	Count	% Diff	Dish 2	Count	% Diff	Dish 3	Count	% Diff
COOH-T #1	60	4%	OH-T #1	54	-22%	CF3-T #1	54	77%
COOH-T #2	60	4%	OH-T #2	70	1%	CF3-T #2	40	31%
COOH-T #3	47	-18%	OH-T #3	46	-33%	CF3-T #3	17	-44%
Avg COOH-T	56	-3%	Avg OH-T	57	-18%	Avg CF3-T	37	21%
St.Dev. COOH	8	13%	St.Dev. OH-T	12	18%	St.Dev. CF3-T	19	61%
CH3-T #1	59		CH3-T #3	57		CH3-T #5	33	
CH3-T #2	56		CH3-T #4	81		CH3-T #6	28	
Avg CH3-T	58		Avg CH3-T	69		Avg CH3-T	31	

Table 3: Assay data testing COOH-T, OH-T, and CF₃-T SAMs. The surface were arranged in the dishes as shown in Figure 18.

The data from third set of antibacterial assays again begin to show a very large variance from which no significant conclusions can be made. Calculating the pooled standard deviation and relative standard deviation, shown in Table 4, for the three surfaces reveals significant random error.

	COOH-T	OH-T	CF3-T
Pool. SD	29%	14%	50%
RSD	-14500	-519	1923

Table 4: Variation statistics for data from Table 3.

The large variability in the results is likely due in part to the use the methyl terminated SAMs as the reference. It is not certain that each surface forms monolayers of equal quality. Some monolayers may have more defects that could affect the number of viable bacteria. To eliminate this possible source of error, the next assays performed used clean gold slides as the reference surface. The gold reference slides were cleaned in piranha

solution and stored in deionized water prior to the assay. Three SAMs were placed in a Petri dish with one clean gold slide. Each surface was sprayed with bacteria, the dish was covered, and after 45 seconds the melted agar was added. Each assay tested the 16-C CH_3 , COOH , OH , and 10-C CF_3 terminated SAMs. The experiment was repeated seven times for a total of eight trials. For each SAM, the percent difference between the colony count for the SAM and the colony count for the clean gold reference surface was determined. The average percent difference and pooled standard deviation were determined using all of the percent differences for each of the four SAMs investigated. Table 5 reports the statistical data.

End Grp	Mean % Diff	Pooled St.DEV
CH_3	18%	25%
COOH	0%	24%
OH	40%	25%
CF_3	-4%	15%

Table 5: Mean percent difference of average SAM colony counts from clean gold colony counts. Pooled standard deviations are from data of 8 experiments.

The data in Table 5 is displayed graphically in Figure 19. The overlapping error bars of the data indicate that the experimental error is too great to detect differences in bacteria viability for the four SAMs investigated. A more powerful way to determine the existence of statistical differences is the analysis of variance test, or ANOVA.

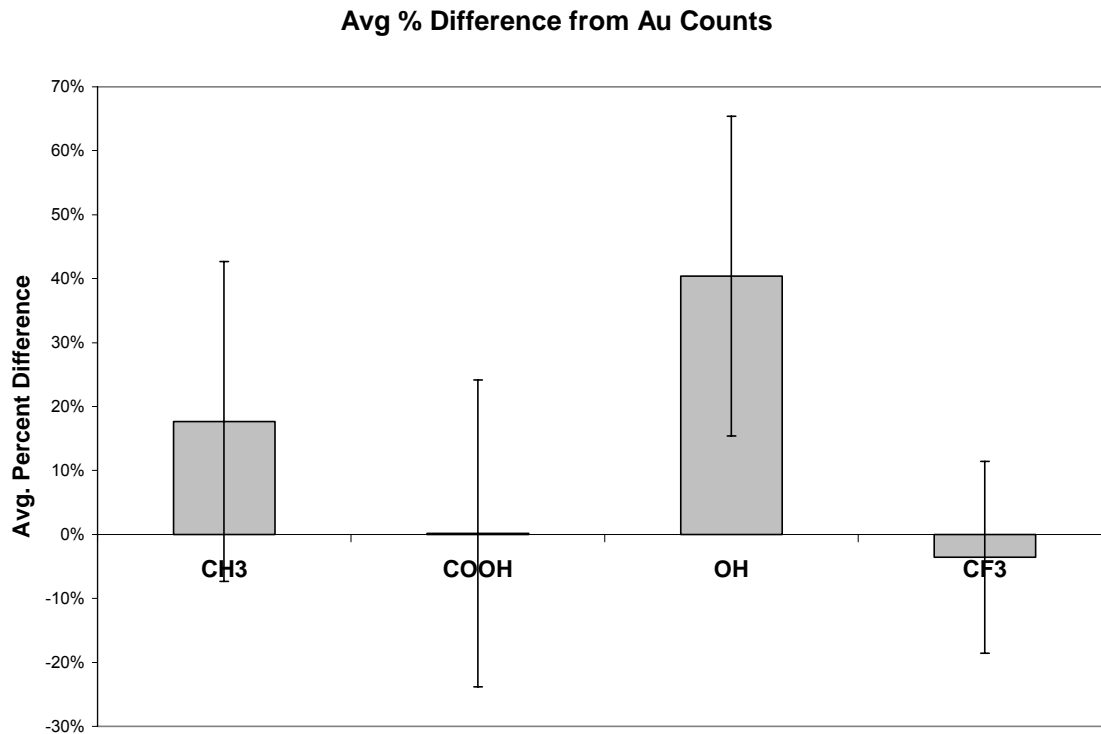


Figure 19: Graphical representation of the data in Table 5. The error bars represent the standard deviation for eight replicate analyses. The large, overlapping error bars indicate that the experiment was not able to quantify the effect of surface composition on bacteria viability.

3.6 Analysis of Variance Tests (ANOVA)

A more powerful tool for testing variances among samples that undergo different treatments is the Analysis of Variance, or ANOVA. ANOVA can separate and identify variances caused by random error and controlled or fixed-effect error.¹⁵⁴ ANOVA can also be used to separate more than one source of random variation, known as a random-effect or uncontrolled factor. When there is one factor, either random or controlled, in addition to the random error, the ANOVA test is called a one-way ANOVA. When there are two random or controlled factors in addition to the random error, the ANOVA test is called a two-way ANOVA.

The mathematics of the one-way ANOVA are based on data arranged as shown in Figure 20.

	1	2	...	k	
	-	-		-	
	-	-		-	
	-	-		-	
	-	-		-	Overall Totals
Sample Sizes	n_1	n_2	...	n_k	n
Sample Totals	T_1	T_2	...	T_k	T
Sample Means	\bar{x}_1	\bar{x}_2	...	\bar{x}_k	\bar{x}
Population Means	μ_1	μ_2	...	μ_k	

Figure 20: One-way ANOVA table

The hypothesis is tested in ANOVA by using the F-test to test for variances between standard deviations. The null hypothesis is generally that all of the sample means are equal, meaning that there is no deviation. The variances compared by the F-test are derived as follows. A variance is defined as the square of the standard deviation. With an ANOVA test, there are three sums of squares that need to be defined. The first one is called the **total sum of squares** (SSTO) and is the sum of the squared deviations of the observations from the overall mean.

$$SSTO = \sum \sum (x_i - \bar{x})^2 \quad (8)$$

The second sum of squares is the **treatment sum of squares** (SSTR). This is defined as the sum of the squared deviations between the sample means and the overall mean.

$$SSTR = n_1(\bar{x}_1 - \bar{x})^2 + n_2(\bar{x}_2 - \bar{x})^2 + \dots + n_k(\bar{x}_k - \bar{x})^2 \quad (9)$$

The final sum of squares is the **error sum of squares** (SSE). This is defined as the sum of the squared deviations from each observation from its own sample mean.

$$SSE = \sum \sum (x_i - \bar{x}_i)^2 \quad (10)$$

It can be shown that the total sum of squares is equal to the sum of the treatment and error sum of squares: $SSTO = SSTR + SSE$.

The F-test performed by ANOVA is calculated with the ratio of the **treatment mean square** (MSTR) with the **error mean square** (MSE). The treatment mean square is equal to the treatment sum of squares divided by the number of treatments (number of columns)

minus 1. The error mean square is the error sum of squares divided by the number of observations minus the number of treatments (columns).

$$\frac{MSTR}{MSE} = \frac{SSTR / (k - 1)}{SSE / (n - k)} \quad (11)$$

The division of the SSTR by k-1 and SSE by n-k gives a ratio that has an F distribution if the null hypothesis is true. This ratio is then compared to the standard accepted value found for the specific degrees of freedom at the confidence level of interest. If the calculated value exceeds the critical value, then the null hypothesis is rejected, meaning that there is a significant difference between the sample means that cannot be explained by random error.

The one-way analysis of variance was performed on the data from the 16-C CH₃, COOH, OH, and 10-C CF₃-T samples to see if there was significant variation in percent difference values from day to day, or the between-run reproducibility. The null hypothesis for this experiment states that there is no significant variation in the percent difference values between-runs (days). The F-test was performed at the 95% confidence level (F=0.05). Tables 6-9 give the ANOVA results calculated using Microsoft Excel.

Anova: Single Factor

16-C CH₃-T

SUMMARY

<i>Groups</i>	<i>Count</i>	<i>Sum</i>	<i>Average</i>	<i>Variance</i>
Assay1	3	1.07	0.357	0.201
Assay2	3	-0.41	-0.137	0.029
Assay3	3	0.07	0.023	0.135
Assay4	3	1.38	0.460	0.030
Assay5	3	0.46	0.153	0.006
Assay6	3	0.43	0.143	0.023
Assay7	3	1.27	0.423	0.039
Assay8	2	-0.22	-0.110	0.010

ANOVA

<i>Source of Variation</i>	<i>SS</i>	<i>df</i>	<i>MS</i>	<i>F</i>	<i>P-value</i>	<i>F crit</i>
SSTR	1.05	7	0.151	2.418	0.072	2.707
SSE	0.94	15	0.062			
SSTO	1.99	22				

Table 6: 16-C CH₃-T ANOVA results

Anova: Single Factor

16-C COOH-T

SUMMARY

<i>Groups</i>	<i>Count</i>	<i>Sum</i>	<i>Average</i>	<i>Variance</i>
Assay2	3	-0.140	-0.047	0.036
Assay3	3	-0.510	-0.170	0.020
Assay4	3	-0.270	-0.090	0.062
Assay5	2	1.000	0.500	0.045
Assay6	3	0.970	0.323	0.349
Assay7	3	-0.830	-0.277	0.014
Assay8	3	-0.020	-0.007	0.063

ANOVA

<i>Source of Variation</i>	<i>SS</i>	<i>df</i>	<i>MS</i>	<i>F</i>	<i>P-value</i>	<i>F crit</i>
SSTR	1.16	6	0.193	2.218	0.108	2.915
SSE	1.13	13	0.087			
SSTO	2.29	19				

Table 7: 16-C COOH-T ANOVA results

Anova: Single Factor

16-C OH-T

SUMMARY

<i>Groups</i>	<i>Count</i>	<i>Sum</i>	<i>Average</i>	<i>Variance</i>
Assay2	3	0.490	0.163	0.039
Assay3	3	1.280	0.427	0.099
Assay4	3	0.960	0.320	0.067
Assay5	3	0.920	0.307	0.091
Assay6	3	0.690	0.230	0.030
Assay7	3	2.490	0.830	0.011

ANOVA

<i>Source of Variation</i>	<i>SS</i>	<i>df</i>	<i>MS</i>	<i>F</i>	<i>P-value</i>	<i>F crit</i>
SSTR	0.85	5	0.170	3.013	0.055	3.106
SSE	0.68	12	0.056			
SSTO	1.53	17				

Table 8: 16-C OH-T ANOVA results

Anova: Single Factor

SUMMARY

<i>Groups</i>	<i>Count</i>	<i>Sum</i>	<i>Average</i>	<i>Variance</i>
Assay1	3	-0.720	-0.240	0.011
Assay2	3	-0.340	-0.113	0.001
Assay3	3	-0.420	-0.140	0.024
Assay4	3	-0.300	-0.100	0.033
Assay5	3	0.640	0.213	0.039
Assay6	3	0.140	0.047	0.035
Assay7	3	0.240	0.080	0.013

ANOVA

<i>Source of Variation</i>	<i>SS</i>	<i>df</i>	<i>MS</i>	<i>F</i>	<i>P-value</i>	<i>F crit</i>
SSTR	0.435	6	0.072	3.267	0.032	2.848
SSE	0.311	14	0.022			
SSTO	0.745	20				

Table 9: 10-C CF₃-T ANOVA results

For every SAM tested except for the CF₃-T, the calculated F value was less than the critical F value, as shown in Table 10. The F-test values imply that the mean percent difference values for the methyl, carboxylic acid, and hydroxyl terminated SAMs, determined by experiments on different days, are not statistically different at the 95% confidence level. To determine if the average percent difference values of the different SAMs are statistically different, a two-way ANOVA test was performed.

SAM	F-calc	F-crit
CH ₃ -T	2.42	2.71
OH-T	3.01	3.11
COOH-T	2.22	2.92
CF ₃ -T	3.27	2.85

Table 10: Summary of F-test values for one-way ANOVA. Only the CF₃-T SAM had F-calc greater than F-crit.

The two-way ANOVA setup is very similar to the one-way setup, shown in Figure 21.

	Treatments				Block Totals
	1	2	...	k	
Blocks	-	-	-	-	B ₁
	-	-	-	-	B ₂
	-	-	-	-	⋮
	-	-	-	-	⋮
	-	-	-	-	B _b
Sample Sizes	b	b	b	b	n
Sample Totals	T ₁	T ₂	...	T _k	T
Sample Means	\bar{x}_1	\bar{x}_2	...	\bar{x}_k	\bar{x}
Population Means	μ ₁	μ ₂	...	μ _k	

Figure 21: Two-way ANOVA setup

In this setup, the rows are designated as the blocks and the columns as the treatments. The F-test proceeds similarly to the F-test for the one-way ANOVA, but with one new term called the *block sum of squares* (SSB), which is defined as the sum of the squared deviations of the block means from the overall mean. For k treatments in block i , $i=1,2,\dots,b$,

$$SSB = \sum \sum (\bar{x}_i - \bar{x})^2 = \sum k(\bar{x}_i - \bar{x})^2 \quad (12)$$

For the two-way ANOVA, the error sum of squares is now equal to the total sum of squares minus the treatment sum of squares minus the block sum of squares.

$$SSE = SSTO - SSTR - SSB \quad (13)$$

The two-way ANOVA then performs the F-test on both the between treatment (column) interaction and the between block (row) interactions. For the experiments discussed here, the treatments were the four different types of SAMs and the blocks were the different test days. The between treatment F-test is performed by calculating F using the following equation:

$$F = \frac{SSTR / (k - 1)}{SSE / (k - 1)(b - 1)} = \frac{MSTR}{MSE} \quad (14)$$

where k is the number of treatments, b is the number of blocks, MSTR is the treatment mean square and MSE is the error mean square. If the calculated F value is greater than the critical F value for the desired confidence and degrees of freedom, then there is a

statistical difference between the means of the treatments. The between block F-test is performed similarly:

$$F = \frac{SSB / (b - 1)}{SSE / (k - 1)(b - 1)} = \frac{MSB}{MSE} \quad (15)$$

where MSB is the block mean square. Again, if the F value is greater than the critical F value, then there is a statistical difference between the means of the blocks.

For the experiments performed here, the blocks were the different days the experiments were performed and the treatments were the different surfaces used in the assays. The two-way ANOVA will verify if there is a statistical distance among the results obtained on different days and if there is a statistical difference among the results obtained for the different surfaces used. Table 11 shows the data used in the ANOVA calculation. Not all the results from each of the eight test days were used because some of the trials on the days not listed had poor results stemming from gross errors, such improper spraying technique or the gold slides becoming detached from the bottom of the Petri dish, which resulted in the slides floating in the agar. The experimental data used had a result for each of the three trials for all four SAMs. Table 12 shows the two-way ANOVA calculations.

Day	CH3	COOH	OH	CF3
Day 2	-15%	-9%	23%	-9%
	4%	16%	32%	-11%
	-30%	-21%	-6%	-14%
Day 3	22%	-17%	43%	-4%
	25%	-3%	74%	-6%
	-40%	-31%	11%	-32%
Day 4	56%	-29%	3%	5%
	56%	19%	40%	-5%
	26%	-17%	53%	-30%
Day 6	17%	90%	51%	13%
	28%	-28%	45%	44%
	-2%	35%	-4%	7%
Day 7	38%	-41%	43%	26%
	64%	-24%	12%	-4%
	25%	-18%	14%	-8%

Table 11: Two-way ANOVA data

ANOVA						
<i>Source of Variation</i>	<i>SS</i>	<i>df</i>	<i>MS</i>	<i>F</i>	<i>P-value</i>	<i>F crit</i>
Blocks	0.550	4	0.137	2.299	0.076	2.606
Treatments	1.198	3	0.399	6.682	0.001	2.839
Interaction	1.245	12	0.104	1.737	0.095	2.003
Residual	2.390	40	0.060			
Total	5.384	59				

Table 12: Two-way ANOVA calculations

The interaction row is random error between replicate samples for a specific SAM on one test day. The calculated F value is less than the critical F value indicating that there is no significant interaction error among the daily replicate samples ($1.737 < 2.003$). The between blocks, or between days variation has a calculated F value less than the critical F ($2.299 < 2.606$). This agrees with the one-way ANOVA results discussed prior, indicating that there is no significant variation between the different test days. The between treatments, or between different SAMs variation has a larger critical F than calculated F ($6.682 > 2.839$). The larger F-critical value indicates that there is a demonstrated significant difference between the data of the different SAMs. Based on the significantly different results, it could be possible to conclude that the structure of the SAMs assayed has an effect on the viability of the bacteria.

3.7 Discussion

This result obtained from the one-way and the two-way between block ANOVA tests contradict the variance reported by the pooled standard deviation in Table 5. One of the key assumptions of the ANOVA test is that the population standard deviation has a Gaussian distribution. However, without a sufficient number of replicate samples one cannot be totally certain that the population standard deviation obeys the Gaussian distribution assumption because not enough measurements were taken.

Confidence limits can provide a reliable indication of the variation among replicate data. Large confidence limits indicate more replicate measurements are needed to obtain the true value of the data. Confidence limits for a population mean are calculated using Equation 16:

$$CL = \bar{x} \pm \frac{z\sigma}{\sqrt{N}} \quad (16)$$

where σ is the sample standard deviation, \bar{x} is the sample mean, N is the number of replicate measurements, and z is a statistical parameter that changes based on the confidence level percentage. Table 13 lists the confidence limits for the four SAMs tested at the 95% confidence limits with $z=1.96$. The data can be interpreted by stating that 95 times out of 100 the real percent difference will fall within the range indicated by the confidence limits.

End Grp	Mean % Diff	Pooled St.DEV	95% Conf Lim.	For a 1% CL
CH3	18%	25%	10.22%	2401
COOH	0%	24%	9.81%	2213
OH	40%	25%	11.24%	2401
CF3	-4%	15%	6.42%	864

Table 13: 95% confidence limits for four SAMs tested via the antibacterial assay. The large limits signify that there was large random error in the analyses.

The confidence limits are rather large and indicate that the true percent differences could be anywhere over a large range. To lower the confidence limits, more replicate measurements are needed. The last column of Table 13 gives the number of replicate measurements one would need to achieve a one percent confidence limit for each of the four surfaces studied. The numbers indicate that many more replicate measurements are needed to obtain the “true” values.

The large variation in the percent difference data from the antibacterial assay are caused by a combination of multiple sources of error. Environmental variation, including temperature and humidity, were not controlled for each experiment. Bacteria are affected by changes in environmental conditions; however, the differences in the environmental variables might not be large enough to significantly contribute the variation in the data. The most significant contribution to the variation of data is likely from the considerable number of experimental variables. The most important variable is the actual number of bacteria initially sprayed onto the surface. Although the concentration of bacteria in solution is controlled, the amount sprayed onto the surface is dependent on a number of factors. The air flow rate through the sprayer was not measured and might have been different for each experiment. The rate at which the sprayer was passed over the surface varied, as did the angle of the spray relative to the surface. Control over the experimental variables was very difficult and most likely led to the large data variation observed.

In addition to the observed data variation, all of the SAMs possessed little to no antibacterial activity. The lack of antibacterial activity can be explained by the fact that none of the four SAMs tested possessed any known antibacterial functionality. Surface-bound antibacterial molecules normally contain cationic groups that disrupt the outer cell membranes of the bacteria which initiate the death of the cell. The four SAMs tested did not contain any cationic groups. Because the SAMs did not contain any antibacterial properties, the viability of the bacteria on the SAMs was probably an adhesion phenomenon.

The antibacterial assay experiments provided little data to gain insight about the viability of bacteria on the limited set of SAMs tested. The conclusion of the initial assays is that *E. coli* is viable on well-ordered methyl, hydroxyl, carboxylic acid, and trifluoro terminated SAM. In the next chapter, the antibacterial assay will be used to show that a carboxylic acid terminated SAM, complexed with a known antibacterial agent, silver ions, is antibacterial.

Chapter 4: Antibacterial Silver Carboxylate Self-Assembled Monolayers

4.1 Introduction

In Chapter 1, two previously studied antibacterial surfaces were discussed along with questions remaining from those studies. The main question remaining from the studies were how the molecular scale surface structure and composition affect the antibacterial activity. Self-assembled monolayers (SAMs) of alkanethiols on gold were introduced in Chapter 2 as a model system to investigate the fundamental questions. In this chapter, experiments where simple carboxylic acid terminated monolayers are complexed with silver(I) ions are discussed. The resulting silver carboxylate terminated SAM demonstrated biocidal activity as shown by the antibacterial assay. Although using silver ions to create a biocidal surface is not a novel idea, this study represents the first demonstration of an antibacterial alkanethiol monolayer on gold. The experiments also demonstrated that the well-ordered structure of the SAM is not perturbed even after colony growth and subsequent washing procedure.

The motivation to complex a carboxylic acid terminated SAM with silver stems from the well known antibacterial effects of silver ions. Many commercial antibacterial plastics are based upon slow release of silver ions from a polymer matrix.¹⁵⁵ In fact, the use of silver as an antibacterial agent goes back much further than modern times. Perhaps as far back as 1000 B.C., water kept in silver or copper vessels could be rendered drinkable if exposed to light.¹⁵⁶ In 1869, Revelin was the first to report the low concentrations at which silver could exert its antimicrobial effect.¹⁵⁷ von Naegeli followed up Revelin's study in 1893 and found that silver ions at a concentration of 9.2×10^{-9} M killed the common freshwater *Spirogyra*.¹⁵⁸ He subsequently coined the term 'oligodynamic' which means 'active with few'.¹⁵⁹ Credé, in 1881, published a manuscript that advocated the use of silver in the prevention of ophthalmia neonatorum in newborns, a practice still in use today.¹⁶⁰ Gibbard investigated factors that effected the antibacterial activity of silver.¹⁶¹ He found that if silver is mechanically cleaned with rough cloth or paper, the silver becomes inactive. Cooling molten silver in an atmosphere of hydrogen gives no activity, whereas cooling in air does. The conclusion

reached by the experiments of Gibbard is that pure silver (Ag^0) is inactive and the active form was the silver ion (Ag^+). Gibbard also noted that colloidal silver, silver oxide, and silver nitrate were always active.¹⁶¹

The goals of the silver carboxylate self-assembled monolayer experiments described below were to explore whether a carboxylate SAM on gold that presents a single monolayer of silver ions to the environment is antibacterial, and how the well-ordered structure of the SAM is affected by the bacteria. To obtain the necessary data, the surfaces were characterized, tested for antibacterial activity, and then re-characterized.

4.2 Experimental Details

The experimental procedure is split up into three main parts; surface formation, surface characterization, and assessment of surface antibacterial activity. During surface formation, the alkanethiol self-assembled monolayers are created and modified. Surface characterization provides information about the structure of the surface, which includes ordering of the surface molecules and the presence and concentration of specific chemical species. The characterization information is primarily provided by reflection-absorption infrared spectroscopy (RAIRS) and X-ray photoelectron spectroscopy (XPS). The specifics of RAIRS and XPS techniques were discussed in Chapter 3. The assessment of surface antibacterial activity is determined by the antibacterial assay. The specifics of the assay were also discussed in Chapter 3.

4.2.1 Materials

Absolute ethanol was obtained from Aaeper Alcohol and Chemical Co. 16-mercaptohexadecanoic acid (90%), 1-hexadecanethiol (92%), and silver nitrate (>99%) were purchased from Sigma-Aldrich and used as received.

Escherichia coli (strain JM109) was purchased from New England Bio Labs. Tryptone and yeast extract were purchased from Difco. Sodium chloride, sodium dodecyl sulfate (99%), ammonium sulfate, potassium hydrogen phosphate, potassium dihydrogen phosphate, and sodium citrate dihydrate were purchased from Fisher Scientific and used as received. Media used in the preparation of bacteria had the following compositions:

2XYT: 16 g tryptone, 10 g yeast extract, 5 g NaCl in 1 L of deionized H_2O

LB: 10 g tryptone, 5 g yeast extract, 10 g NaCl in 1 L of deionized H_2O

SMS: 2 g NH_4SO_4 , 14 g K_2HPO_4 , 6 g KH_2PO_4 , 1 g $\text{Na}_3\text{CH}_3\text{CH}_2\text{COO} \cdot 2\text{H}_2\text{O}$ in 1L of deionized water.

4.2.2 Preparation of Self-Assembled Monolayers

Gold substrates were purchased from EMF Corporation (Ithaca, NY). The substrates were prepared by evaporation of a 5 nm titanium or chromium adhesion layer onto a silica substrate, 1" x 1" x 0.62" or 1 cm x 1 cm x 1 mm, followed by coating with 100 nm of gold. It should be noted that antibacterial assay experiments performed on bare gold surfaces revealed that the small amounts of titanium or chromium did not affect the viability of the bacteria. The substrates were cleaned in "piranha solution", a 7:3 mixture of H_2SO_4 (concentrated) / H_2O_2 (30%) ("*piranha solution*" is an oxidizing mixture that can be explosive) for one hour at room temperature. The substrates were removed from piranha, rinsed with copious amounts of deionized water (Millipore Purification Systems, 18.2 M Ω), dried with ultra-high pure nitrogen, and placed in a 1 mM ethanolic solution of the thiol for 18-24 hours. Prior to analysis, the SAMs were removed from the thiol solution, rinsed with absolute ethanol and deionized water, and finally dried in a stream of ultra-pure nitrogen.

4.2.3 Preparation of Silver Carboxylate Self-Assembled Monolayers

The COOH-terminated monolayers were rinsed with absolute ethanol and deionized water, dried with ultra-pure nitrogen, and placed into a 1-2 mM ethanolic solution of AgNO_3 for 15-30 minutes. The complexation reactions were performed in the dark due to the sensitivity of silver nitrate to light. The SAMs were then removed from the solution, rinsed with absolute ethanol, dried with ultra-pure nitrogen, and used for further analysis.

4.2.4 Reflection-Absorption Infrared Spectroscopy

RAIR spectra were collected using a Bruker IFS 66v/S spectrometer equipped with a liquid nitrogen mercury-cadmium-telluride (MCT) detector. The infrared radiation is p-polarized and was directed onto the surface at a grazing angle of 86° relative to the surface normal. The background references for all spectra were clean gold

substrates. Each spectrum was collected using a resolution of 2 cm^{-1} and represents the average of 100 scans.

4.2.5 X-ray Photoelectron Spectroscopy

XP spectra were collected on a Perkin Elmer 5400 X-ray Photoelectron Spectrometer. A monochromatized Mg(K α) radiation source (1253.6 eV) and a position sensitive, multi-channel plate detector were used to make the measurements. The vacuum chamber was maintained at a background pressure of $\sim 10^{-7}$ mbar during data collection. To ensure surface sensitivity, the measurements were conducted using a take-off angle of 15° relative to the surface normal. The binding energies of each spectrum are referenced to the Au (4f^{7/2}) peak at 83.9 eV. Survey spectra were recorded with a pass energy of 89.45 eV for ten minutes on a 1 mm x 3.5 mm spot size and 250 W X-ray source power. High resolution multiplex spectra were collected with an acquisition time of 8 minutes per region. Atomic percent composition was determined using instrument specific sensitivity factors.

4.2.6 Antibacterial Assays

The antibacterial assays were performed in a similar manner to those described in Chapter 3. *E. coli* was cultured in 2XYT media to reach a concentration of 10^8 cells/mL. The culture was then diluted to 10^5 cells/mL in SMS (Spizizen's Mineral Salts). The SAMs were removed from the silver nitrate solution, rinsed with absolute ethanol, dried in a stream of air that had been filtered through a 0.2 μm filter, and placed into a 5.5 cm diameter Petri dish. The chromatography sprayer was prepared by spraying absolute ethanol for 30 seconds, followed by deionized water for 30 seconds. The bacteria were then sprayed onto the SAM until a uniform coverage was achieved. The Petri dishes were covered for 45 seconds before 10 mL of melted LB growth agar was poured into the dish. The Petri dishes were re-covered and the agar was allowed to solidify. After the agar had solidified (15-25 minutes), the Petri dishes were inverted and stored in a 37°C incubator overnight. The viability of the bacteria was assessed the following day using a digital camera equipped light box. The camera is controlled by AlphaImager Imaging System software. The images were manually analyzed for bacterial growth. Images that

contained growths were labeled antibacterial inactive and images that did not contain growth were labeled antibacterial active. The number of viable colonies was not counted.

4.2.7 Cleaning of Surfaces After Antibacterial Assay

Analysis of the SAMs after the antibacterial assay required removal of all material accumulated on the surface during the assay. The accumulated material included the nutrient agar, which has a gelatinous consistency, and remaining bacteria material. To clean the surfaces and allow for post-assay analysis, the SAMs were removed from the solidified agar. Large pieces of agar were manually removed with sterile picks. The SAMs were then rinsed with deionized water and placed into a 1% aqueous solution of sodium dodecyl sulfate (SDS) in 0.5 M sodium chloride for 5-10 minutes. The SDS/NaCl mixture is a detergent solution that desorbed the remaining material from the surfaces without affecting the structure of the SAMs. The SAMs were then removed from the SDS/NaCl solution, rinsed with deionized water, and stored in deionized water prior to analysis.

4.3 Results and Discussion

4.3.1 Characterization of Self-Assembled Monolayers Before Antibacterial Assay

The self-assembled monolayers were characterized using reflection-absorption infrared spectroscopy and x-ray photoelectron spectroscopy. RAIR and XP spectra were taken on 16-mercaptohexadecanoic acid (16-C COOH-T) and 1-hexadecanethiol (16-C CH₃-T) SAMs before and after reaction with silver nitrate. The methyl terminated SAM was used as a control to demonstrate that the surface silver ions are primarily bound to the terminal carboxylate group and not to other chemical moieties within the alkanethiol monolayer.

4.3.1.1 Reflection-Absorption Infrared Spectra

Figure 22 shows the RAIR spectra for a 16-C CH₃-T SAM before and after immersion in silver nitrate.

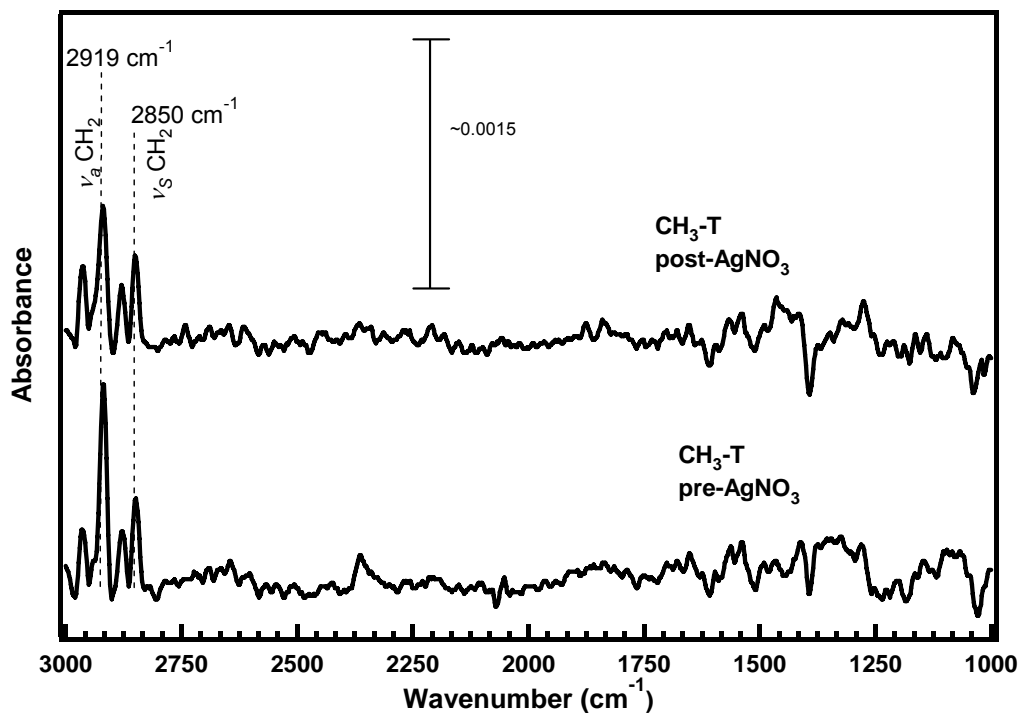


Figure 22: RAIR spectra of a 16-C CH₃-T SAM pre- and post-immersion in silver nitrate.

The important spectral features are the C-H absorption modes occurring near 3000 cm⁻¹. The position, shape, and intensity of the C-H stretching peaks give a wealth of information about the structure of alkanethiol monolayers.¹⁰³ Here, the asymmetric (ν_a) and symmetric (ν_s) methylene stretching vibrations at 2919 and 2850 cm⁻¹, respectively, indicate that the molecular organization of the surface molecules resembles that of a crystalline solid.¹⁰³ The methylene stretching peaks are also narrow, exhibiting small full-width-half-maximum (FWHM) values, which is a spectral feature that also signifies a well-ordered surface.¹⁰³

The position and FWHM values of the spectra after soaking in AgNO₃ do not appear different than those of the original spectra, which indicate that the silver nitrate does not significantly perturb the structure of the monolayer. Further evidence for the lack of significant structural perturbation comes from the persistence of the asymmetric and symmetric stretching vibrations of the terminal methyl groups, which appear at 2964 and 2878 cm⁻¹, respectively. The methyl vibration peaks do not change in position or appearance, indicating that the SAM remains well-ordered.

Figure 23 shows the RAIR spectra for the 16-C COOH-T SAM before and after immersion in silver nitrate.

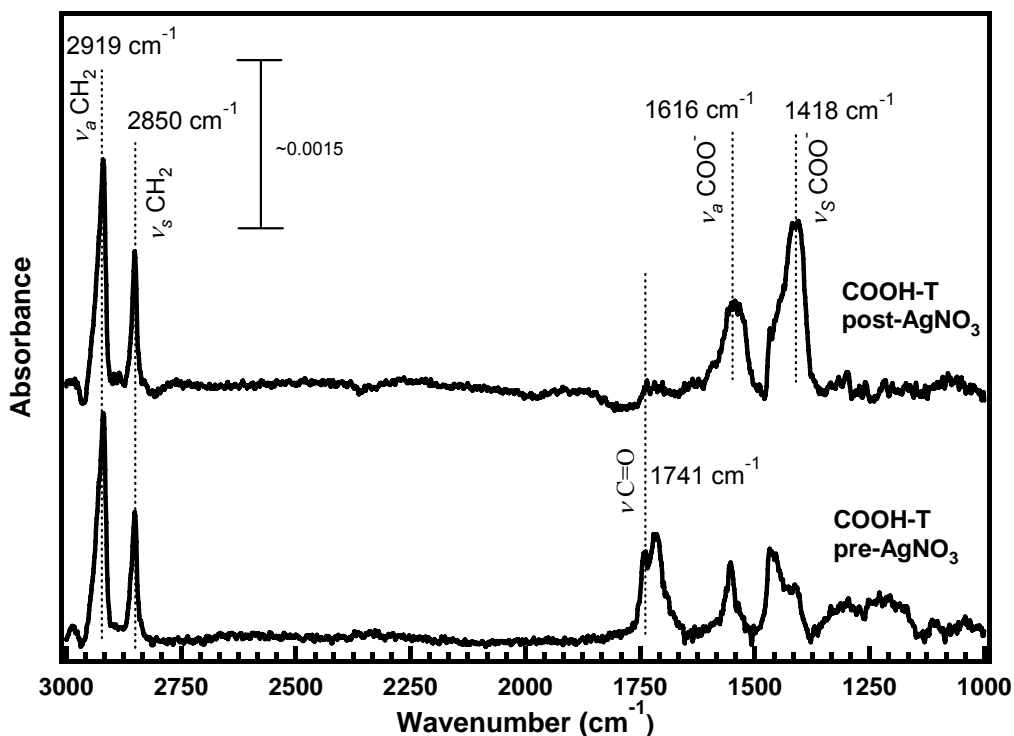


Figure 23: RAIR spectra of a 16-C COOH-T SAM pre- and post-immersion in silver nitrate. The disappearance of the carbonyl stretching mode at 1741 cm^{-1} provides evidence that the carbonyl groups have converted to carboxylate groups.

Both spectra for the pre- and post- AgNO_3 treated SAMs exhibit asymmetric and symmetric methylene stretching vibrations at 2919 and 2850 cm^{-1} , respectively. Again, the position of the methylene peaks, along with small FWHM values indicates that the SAMs remain well-ordered after treatment.

The vibrational modes in the lower frequency region of the RAIR spectra are from the functional groups present within the surface. The particular mode to observe on the spectra in Figure 23 is near 1750 cm^{-1} and is a large doublet peak stemming from the carbonyl stretch of the carboxylic acid functional group. The doublet can be resolved into two peaks; one at 1741 cm^{-1} and the other at 1718 cm^{-1} . The splitting is the result of nearest-neighbor hydrogen bonding of some fraction of carboxylic acid groups,¹⁰³ which lowers the energy of the carbonyl stretch by 23 cm^{-1} . The peak assignments are in agreement with literature precedents.¹⁰³

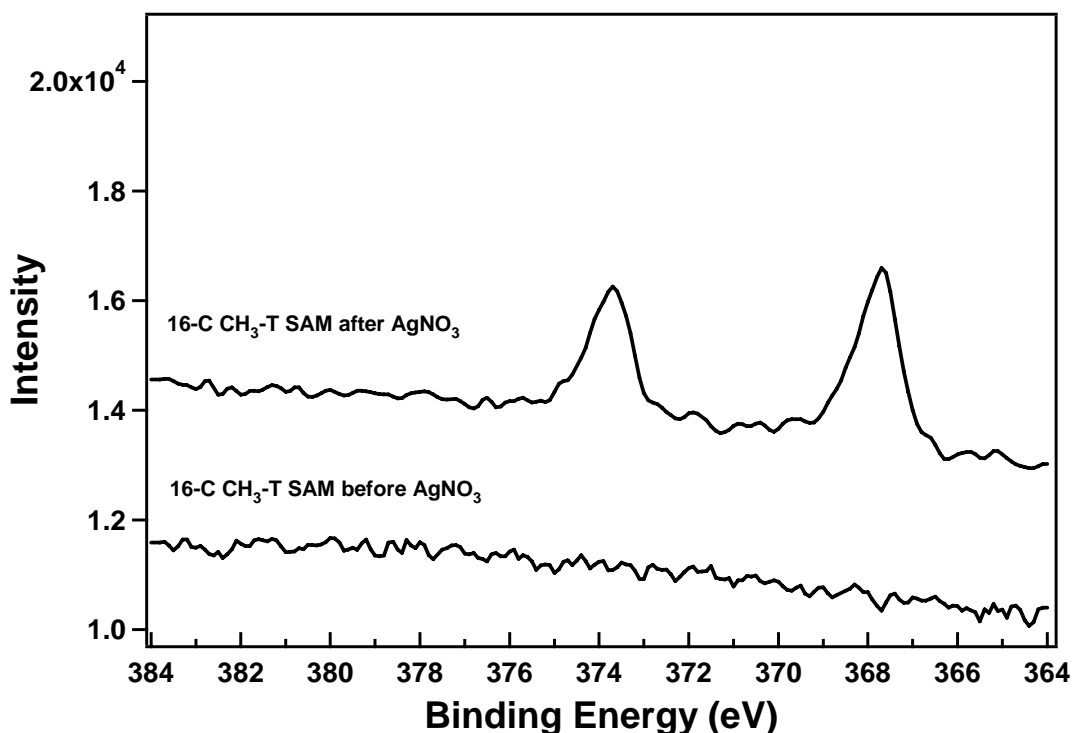


Figure 25: XP spectra of the Ag 3d multiplex for a 16-C CH₃-T SAM pre-and post-immersion in silver nitrate solution. The spectra indicate that silver remains on the surface after treatment with AgNO₃.

The spectra indicate that there is silver present on the methyl terminated SAM after immersion in silver nitrate solution. The explanation of the presence of silver involves monolayer defects and the affinity of silver for sulfur and thiols.^{162, 163} The presence of monolayer defects^{133, 135, 164-168} would allow for migration of the silver ions to the underlying sulfur moieties.¹⁶⁹ The defects can increase the spacing between adjacent alkyl chains, allowing for easier diffusion of silver ions to the sulfur head groups. The interaction of the alkyl chains with silver ions is supported by the earlier RAIR spectra (Figure 22). The intensity of the methylene stretching modes of the post-treatment spectra is slightly diminished compared to the pre-treatment spectra, which is consistent with a decrease in total methylene groups within the surface. Reaction of silver ions with the sulfur head group may remove of a small number of chains from the surface, resulting in fewer methylene groups. Interestingly, the small amount of Ag adsorbed within the

CH₃-T SAM does not appear to have a deleterious affect on cell growth (see section 4.3.2)

The multiplex Ag 3d region of the 16-C COOH-T SAM both before and after reaction with silver nitrate is shown in Figure 26. Both the positions and symmetric shape of the 3d photoelectron peaks are consistent with silver(I) ions.¹⁷⁰ The amount of silver on the surface was quantified by calculating the atomic percent composition. The calculation is performed by using instrument specific sensitivity factors, as explained in Chapter 3. Predicted percent composition values were determined by using a single sixteen carbon chain containing two oxygen atoms and one silver atom. Figure 27 presents the percent atomic composition values. The experimental values are the average of three analyses with the error bars representing the standard deviation.

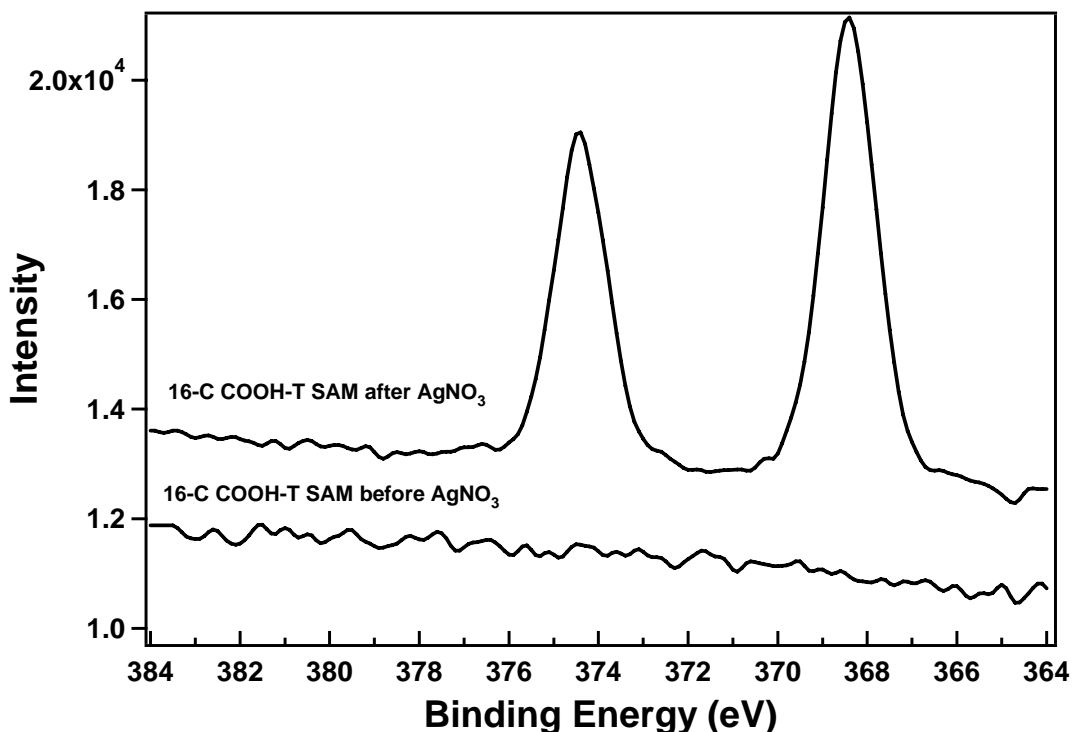


Figure 26: XP spectra of the Ag 3d multiplex for a 16-C COOH-T SAM before and after immersion in silver nitrate solution. The positions and symmetry of Ag 3d photoelectron peaks in the pre-treatment spectra indicate that all of the silver ions are in the oxidized 1+ state. The increased peak heights and area compared to the 16-C CH₃-T XP spectra (Figure 25) show that the 16-C COOH-T SAM after reaction with silver nitrate has a larger surface concentration of silver.

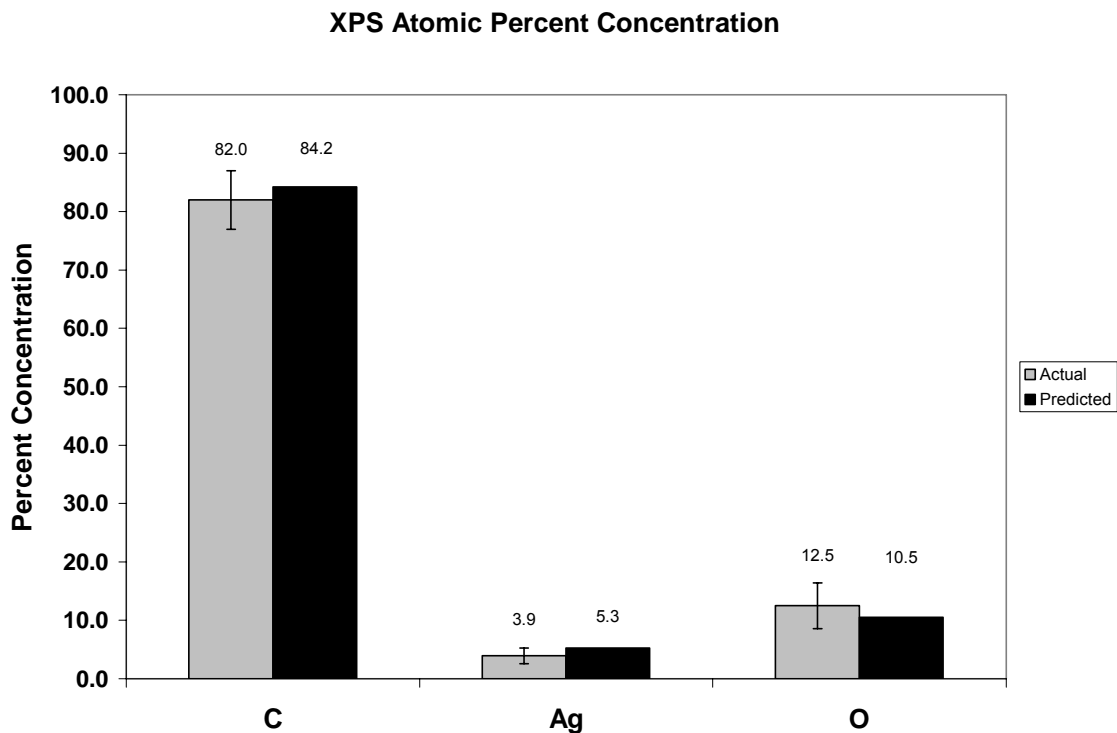


Figure 27: Atomic percent composition of a silver carboxylate terminated SAM. The error bars represent the standard deviation of 4 analyses. The predicted values were calculated using a molecule composed of 16 carbons, 2 oxygens, and one silver atom.

Within experimental error, the experimental data agrees with the prediction of a 1:1 ratio of silver cation to carboxylate anion. This suggests that each surface carboxylate group is complexed with one silver ion, resulting in a single monolayer of silver ions at the interface. The surface concentration of alkanethiol SAMs on Au(111) is approximately 4.5×10^{14} molecules/cm²,¹¹⁰ or about 4.5 nmol/cm². The XPS data suggests that one silver ion is bound to one carboxylate group, therefore the surface silver concentration could be considered approximately 4.5 nmol/cm².

4.3.2 Antibacterial Assays

After characterization of the SAMs, antibacterial assays were performed. Figure 28 displays the digital images of the surfaces after the antibacterial assay using *E coli* (see section 3.4). Each small light spot on the surface is known as a colony-forming-unit, or CFU. A colony forming unit is formed by the multiplication of a single bacterium that had attached to the surface. If the bacteria that are sprayed onto the surface are killed, no colony forming units will be present.

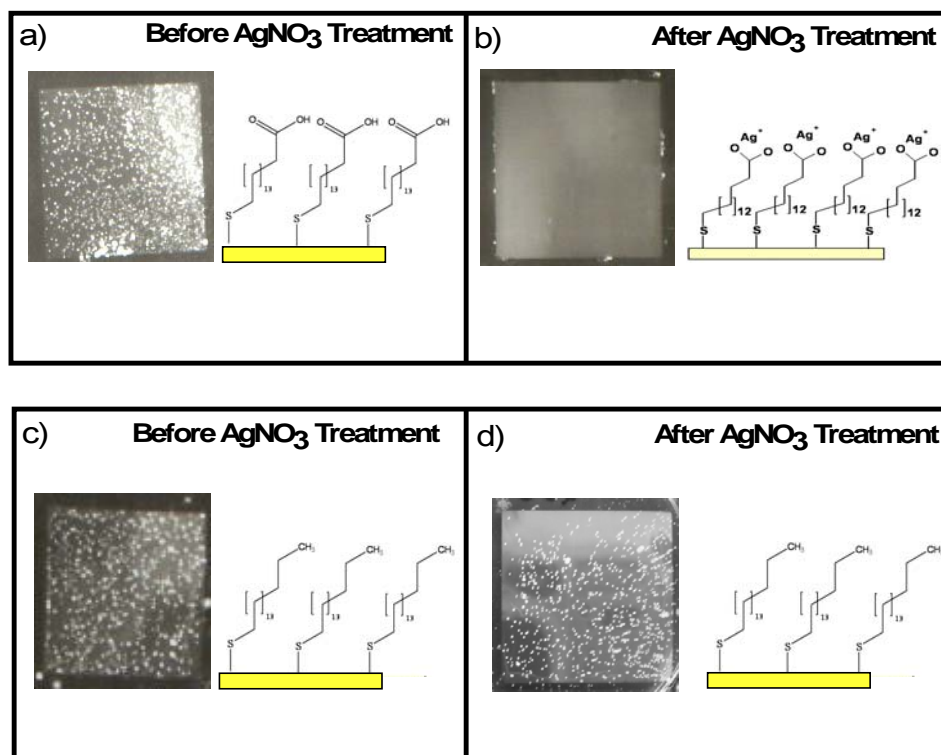


Figure 28: Antibacterial assay images for a 16-C COOH-T SAM before (a) and after (b) and a 16-C CH₃-T SAM before (c) and after (d) immersion in a silver nitrate solution. The 16-C COOH-T SAM after reaction with silver nitrate showed antibacterial activity.

The assay was performed on both a 16-C CH₃-T and 16-C COOH-T SAM before and after reaction with silver nitrate. On both the methyl and carboxylic acid terminated SAMs, bacteria remained viable and formed a large number of colony forming units. After reaction with silver nitrate, bacteria remained viable on only the methyl terminated SAM. In contrast to this, the bacteria were non-viable on the post-AgNO₃ treated carboxylic acid terminated SAM after reaction with silver nitrate.

The antibacterial activity of the silver carboxylate SAM was not unexpected; however the initial assay result did help provide information about the structural requirements for antibacterial activity of the simple alkanethiol SAMs investigated. Both the methyl and carboxylic acid terminated SAMs underwent a reaction with silver ions as evidenced by RAIRS and XPS data. The antibacterial assay result helps confirm the earlier assumption that the silver reacts at different locations on the different SAMs. The silver ions detected via XPS on the methyl terminated SAMs were probably located near the sulfur headgroups and away from the interface. The silver ions detected on the

carboxylic acid terminated SAMs were most likely bound to a terminal carboxylate anion species formed by the metal complexation reaction of silver ions and the carboxylate anions. The complexation reaction occurs at the terminal end of the SAM, placing the silver ions at the interface. XPS data also helped determine that there was a higher surface concentration of silver ions on the carboxylic acid terminated SAM (~ 4.5 nmol/cm²) than for the methyl terminated SAM (~ 1.7 nmol/cm²). Both the surface concentration and location relative to the interface of the silver ions likely contribute to the antibacterial activity of the silver complexed carboxylic acid terminated SAM and the antibacterial inactivity of the methyl terminated SAM.

4.3.3 Stability of a Silver Carboxylate SAM

The next part of the study was performed to establish if the silver carboxylate SAMs retained antibacterial activity after the initial assay. The experiment was performed by simply repeating the antibacterial assay. First, the surfaces were removed from the Petri dish of the initial assay and cleaned. The cleaning step involved manual removal of large piece of growth agar followed by soaking in an aqueous solution of one percent sodium dodecyl sulfate and 0.5 M NaCl. The surface was then rinsed with DI water and re-assayed. Figure 29 shows the digital images of the initial and second assay.

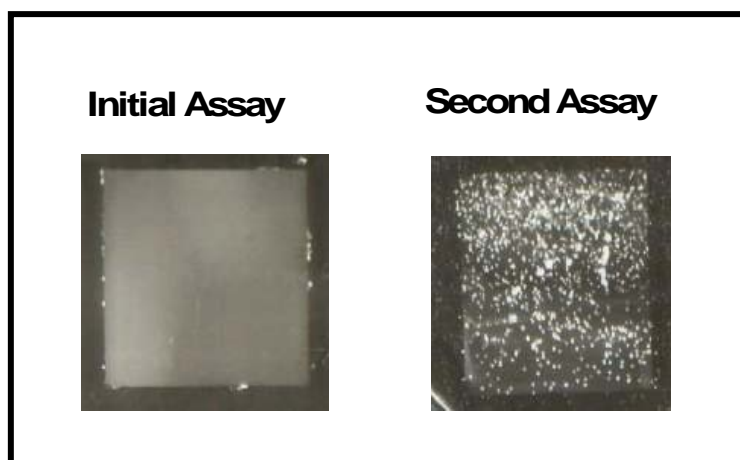


Figure 29: Antibacterial assay images for a silver carboxylate SAM. The second assay was performed after cleaning the surface with SDS/NaCl solution. The image of the second assay reveals that the silver carboxylate SAM does not retain its antibacterial activity.

The image of the second assay reveals that the silver carboxylate SAM did not retain antibacterial activity as there is a large number of colony forming units on the

surface. The loss of activity signifies that a change in composition of the surface occurred during the initial antibacterial assay. Changes in the SAMs are evidenced by key differences in pre- and post- AgNO_3 treatment RAIR spectra. Figure 30 shows the RAIR spectra of a 16-C COOH-T SAM before reaction with silver nitrate, after reaction with silver nitrate, and after the antibacterial assay.

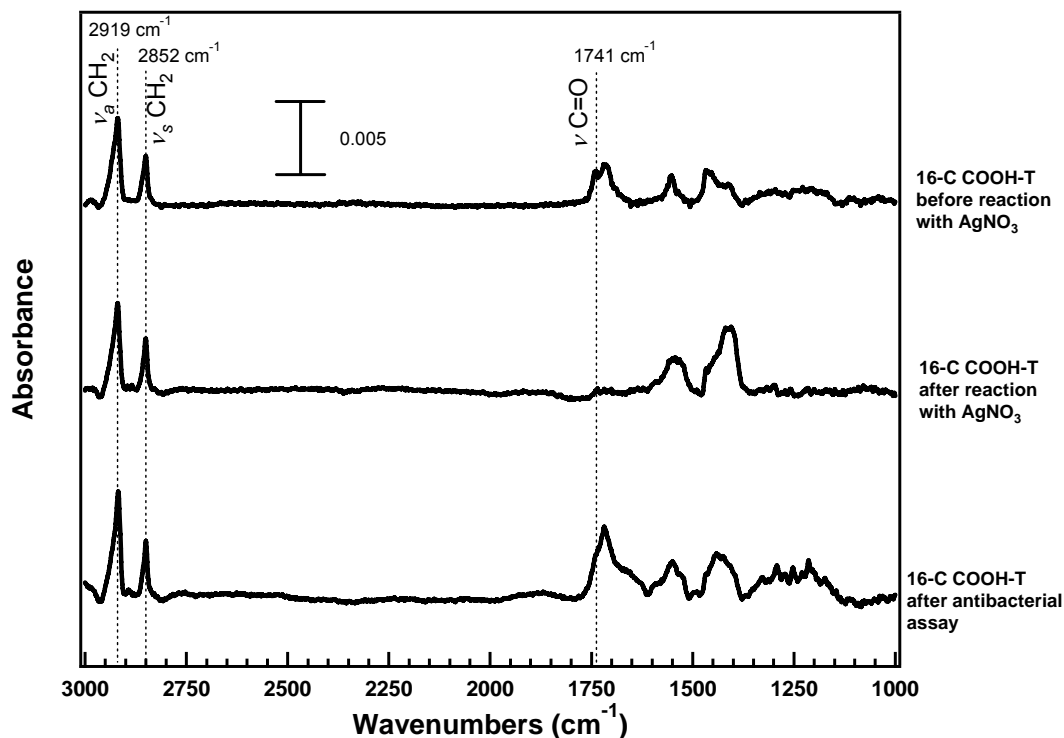


Figure 30: RAIR spectra of a 16-C COOH-T SAM before reaction with silver nitrate, after reaction, and after an antibacterial assay. The spectrum after the assay shows evidence that the silver carboxylate complex is lost and the acid functional group is reformed.

There are two important regions of the spectra to discuss. First, the lower frequency range provides evidence for a change in the composition of the surface-bound carboxylic acid groups during the antibacterial assay. In the top spectrum of the unreacted carboxylic acid terminated SAM, the carbonyl of the acid functional group is present at 1741 cm^{-1} . In the middle spectrum of the same acid terminated SAM after reaction with silver nitrate, the carbonyl mode has disappeared and is replaced by modes corresponding to the asymmetric and symmetric stretching modes of a carboxylate group. The disappearance of the carbonyl and introduction of the carboxylate modes indicates the formation of a silver carboxylate complex. In the bottom spectrum of the same

surface after the antibacterial assay, the carbonyl stretch has reappeared. The reappearance of the carbonyl stretching mode suggests that the silver carboxylate complex is no longer present on the surface and the carboxylic acid group has been reformed. The disappearance of the silver carboxylate complex agrees with the antibacterial inactivity of the surface after the initial assay; without any surface-bound silver ions, the surface is rendered non-antibacterial.

The second important part of the spectra from Figure 30 is the high frequency region containing the C-H stretching modes. The position, intensity, and shape of the asymmetric and symmetric methylene stretching vibrations provide important information about the organization of the monolayer. The asymmetric and symmetric methylene vibrations on all three spectra in Figure 30 appear quite similar. The modes appear at wavenumbers characteristic of well ordered, all-trans configured alkane chains.¹⁰³ The peaks are also narrow and intense, characteristics that also arise from well-ordered, crystalline like chain conformations.¹⁰³ The lack of change in the methylene stretching vibrations for the SAM after the antibacterial assay indicates that the well-ordered monolayer structure is not significantly disrupted by the antibacterial assay.

4.3.4 Regeneration of a Silver Carboxylate SAM

The RAIR spectra of the silver carboxylate SAM after the antibacterial assay revealed that the silver ions are removed and that the carboxylic acid group is reformed. We hypothesized that the surface loses antibacterial activity as a result the removal of the silver ions. To test the hypothesis, a second assay was performed on the same acid-terminated surface. We also hypothesized that the silver carboxylate complex could be reformed on the original acid-terminated surface, thereby restoring antibacterial activity. This hypothesis was tested by cleaning the surface with the SDS/NaCl solution followed by re-immersing the surface in silver nitrate for approximately 15-30 minutes followed by a second assay. Images of the secondary assays are shown in Figure 31.

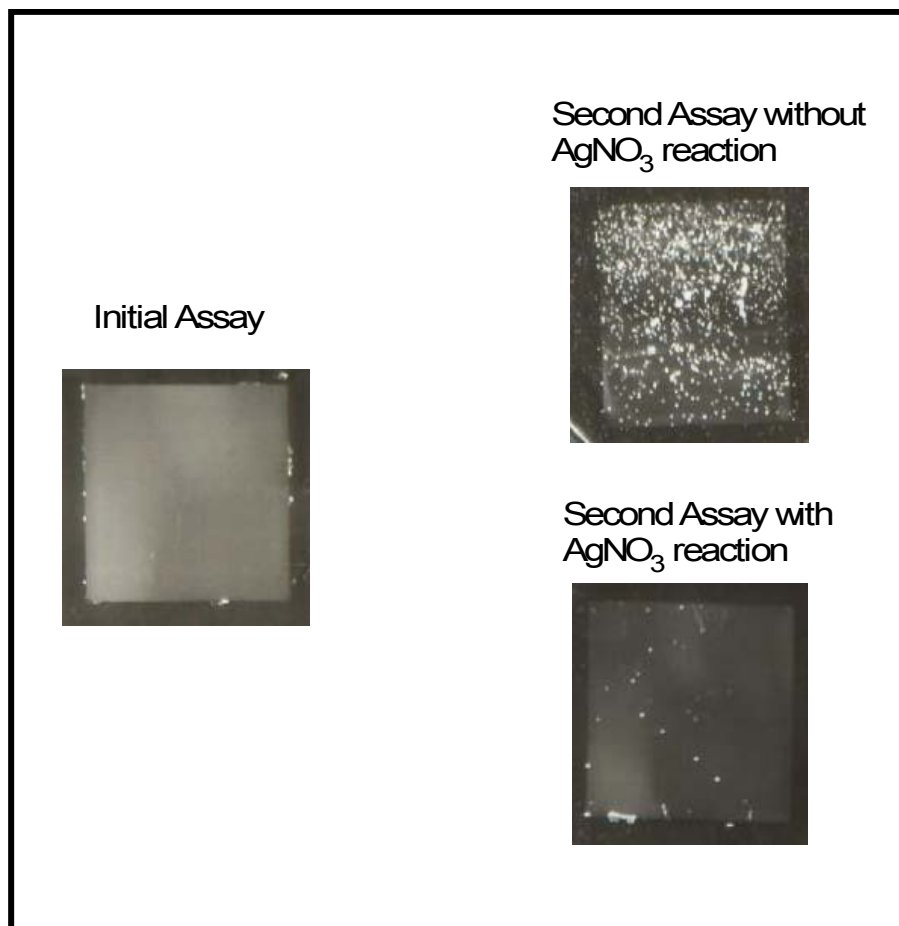


Figure 31: Antibacterial assay images demonstrating the regeneration of the antibacterial silver carboxylate SAM. The antibacterial activity was restored when the SAM was re-exposed to silver nitrate for 15-30 minutes.

The image of the second assay after reaction with silver nitrate shows very few colony forming units compared to the image from the second assay without silver nitrate reaction. The tremendously diminished number of colony forming units indicates that the antibacterial surface was regenerated by re-immersing the SAM in silver nitrate solution. The most probable explanation for the regenerated antibacterial activity is that the silver carboxylate complex is reformed by the complexation reaction of the carboxylic acid groups and silver ions. However, it is interesting to note that approximately 20 CFU's survive on the re-complexed Ag^+ SAM. We speculate that this is due to some of the carboxylic acid groups not undergoing reaction with silver ions.

4.3.5 Antibacterial Assay of Other Metal Carboxylate SAMs

The antibacterial assays provided evidence that the silver ions were responsible for the antibacterial activity. To prove that the silver ion is responsible for the activity and not the carboxylate complex, carboxylic acid SAMs were reacted with a series of other metal salts. The metal salts tested were zinc nitrate hexahydrate $[\text{Zn}(\text{NO}_3)_2 \cdot 6\text{H}_2\text{O}]$, iron (III) perchlorate hexahydrate $[\text{Fe}(\text{ClO}_4)_3 \cdot 6\text{H}_2\text{O}]$, nickel (II) perchlorate hexahydrate $[\text{Ni}(\text{ClO}_4)_2 \cdot 6\text{H}_2\text{O}]$, and copper (II) chloride. The metal carboxylate SAMs were formed by immersing a carboxylic acid terminated SAM for 15-30 minutes in a 1-2 mM ethanolic solution of the metal salt. The SAMs were characterized by RAIRs after immersion. The RAIR spectra are shown in Figure 32.

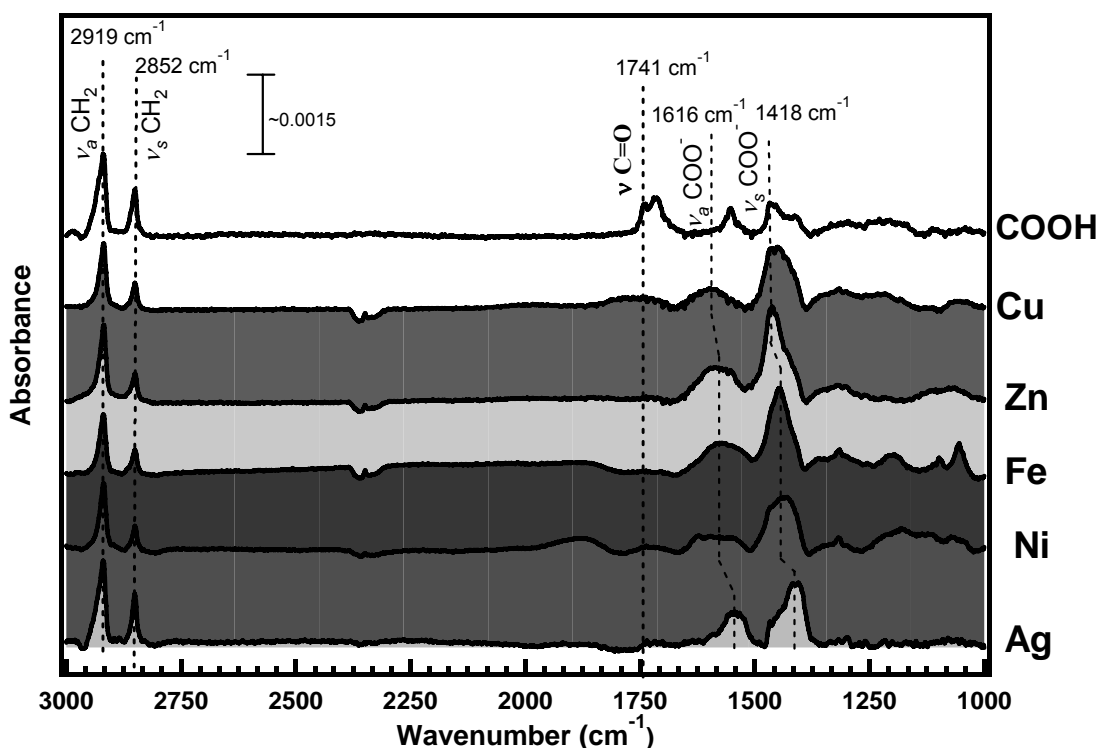


Figure 32: RAIR spectra of 16-C COOH-T SAMs after complexation reactions with different metal salts. Evidence for the reactions comes from the disappearance of the carbonyl stretching mode at 1741 cm^{-1} and the increased intensity of the asymmetric and symmetric carboxylate stretching modes at ~ 1616 and 1418 cm^{-1} , respectively.

The RAIR spectra of the copper, zinc, iron, and nickel carboxylate SAMs are very similar to the spectrum of the silver carboxylate SAM. The carbonyl stretching vibration present at 1741 cm^{-1} in the acid spectrum is absent from all of the metal carboxylate

spectra. The asymmetric and symmetric carboxylate stretches, all located near 1616 and 1418 cm^{-1} , respectively, are more prominent in the metal carboxylate spectra than in the acid spectrum. Both the disappearance of the carbonyl stretching vibration and the increased intensity of the asymmetric and symmetric carboxylate stretching vibrations suggest that the carboxylic acid SAMs have undergone a complexation reaction with the metal salts.

The antibacterial assay was performed on each of the metal carboxylate SAMs. Images from each assay are shown in Figure 33. Except for the silver carboxylate SAM, all of the SAMs show a significant number of colony forming units. The results shown by the antibacterial assay of the other metal carboxylate SAMs isolates the silver ion as the key antibacterial agent.

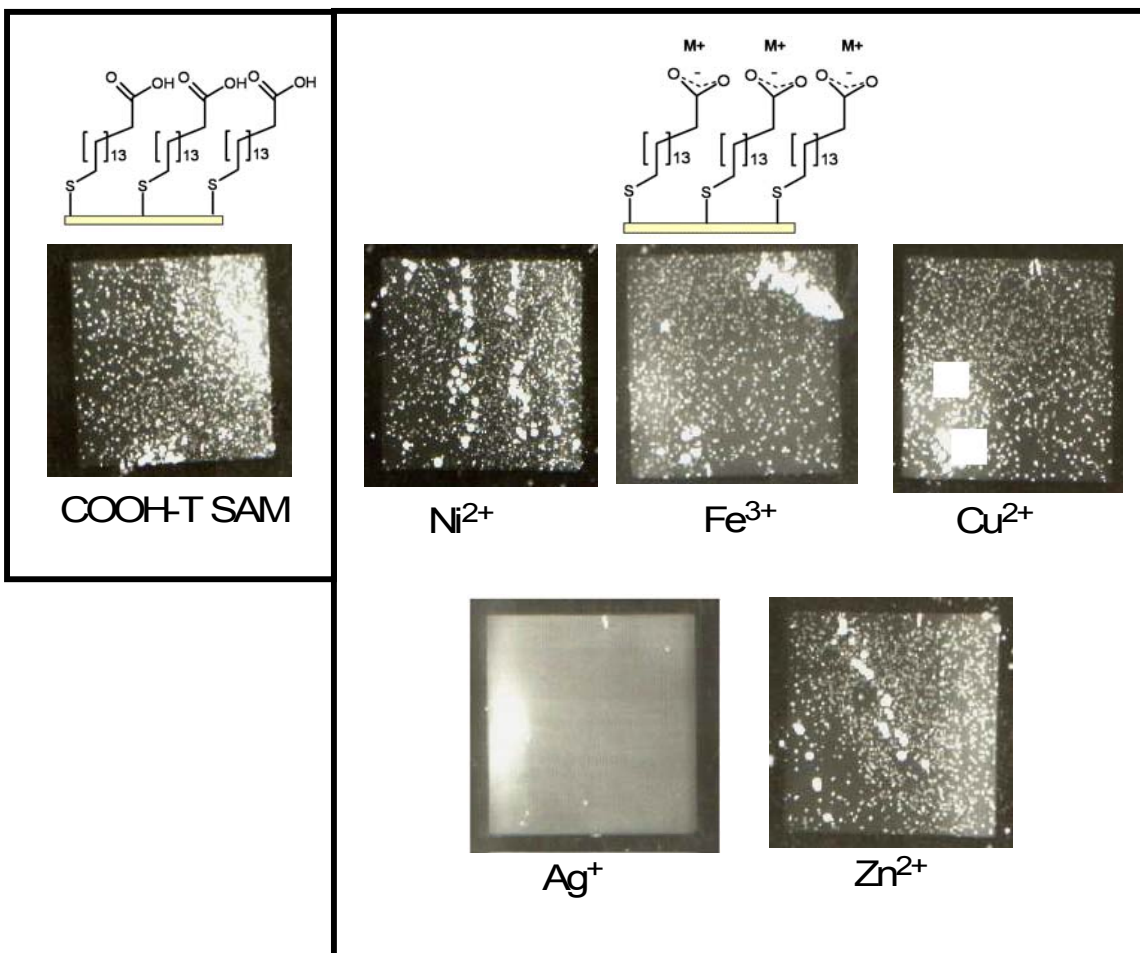


Figure 33: Images from the antibacterial assay of a series of metal carboxylate SAMs. Only the silver carboxylate showed antibacterial activity.

4.3.6 Discussion of the Antibacterial Activity of a Silver Carboxylate SAM

RAIRS data in combination with the results of the antibacterial assay demonstrated that the silver ions are responsible for the antibacterial activity. However, the silver carboxylate group was shown to be unstable during assay. The instability of the silver carboxylate group is important in the mechanism of the biocidal activity. Closer inspection of an antibacterial assay image of a silver carboxylate SAM reveals another important clue about the mechanism. In Figure 34, the immediate vicinity of the surface shows a lack of colony forming units, similar to the SAM surface. The area surrounding the surface with little bacteria growth is known as the zone of inhibition and is characteristic of antibacterial agents that have leached from the surface.⁷² The leaching of silver ions into the environment is expected as a result of the low formation constant of a silver acetate complex. The formation constants of a silver acetate complex are $K_1=5.37$ and $K_2=0.13$.¹⁷¹ As a result of the instability of the silver acetate complex, the silver ions can easily enter the melted agar solution used during the antibacterial assay and interact with bacteria not directly sprayed onto the SAM.

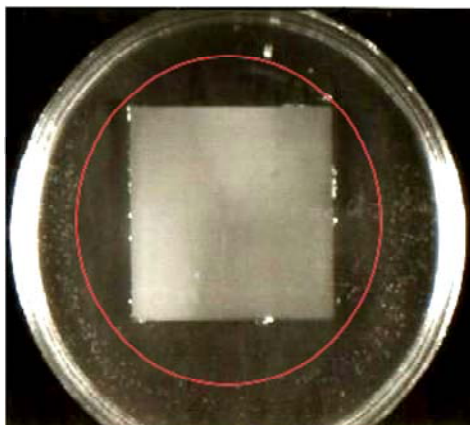


Figure 34: Antibacterial assay image of a silver carboxylate SAM. The red circle outlines the zone of inhibition. The zone of inhibition is characteristic of antibacterial agents that leech from the surface.⁷²

The leaching of silver ions is necessary for the antibacterial activity of the silver carboxylate SAM. In order for silver ions to kill bacteria, they must be taken up by the bacteria. The known antibacterial mechanisms of silver ions all occur inside of the cell, where they react with enzymes,^{172, 173} thiol groups,^{162, 163} and nucleic acid bases.¹⁷⁴⁻¹⁷⁹ If

the silver ions did not leach from the surface, they would not be able to enter the bacterial cell.

4.4 Conclusions

Silver carboxylate terminated SAMs showed antibacterial activity against *E. coli*. The silver carboxylate SAM was formed by the complexation reaction of carboxylic acid terminal groups and silver ions. The presence of complexed silver ions was detected via RAIRS and XPS. RAIR spectra showed that the carbonyl stretching vibration from the carboxylic acid disappeared after formation of the silver carboxylate complex. XPS spectra showed the presence of surface-bound silver via the Ag 3d photoelectron peaks. The surface concentration of silver ions was determined to be approximately 4.5 nmol/cm².

Antibacterial assay experiments demonstrated that the silver carboxylate terminated SAMs are antibacterial. A subsequent assay performed after cleaning the surface showed that the antibacterial activity of Ag⁺-complexed SAMs is not permanent. The loss of antibacterial activity is caused by leaching of silver ions from the surface during or after the initial assay. The leaching of the silver ions is evident from the zone of inhibition surrounding the surface of the initial assay. RAIR spectra taken after the initial assay showed that the reappearance of the carbonyl stretching vibration, which indicates that the silver carboxylate complex is lost, resulting in the reformation of the carboxylic acid group.

Antibacterial activity could be restored if the SAM was reacted with silver nitrate after the initial assay. The second reaction with silver nitrate appeared to reform the silver carboxylate complex to restore the antibacterial activity.

The mechanism of the antibacterial activity of the silver carboxylate SAMs was dependent on the uptake of silver ions into the bacterial cell. The known antibacterial effects of silver ions all occur at locations inside of the cell, not on the outer cell wall or membrane. The likely diffusion of the silver ions into the cells is supported by the observed leaching effect and the low binding constants of the silver carboxylate complex.

Perhaps the most important conclusion reached was that alkanethiol SAMs are remarkably stable after the antibacterial assay. RAIR spectra showed that the well-ordered crystalline-like arrangement of the alkyl chains was not significantly perturbed

by the bacteria or conditions of the assay. The stability of the SAMs helps to justify the use of alkanethiol SAMs to study the interactions between bacteria and surfaces. The stability of the well-ordered alkyl chain will allow for future studies of SAMs with more complicated terminal groups. The novel synthesis and systematic alteration of terminal functional groups and the resulting effects on bacteria viability will encompass the future of the project. Future work is briefly outlined in Chapter 5.

Chapter 5: Conclusions and Future Work

5.1 Conclusions

The primary objective of the work presented here was to establish use of alkanethiol SAMs as a tool to investigate the fundamental relationships between surface structure and bacteria viability. Significant work was done in developing the antibacterial assay an experimental method to observe the viability of bacteria on SAMs. These efforts led to the discovery that a simple layer of Ag^+ ions residing on an organic surface kills 100% of the *E. coli* that interact with the surface.

Chapter 3 presented the antibacterial assay method development. Well-ordered SAMs composed of methyl, hydroxyl, carboxylic acid, and perfluoro terminated groups were assayed and the remaining colony forming units were counted. Statistical analyses showed that there was significant variation in the results. The variation was caused by a combination of environmental and experimental factors. Bacterial growth can vary with differing environmental factors, such as temperature and humidity. The manual operation of the chromatography sprayer used to spray the bacteria onto the surfaces contributed to the experimental errors. Control of the amount of bacteria sprayed onto the surface proved to be extremely difficult.

The large variation of viable bacteria counts led to the conclusion that there was no difference in bacteria viability on the well-ordered methyl, hydroxyl, carboxylic acid, and perfluoro terminated SAMs. Within our ability to distinguish differences in colony growth on different SAMs, none of the SAMs had antibacterial activity. The inactivity of the methyl, carboxylic acid, and perfluoro terminated SAMs was expected as none of the four SAMs contained known antibacterial functional groups. The assay of the hydroxyl terminated SAM showed that a surface-bound long chain alcohol does not possess antibacterial activity, which is in direct contrast to the biocidal activity of ethanol and isopropanol.

In Chapter 4, a carboxylic acid terminated SAM complexed with silver ions was shown to be antibacterial. The weak silver carboxylate complex allowed for the release of silver ions into the surrounding media where they are taken up by the bacteria. A zone

of inhibition provided evidence for leaching of silver from the surface, which was further supported by RAIRs data that showed the loss of carboxylate groups and the reformation of carbonyl groups. Because the silver ions were removed from the surface, the biocidal activity was not retained as shown in a second assay.

The antibacterial silver carboxylate surface could be regenerated by a second reaction between the surface and silver nitrate, which regenerated the silver carboxylate groups and restored the antibacterial activity due to the replenishing of silver ions at the surface. Zinc, iron, nickel, and copper ions were complexed with the carboxylate species, but none of those metal carboxylate surfaces showed antibacterial activity. The antibacterial inactivity of the other metal ions indirectly showed that the silver ions were responsible for the antibacterial activity.

The well-ordered crystalline-like structure of the alkyl chains of the SAMs were not significantly perturbed by the conditions of the antibacterial assay. RAIR spectra recorded after the assay showed that the peaks of the methylene stretching vibrations did not differ from the same peaks of the RAIR spectra recorded before the assay. The observation of preserved well-ordered alkyl chain structure helped to conclude that the functionalized alkanethiol SAMs are sufficiently stable to use as a tool for investigating the relationship between surface structure and viability of bacteria.

5.2 Future Work

The future work of this project will focus on creating SAMs containing quaternary ammonium groups. Quaternary ammonium groups covalently bound to surfaces have shown antibacterial properties, however the surfaces were not fully characterized. A covalently bound antibacterial group will allow for subsequent systematic alteration of the surface structure, such as ordering, density, surface concentration, and various alkane chain lengths. Systematic alteration of a non-covalently bound antibacterial group is not feasible because of leaching issues, which were observed for the silver carboxylate surfaces.

The initial part of the work will be to synthesize SAMs containing covalently bound quaternary ammonium groups. The synthesis will be conducted on two fronts; synthesizing the entire thiol molecules before forming the SAM and modification of a

SAM after formation. Preliminary work has shown that each route appears feasible to creating SAMs with quaternary ammonium groups.

The total synthesis route will occur via three steps, outlined in Figure 35. The first step will convert a bromoalcohol into a bromotriflate.¹⁸⁰ The highly reactive bromotriflate group is then reacted with a tertiary amine to form a quaternary ammonium salt.¹⁸¹ The final step converts the terminal bromine of the quaternary ammonium salt into a thiol.¹⁸² Once the total synthesis has been verified, a SAM will be formed, characterized, and tested for antibacterial activity. The structure of the SAMs will then be systematically altered by changing the alkyl chain of the SAM molecules. The alteration will be done by using starting material containing the desired chain lengths. Preliminary nuclear magnetic resonance spectra have shown evidence for the formation of the bromine terminated quaternary ammonium salt shown in step 2 of Figure 35.

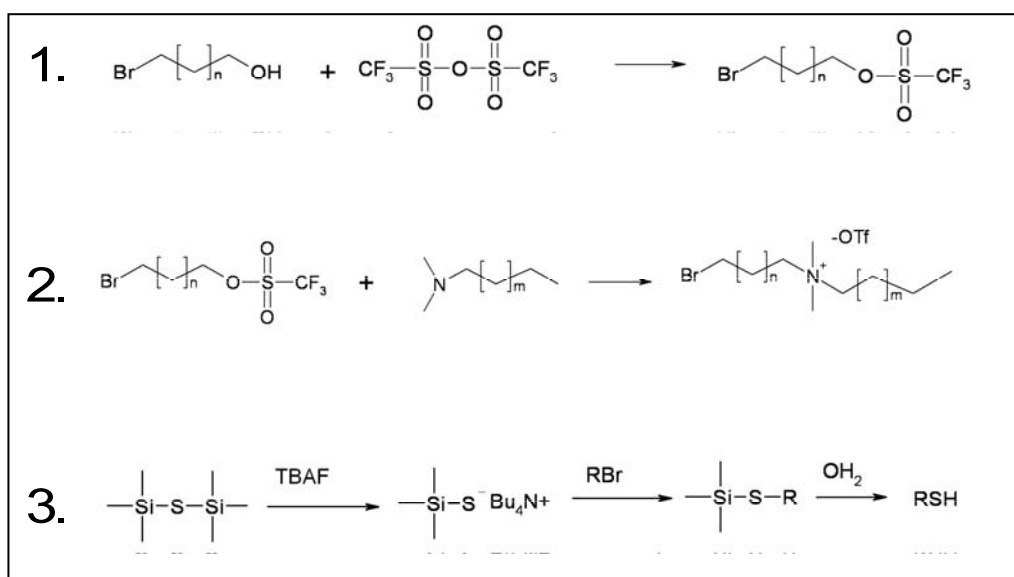


Figure 35: Synthetic route for the total synthesis of a quaternary ammonium containing thiol. The synthesis will involve forming a bromotriflate followed by conversion to a quaternary ammonium salt. The terminal bromine group is then converted to the thiol. Alkyl chain lengths can be varied by using different starting material.

The second synthetic route will be carried out in three steps as outlined in Figure 36. First, a carboxylic terminated SAM will be formed and characterized (see sections 3.1-3.3). Next, the carboxylic acid terminal groups will be converted into amide groups via reaction with a diamine catalyzed by 1-ethyl-3-[3-

(dimethylamino)propyl]carbodiimide.^{145, 146} After characterization of the modified surface, the terminal tertiary amine groups will be reacted with a 2-bromoketone to create quaternary ammonium groups. The surface will again be characterized followed by assessment of antibacterial activity via the antibacterial assay. The chain lengths in the n, m, and x positions shown in Figure 36 will be systematically altered by using starting materials of the desired chain lengths.

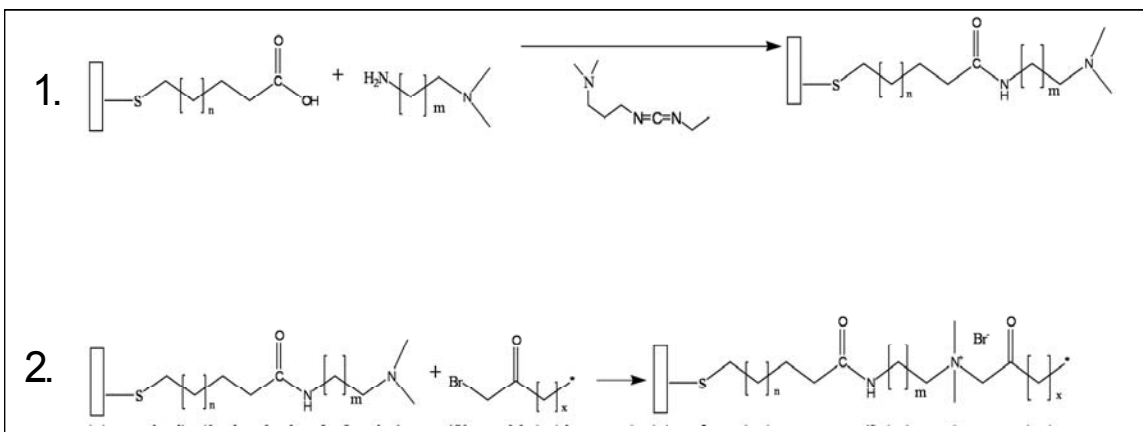


Figure 36: Synthetic route of quaternary ammonium SAMs via modification of an initial carboxylic acid terminated SAM. The structure of the molecules will be systematically varied in the m, n, and x positions by using starting materials with the desired chain lengths.

The primary advantage of the second synthetic route is lack of a product separation step. One of the largest drawbacks of total synthesis of a thiol is the difficult separation of intermediates and products. By anchoring the thiol molecules to the surface initially, they are essential pre-separated from unwanted reaction byproducts and intermediates. Anchoring the thiol to the gold substrate also serves to protect the thiol from unwanted reactions, which is a situation frequently encountered during the synthesis of functionalized thiols.

Preliminary RAIRS and XPS data provided evidence for quaternary ammonium containing SAM with chain lengths n=7, m=1, and x=13 via the synthetic route shown in Figure 36. The initial quaternary ammonium containing SAM did not exhibit any antibacterial activity. The lack of activity is probably the result of a low surface concentration of quaternary ammonium groups.

In summary, the future work of this project will involve refining the synthesis of quaternary ammonium containing SAMs followed by systematic alteration of the alkyl

chain length within the SAMs. The different chain lengths will change the structure of the surfaces, and possibly the viability of bacteria on those surfaces. By utilizing the versatility of self-assembled monolayers of functionalized alkanethiols on gold, a fundamental understanding of the relationship between molecular scale surface structure and the viability of bacteria can be obtained.

References

1. Beveridge, T. J., *Metal Ions and Bacteria*. John Wiley & Sons, Inc.: New York, R.J. Doyle.
2. Srivastava, S.; Srivastava, P. S., *Understanding Bacteria*. Kluwer Academic Publishers: Dordrecht, The Netherlands, 2003.
3. Harden, V. P.; Harris, J. O., The isoelectric point of bacterial cells. *J. Bacteriol.* **1953**, 65, 198-202.
4. James, A. M., The electrical properties and topochemistry of bacterial cells. *Adv. Colloid Interface Sci.* **1982**, 15, 171-221.
5. Neihof, R.; Echols, W. H., Physicochemical studies of microbial cell walls. 1. Comparative electrophoretic behavior of intact cells and isolated cell walls. *Biochim. Biophys. Acta* **1973**, 318, 22-32.
6. Richmond, D. V.; Fisher, D. J., The electrophoretic mobility of microorganisms. *Adv. Microb. Physiol.* **1973**, 9, 1-27.
7. Burger, M. M., Teichoic acids: antigenic determinants, chain separation, and their location in the cell wall. *Proc. Natl. Acad. Sci. USA* **1966**, 56, 910-917.
8. Doyle, R. J.; McDaniel, M. L.; Helman, J. R.; Streips, U. N., Distribution of teichoic acid in the cell wall of *Bacillus subtilis*. *J. Bacteriol.* **1975**, 122, 152-158.
9. Garland, J. M.; Archibald, A. R.; Baddiley, J., An electron microscope study of the location of teichoic acid and its contribution to staining reactions in walls of *Streptococcus faecalis* 8191. *J. Gen. Microbiol.* **1975**, 89, 73-86.
10. Sonnenfeld, E. M.; Beveridge, T. J.; Doyle, R. J., Asymmetric distribution of charge on the cell wall of *Bacillus Subtilis*. *J. Bacteriol.* **1985**, 163, 1167-1171.
11. Umeda, A.; Ueki, Y.; Amako, K., Structure of the *Staphylococcus aureus* cell wall determined by freeze-substitution method. *J. Bacteriol.* **1987**, 169, 2482-2487.
12. Weiss, L., The pH value at the surface of *Bacillus subtilis*. *J. Gen. Microbiol.* **1963**, 32, 331-340.
13. Beveridge, T. J., Ultrastructure, chemistry, and function of the bacterial wall. *Int. Rev. Cytol.* **1981**, 72, 229.
14. Cronan, J. E., *Phospholipid synthesis and assembly*. Wiley: New York, 1979; p p. 35.

15. Lugtenberg, E. J. J.; Peters, R., Distribution of lipids in cytoplasmic and outer membranes of *Escherichia coli*. *Biochim. Biophys. Acta* **1976**, 441, 38.
16. Jain, M. K., "*Nonrandom lateral organization in bilayers and biomembranes*". Academic: New York, 1983; Vol. 1, p p. 1.
17. Ferris, F. G.; Beveridge, T. J., Functions of bacterial cell surface structures. *BioScience* **1985**, 35, 172.
18. Yuehuei, H.; Friedman, R. J., Concise Review of Mechanisms of Bacterial Adhesion to Biomaterial Surfaces. *J. Biomed. Mater. Res.* **1998**, 43, 338-348.
19. Marshall, K. C., Mechanisms of bacterial adhesion at solid-water interfaces. In *Bacterial Adhesion. Mechanisms and Physiological Significance*, Savage, D. C.; Fletcher, M., Eds. Plenum Press: New York, 1985; pp 133-161.
20. Marshall, K. C.; Stout, R.; Mitchell, R., Mechanism of initial events in the sorption of marine bacteria to surfaces. *J. Gen. Microbiol.* **1971**, 68, 337-348.
21. Costerton, J. W.; Lappin-Scott, H. M., Behavior of bacteria in biofilm. *ASM News* **1989**, 55, 650-654.
22. Orstavik, D., Sorption of *Streptococcus faecium* to glass. *Acta Pathol. Microbiol. Scand.* **1977**, 85B, 38-46.
23. Fletcher, M.; Floodgate, G. D., An electron-microscopic demonstration of as acidic polysaccharide involved in the adhesion of a marine bacterium to solid surfaces. *J. Gen. Microbiol.* **1973**, 74, 325-334.
24. Satou, N.; Satou, J.; Shintani, H.; Okuda, K., Adherence of streptococci to surface-modified glass. *J. Gen. Microbiol.* **1988**, 134, 1299-1305.
25. Abbot, A.; Rutter, P. R.; Berkeley, R. C. W., The influence of ionic strength, pH and a protein layer on the interaction between *Streptococcus mutans* and glass surfaces. *J. Gen. Microbiol.* **1983**, 129, 439-445.
26. Denyer, S. P.; Davies, M. C.; Evans, J. A.; al., e., *Clin. Microbiol.* **1990**, 28, 1813-1817.
27. Gordon, A. S.; Gerchakov, S. M.; Udey, L. R., The effect of polarization on the attachment of marine bacteria to copper and platinum surfaces. *Can. J. Microbiol.* **1981**, 27, 698-703.
28. Harber, M. J.; Mackenzie, R.; Asscher, A. W., A rapid bioluminescence method for quantifying bacteria adhesion to polystyrene. *J. Gen. Microbiol.* **1982**, 129, 621-632.

29. Hogt, A. H.; Dankert, J.; Vries, J. A. d.; Feijen, J., Adhesion of coagulase-negative staphylococci to biomaterials. *J. Gen. Microbiol.* **1983**, 129, 1959-1968.
30. Loosdrecht, M. C. M. v.; Lyklema, J.; Norde, W.; Schraa, G.; Zehnder, A. J. B., The role of bacterial cell wall hydrophobicity in adhesion. *Appl. Environ. Microbiol.* **1987**, 53, 1893-1897.
31. Dankert, J.; Hogt, A. H.; Feijen, J., J. Biomedical polymers: bacterial adhesion, colonization, and infection. *CRC Crit. Rev. Biocompat.* **1986**, 2, 219-301.
32. Hogt, A. H.; Dankert, J.; Feijen, J., Adhesion of *Staphylococcus epidermidis* and *Staphylococcus saprophyticus* to a hydrophobic biomaterials. *J. Gen. Microbiol.* **1985**, 131, 2485-2491.
33. Barth, E.; Myrvik, Q. M.; Wagner, W.; Gristina, A. G., *In Vitro* and *vivo* comparative colonization of *Staphylococcus aureus* and *Staphylococcus epidermidis* orthopedic implant materials. *Biomaterials* **1989**, 10, 325-328.
34. Oga, M.; Sugioka, Y.; Hobgood, C. D.; Gristina, A. G.; Myrvik, Q. N., Surgical biomaterials and differential colonization by *Staphylococcus epidermidis*. *Biomaterials* **1988**, 9, 285-289.
35. Pringle, J. H.; Fletcher, M., Influence of substratum hydration and adsorbed macromolecules on bacterial attachment to surfaces. *Appl. Environ. Microbiol.* **1986**, 51, (1321-1325).
36. Reynolds, E. C.; Wong, A., Effect of adsorbed protein on hydroxyapatite zeta potential and *Streptococcus mutans* adherence. *Infect. Immunol.* **1983**, 39, 1285-1290.
37. An, Y. H.; Friedman, R. J.; Draughn, R. A.; Smith, E. A.; Nicholson, J.; John, J. F., Rapid Quantification of staphylococci adhered to titanium surfaces using image analyzed epifluorescence microscopy. *J. Microbiol. Methods* **1995**, 24, 29-40.
38. Locci, R.; Peters, G.; Pulverer, G., Microbial colonization of prosthetic devices. I. Microtopographical characteristics of intravenous catheters as detected by scanning electron microscopy. *Zbl. Bakt. Hyg. I. Abt. Orig. B* **1981**, 173, 285-292.
39. Gristina, A. G., Biomaterial-centered infection: microbial adhesion versus tissue integration. *Science* **1987**, 237, 1595.
40. Gristina, A. G.; Hobgood, C. D.; Barth, E., Biomaterial specificity, molecular mechanisms, and clinical relevance of *S. epidermidis* and *S. aureus* infections in surgery. In *Pathogenesis and Clinical Significance of Coagulase-Negative Staphylococci*, Pulverer, G.; Quie, P. G.; Peters, G., Eds. Fisher Verlag: Stuttgart, 1987; pp 143-157.

41. Chu, C. C.; Williams, D. F., Effects of physical configuration and chemical structure of surface materials on bacterial adhesion. *Am. J. Surg.* **1984**, 147, 197-204.
42. Duran, L. W.; Pietig, J. A.; Driemeyer, J. E.; al., e., Prevention of microbial colonization on medical devices by photochemical immobilization of antimicrobial peptides. *Trans. Soc. Biomater.* **1993**, 16, 35.
43. Bridgett, M. J.; Davies, M. C.; Denyer, S. P., *Biomaterials* **1992**, 13, 411-416.
44. Farber, B. F.; Wolff, A. G., The use of nonsteroidal anti-inflammatory drugs to prevent the adherence of *Staphylococcus epidermidis* to medicinal polymers. *J. Infect. Dis.* **1992**, 166, 861-865.
45. Speier, J. L.; Malek, J. R., Destruction of microorganisms by contact with solid surfaces. *J. Colloid Interface Sci.* **1982**, 89, (68-76).
46. McAllister, E. W.; Carey, L. C.; Brady, P. G.; Heller, R.; Kovacs, S. G., The role of polymeric surface smoothness of biliary stents in bacterial adhesion, biofilm deposition, and stent occlusion. *Gastrointest. Endosc.* **1993**, 39, 422-425.
47. Baker, A. S.; Greenham, L. W., Release of gentamicin from acrylic bone cement: elution and diffusion studies. *J. Bone Joint Surg.* **1988**, 70A, 1551-1557.
48. Merritt, K.; Shafer, J. W.; Brown, S. A., Implant site infection rates with porous and dense materials. *J. Biomed. Mater. Res.* **1979**, 13, 101-108.
49. Sugarman, B.; Musher, D., Adherence of bacteria to suture materials. *Proc. Soc. Exp. Biol. Med.* **1981**, 167, 156-160.
50. Fletcher, M.; Loeb, G. I., Influence of substratum characteristics on the attachment of marine pseudomonad to solid surfaces. *Appl. Environ. Microbol.* **1979**, 37, 67-72.
51. Ludwicka, A.; Jansen, B.; Wadstrom, T.; Pulverer, G., Attachment of staphylococci to various synthetic polymers. *Zbl. Bakt. Hyg. A.* **1984**, 256, 479-489.
52. Fletcher, M.; Marshall, K. C., Bubble contact angle method for evaluating substratum interfacial characteristics and its relevance to bacterial attachment. *Appl. Environ. Microbol.* **1982**, 44, (184-192).
53. Vaara, M., *Microbiol. Rev.* **1992**, 56, 395-411.
54. Hamilton, W. A., Membrane Active Antibacterial Compounds. In *Inhibition and Destruction of the Microbial Cell*, Hugo, W. B., Ed. Academic Press, Inc.: New York, 1971; pp 77-93.

55. Hartmann, M.; Kaig, H., Saure Seifen. *Z. angew. Chem.* **1928**, 41, 127-130.
56. Kuhn, R.; Bielig, H., Uber Inversteifen. I. Die. Einwirkung von Invertseifen aus Eiweiss-Stoffe. *Berichte der Deutschen Chemischen Gesellschaft* **1940**, 73, 1080-1091.
57. Hotchkiss, R. D., Gramicidin, tyrocidin and tyrothricin. *Advances in Ezymology* **1944**, 4, 153-199.
58. Denyer, S. P.; Hugo, W. B., Biocide-induced damage to the cytoplasmic membrane. *Soc. Appl. Bacteriol. Tech. Ser.* **1991**, 27, 171-187.
59. Salton, M. R. J., Lytic agents, cell permeability and monolayer penetrability. *J. Gen. Physiol.* **1968**, 52, 277S-252S.
60. Ackart, W. B.; Camp, R. L.; Byck, W. L.; Byck, J. S., *J. Biomed. Mater. Res.* **1975**, 9, 55-68.
61. Arciola, C. R.; Radin, L.; Alvergnna, P.; Cenni, E.; Pizzoferrato, A., *Biomaterials* **1993**, 14, 1161-1164.
62. Desai, N.; Hossainy, S. F.; Hubbell, J. A., *Biomaterials* **1992**, 13, 417-420.
63. Kohnen, W.; Jansen, B., *Zentralbl. Bakteriolog.* **1995**, 283, 175-186.
64. Park, K. D.; Kim, Y. S.; Han, D. K.; Kim, Y. H.; Lee, E. H. B.; Suh, H.; Choi, K. S., *Biomaterials* **1998**, 19, 851-859.
65. Medlin, J., *Environ. Health Perspect.* **1997**, 105, 290-292.
66. Nohr, R. S.; Macdonald, G. J., *J. Biomater. Sci. Polym. Ed.* **1994**, 5, 607-619.
67. Shearer, A. E. H.; Paik, J. S.; Hoover, D. G.; Haynie, S. L.; Kelley, M. J., *Biotechnol. Bioeng.* **2000**, 67, 141-146.
68. Lin, J.; Tiller, J. C.; Lee, S. B.; Lewis, K.; Klibanov, A., Insights into bactericidal action of surface-attached poly(vinyl-N-hexylpyridinium) chains. *Biotechnology Letters* **2002**, 24, 801-805.
69. Tiller, J. C.; Lee, S. B.; Lewis, K.; Klibanov, A., Polymer Surfaces Derivatized with Poly(Vinyl-N-Hexylpyridinium) Kill Airborne and Waterborne Bacteria. *Biotechnology and Bioengineering* **2002**, 79, (4), 465-471.
70. Tiller, J. C.; Liao, C.-J.; Lewis, K.; Klibanov, A., Designing surfaces that kill bacteria on contact. *PNAS* **2001**, 98, (11), 5981-5985.

71. Kawabata, N.; Nishiguchi, M., Antibacterial Activity of Soluble Pyridinium-Type Polymers. *Applied and Environmental Microbiology* **1988**, 54, (10), 2532-2535.
72. Endo, Y.; Tani, T.; Kodama, M., *Appl. Environ. Microbol.* **1987**, 53, 2050-2055.
73. Isquith, A. J.; Abbott, E. A.; Walters, P. A., Surface-Bound Antimicrobial Activity of an Organosilicon Quaternary Ammonium Chloride. *Appl. Microbiol.* **1972**, 24, (6), 859-863.
74. Lawrence, C. A., Quaternary ammonium surface-active disinfectants. In *Disinfection, sterilization and preservation*, Lawrence, C. A.; Block, S. S., Eds. Lea and Febiger: Philadelphia, 1968; pp 430-452.
75. Allara, D. L., *Langmuir* **1985**, 1, 45.
76. Allara, D. L.; Nuzzo, R. G., *Langmuir* **1985**, 1, 52-66.
77. Ogawa, H.; Chihera, T.; Taya, K. J., *J. Am. Chem. Soc.* **1985**, 107, 1365.
78. Schlotter, N. E.; Porter, M. D.; Bright, T. B.; Allara, D. L., *Chem. Phys. Lett.* **1986**, 132, 93.
79. Brandiss, S.; Margel, S., *Langmuir* **1993**, 9, 1232.
80. Carson, G.; Granick, S., *J. Appl. Polym. Sci.* **1989**, 37, 2767.
81. Finklea, H. O.; Robinson, L. R.; Blackburn, A.; Richter, B.; Allara, D. L.; Bright, T., *Langmuir* **1986**, 2, 239.
82. Gun, J.; Iscovici, R.; Sagiv, J., *J. Colloid Interface Sci.* **1984**, 101, 201.
83. Gun, J.; Sagiv, J., *J. Colloid Interface Sci.* **1986**, 112, 457.
84. Kessel, C. R.; Granick, S., *Langmuir* **1991**, 7, 532.
85. LeGrange, J. D.; Markham, J. L.; Kurjian, C. R., *Langmuir* **1993**, 9, 1749.
86. Maoz, R.; Sagiv, J., *J. Colloid Interface Sci.* **1984**, 100, 465.
87. Mathauser, K.; Frank, C. W., *Langmuir* **1993**, 9, 3002.
88. Mathauser, K.; Frank, C. W., *Langmuir* **1993**, 9, 3446.
89. Rubinstein, I.; Sabatini, E.; Maoz, R.; Sagiv, J., *J. Proc. Electrochem. Soc.* **1987**, 86, 175.

90. Rubinstein, I.; Sabatini, E.; Maoz, R.; Sagiv, J., *J. Electroanal. Chem.* **1987**, 219, 365.
91. Sagiv, J., *J. Am. Chem. Soc.* **1980**, 102, 92.
92. Schwartz, D. K.; Steinberg, S.; Israelachvili, J.; Zasadzinski, Z. A. N., *Phys. Rev. Lett.* **1992**, 69, 3354.
93. Siberzan, P.; Leger, L.; Ausserre, D.; Benattar, J. J., *Langmuir* **1991**, 7, 1647.
94. Tillman, N.; Ulman, A.; Schildkraut, J. S.; Penner, T. L., *J. Am. Chem. Soc.* **1988**, 110, 6136.
95. Wasserman, S. R.; Tao, Y. T.; Whitesides, G. M., *Langmuir* **1989**, 5, (1074).
96. Love, J. C.; Estroff, L. A.; Kriebel, J. K.; Nuzzo, R. G.; Whitesides, G. M., Self-Assembled Monolayers of Thiolates on Metals as a Form of Nanotechnology. *Chem. Rev.* **2005**, 105, 1103-1169.
97. Li, D. Q.; Ratner, M. A.; Marks, T. J.; Zhang, C. H.; Yang, J.; Wong, G. K. J., *J. Am. Chem. Soc.* **1990**, 112, 7389-7390.
98. Hickman, J. J.; Ofer, D.; Laibinis, P. E.; G.M. Whitesides; Wrighton, M. S., *Science* **1991**, 252, 688-691.
99. Kumar, A.; Abbott, N. L.; Biebuyck, H. A.; Kim, E.; Whitesides, G. M., *Accounts of Chemical Research* **1995**, 28, 219-226.
100. Schomburg, K. C.; McCarley, R. L., *Langmuir* **2001**, 17, 1983-1992.
101. Kim, H.; Jang, J., *Polymer* **2000**, 41, 6553-6561.
102. Laibinis, P. E.; Whitesides, G. M.; Allara, D. L.; Tao, Y. T.; Parikh, A. N.; Nuzzo, R. G., *J. Am. Chem. Soc.* **1991**, 113, (7152-7167).
103. Nuzzo, R. G.; Dubois, L. H.; Allara, D. L., *J. Am. Chem. Soc.* **1990**, 112, 558-569.
104. Nuzzo, R. G.; Fusco, F. A.; Allara, D. L., *J. Am. Chem. Soc.* **1987**, 109, 2358-2368.
105. Schmidt, J.; Laitenberger, P.; Palmer, R. E., *Review of Scientific Instruments* **1998**, 69, 313-314.
106. Whitesides, G. M.; Laibinis, P. E., *Langmuir* **1990**, 6, 87-96.

107. Holman, M. W.; Liu, R.; Adams, D. M., *J. Am. Chem. Soc.* **2003**, 125, 12649-12654.
108. Zamborini, F. P.; Crooks, R. M., *Langmuir* **1998**, 14, 3279-3286.
109. Bain, C. D.; Whitesides, G. M., *Adv. Mater.* **1989**, 1, 110-116.
110. Dubois, L. H.; Nuzzo, R. G., *Ann. Phys. Chem.* **1992**, 43, 437-463.
111. Folkers, J. P.; Zerkowski, J. A.; Laibinis, P. E.; Seto, C. T.; Whitesides, G. M. In *Supramolecular architecture*, ACS Symposium Series 499, American Chemical Society: Washington, D.C., 1992; Bein, T., Ed. American Chemical Society: Washington, D.C., 1992; pp 10-23.
112. Lee, T. R.; Laibinis, P. E.; Folkers, J. P.; Whitesides, G. M., *Appl. chem* **1991**, 63, 821.
113. Whitesides, G. M.; Ferguson, G. S., *Chemtrats-Org. Chem.* **1988**, 1, 171.
114. Sellers, H.; Ulman, A.; Shnidman, Y.; Eilers, J. E., *J. Am. Chem. Soc.* **1993**, 115, 9389-9401.
115. Somorjai, G. A., *Chemistry in Two Dimensions - Surfaces*. Cornell University Press: Ithaca, NY, 1982.
116. Bain, C. D.; Evall, J.; Whitesides, G. M., Formation of Monolayers by the Coadsorption of Thiols on Gold: Variation in the Head Group, Tail Group, and Solvent. *J. Am. Chem. Soc.* **1989**, 111, 7155-7164.
117. Buck, M.; Eisert, F.; Fischer, J.; Grunze, M.; Trager, F., *Appl. Phys.* **1991**, A53, 552.
118. Buck, M.; Eisert, F.; Grunze, M., *Ber. Bunsen-Ges. Phys Chem* **1993**, 97, 399.
119. Hahner, G.; Ch., W.; Buck, M.; Grunze, M., *Langmuir* **1993**, 9, 1955-1958.
120. Brust, M.; Walker, M.; Bethell, D.; Schiffrin, D. J.; Whyman, R., *J. Chem. Soc. Chem. Commun.* **1994**, 801.
121. Chailapakul, O.; Sun, L.; Xu, C.; Crooks, M., *J. Am. Chem. Soc.* **1993**, 115, 12459-12467.
122. Thomas, R. C.; Sun, L.; Crooks, M., *Langmuir* **1991**, 7, 620-622.
123. Bain, C. D.; Biebuyck, H. A.; Whitesides, G. M., *Langmuir* **1989**, 5, 723-727.

124. Porter, M. D.; Bright, T. B.; Allara, D. L.; Chidsey, C. E. D., *J. Am. Chem. Soc.* **1987**, 109, 3559-3568.
125. Walczak, M. W.; Chung, C.; Stole, S. M.; Widrig, C. A.; Porter, M. D., *J. Am. Chem. Soc.* **1991**, 113, 2370-2378.
126. Nuzzo, R. G.; Zegarski, B. R.; Dubois, L. H., *J. Am. Chem. Soc.* **1987**, 109, 733-740.
127. Li, Y.; Huang, J.; McIyer, R. T. J.; Hemminger, J. C., *J. Am. Chem. Soc.* **1992**, 114, 2428-2432.
128. Bryant, M. A.; Pemberton, J. E., *J. Am. Chem. Soc.* **1991**, 113, 3630.
129. Widrig, C. A.; Chung, C.; Porter, M. D., *J. Electroanal. Chem.* **1991**, 310, 335.
130. Ulman, A., Formation and Structure of Self-Assembled Monolayers. *Chem. Rev.* **1996**, 96, 1533-1554.
131. Strong, L.; Whitesides, G. M., *Langmuir* **1988**, 4, 546-558.
132. Dubois, L. H.; Zegarski, B. R.; Nuzzo, R. G., *J. Chem. Phys.* **1993**, 98, (678-681), 678-688.
133. Poirier, G. E., *Chem. Rev.* **1997**, 97, 1117.
134. Schreiber, F., *Prog. Surf. Sci.* **1997**, 65, 151.
135. Poirier, G. E., *Langmuir* **1997**, 13, 2019.
136. Hickman, J. J.; Ofer, D.; Zou, C.; Wrighton, M. S.; Laibinis, P. E.; Whitesides, G. M., *J. Am. Chem. Soc.* **1991**, 113, 1128-1132.
137. McPherson, M. K. The Reactivity of Chemical Warfare Agent Simulants on Carbamate Functionalized Monolayers and Ordered Silsesquioxane Films. Dissertation, Virginia Polytechnic Institute and State University, Blacksburg, VA, 2005.
138. Schlenoff, J. B.; Li, M.; Hiep, L., Stability and Self-Exchange in Alkanethiol Monolayers. *J. Am. Chem. Soc.* **1995**, 117, 12528-12536.
139. Flynn, N. T.; Tran, T. N. T.; Cima, M. J.; Langer, R., Long-Term Stability of Self-Assembled Monolayers in Biological Media. *Langmuir* **2003**, 19, 10909-10915.
140. Evans, S. D.; Sharma, R.; Ulman, A., *Langmuir* **1991**, 7, 156-161.

141. Hautman, J.; Bareman, J. P.; Mar, W.; Klein, M. L., *J. Chem. Soc. Faraday Trans.* **1991**, 87, 2031-2037.
142. Hautman, J.; Klein, M. L., *Phys. Rev. Lett.* **1991**, 67, 1763-1766.
143. Duevel, R. V.; Corn, R. M., *Anal. Chem.* **1992**, 64, 337-342.
144. Yan, L. Y.; Marzolin, C.; Terfort, A.; Whitesides, G. M., Formation and Reaction of Interchain Carboxylic Anhydride Groups on Self-Assembled Monolayers on Gold. *Langmuir* **1997**, 13, 6704-6712.
145. Anderson, M. R.; Baltzersen, R., Reductive desorption of 11-mercaptopundecanoic acid monolayers modified by covalent attachment of 1,3- and 1,4-phenylenediamine. *Journal of Colloid and Interface Science* **2003**, 263, 516-521.
146. Mazur, M.; Krysinski, P., Covalently Immobilized 1,4-Phenylenediamine on 11-Mercaptopundecanoic Acid-Coated Gold: Effect of Surface-Confined Monomers on the Chemical in Situ Deposition of Polyaniline and Its Derivatives. *Langmuir* **2001**, 17, 7093-7101.
147. Persson, H. H. J.; Caseri, W. R.; Suter, U. W., Versatile Method for Chemical Reactions with Self-Assembled Monolayers of Alkanethiols on Gold. *Langmuir* **2001**, 17, 3643-3650.
148. Greenler, R. G., *Journal of Chemical Physics* **1966**, 44, 310.
149. Greenler, R. G., *Journal of Chemical Physics* **1969**, 50, 1963-1968.
150. Davis, G. Interfacial Reaction of an Olefin-Terminated Self-Assembled Monolayer Exposed to Nitrogen Dioxide: An Investigation Into the Reaction Rate and Mechanism. Virginia Polytechnic Institute and State University, Blacksburg, 2003.
151. Moulder, J. F.; Stickle, W. F.; Sobol, P. E.; Bomben, K. D., *Handbook of X-ray Photoelectron Spectroscopy*. Physical Electronics, Inc.: Eden Prairie, MN, 1995.
152. Hogt, A. H.; Dankert, J.; Feijen, J., Adhesion of coagulase-negative *Staphylococci* to methacrylate polymers and copolymers. *J. Biomed. Mater. Res.* **1986**, 20, 533-545.
153. Tsao, M. W.; Hoffmann, C. L.; Rabolt, J. F.; Johnson, H. E.; Castner, D. G.; Erdelen, C.; Ringsdorf, H., Studies of Molecular Orientation and Order in Self-Assembled Semifluorinated n-Alkanethiols: Single and Dual Component Mixtures. *Langmuir* **1997**, 13, 4317-4322.
154. Miller, J. C.; Miller, J. N., *Statistics for Analytical Chemistry*. Ellis Horwood Limited: Chichester, West Sussex, England, 1984; p 202.

155. Simmons, J., Antimicrobial additive systems see increased use in polymers. *Plastics Additives & Compounding* 2001, pp 16-18.
156. Hugo, W. B., Principles and Practice of Disinfection, Preservation and Sterilization. In 2nd Edn. ed.; Russel, A. D.; Hugo, W. B.; Ayliffe, G. A. J., Eds. Blackwell Scientific Publications: Oxford, 1992; pp 3-6.
157. Ravelin, J., *Sci. Nat.* **1869**, 11, 93-102.
158. von Naegeli, V., *Deut. schr. Schweiz. Naturforsch. Ges.* **1893**, 33, 174-182.
159. Russell, A. D.; Path, F. R. C.; Hugo, W. B., Antimicrobial Activity and Action of Silver. *Progress in Medicinal Chemistry* **1994**, 31, 351-371.
160. Credé, C. S. F., *Arch. Gynaek.* **1881**, 17, 50.
161. Gibbard, J., *Am. J. Public Health* **1937**, 27, 122-137.
162. Hugo, W. B., Handbuch der Antiseptik. In *Band I, Teil 2*, Weuffen, W.; Kramer, A.; Groschel, D.; Berensci, G.; Bulka, E., Eds. Volk und Gesundheit: Berlin, 1981; pp 361-409.
163. Rose, A. H., An Introduction to Microbial Physiology. In *Chemical Microbiology*, 2nd. Edn ed.; Butterworths: London, 1976; pp 119-120.
164. Hautman, J.; Klein, M. L. J., *J. Chem. Phys.* **1990**, 93, 7483.
165. Mar, W.; Klein, M. L., *Langmuir* **1994**, 10, 188.
166. O'Dwyer, C.; Gay, G.; Lesegno, B. V. d.; Weiner, J., *Langmuir* **2004**, 20, 8172.
167. Sun, L.; Crooks, R. M., *Langmuir* **1993**, (1951).
168. Yang, G.; Liu, G. Y., *J. Phys. Chem.* **2003**, 107, 8746.
169. Zhou, C.; Nagy, G.; Walker, A. V., Toward Molecular Electronic Circuitry: Selective Deposition of Metals on Patterned Self-Assembled Monolayer Surfaces. *J. Am. Chem. Soc.* **2005**, 127, 12160-12161.
170. Gerenser, L. J., *J. Vc. Sci. Technol.* **1990**, A 8, 3682.
171. Skoog, D. A.; West, D. M.; Holler, F. J., *Fundamentals of Analytical Chemistry*. Seventh ed.; Saunders College Publishing: Philadelphia, 1996.
172. Bragg, P. D.; Rannie, D. J., *Can. J. Microbiol.* **1973**, 20, 883-889.

173. Yudkin, J., *Enzymogia* **1937-1938**, 2, 161-170.
174. Duane, M.; Dekker, C. A.; Schachmen, H. K., *Biopolymers* **1966**, 4, 51-76.
175. Izatt, R. M.; Christensen, J. J.; Rytting, J. H., *Chem. Rev.* **1971**, 71, 439-481.
176. Jensen, R. H.; Davidson, N., *Biopolymers* **1966**, 4, 17-32.
177. Richard, H.; Scriber, J. P.; Duane, M., *Biopolymers* **1973**, 12, 1-10.
178. Yakabe, Y.; Sano, T.; Ushio, H.; Yasunaga, T., *Chem. Lett.* **1980**, 4, 373-376.
179. Zavriev, S. K.; Minchenkova, L. E.; Vorlickova, M.; Kolchinsky, A. M.; Volkenstein, M. V.; Ivanov, V. I., *Biochim. Biophys. Acta* **1979**, 564, 212-224.
180. Armstrong-Chong, R. J.; Matthews, K.; Chong, J. M., Sequential alkynylation of α -bromoalkyl triflates: facile access to unsymmetrical non-conjugated diynes including precursors to diene pheromones. *Tetrahedron* **2004**, 60, 10239-10244.
181. Ahmed, Z.; Kazmi, S. N. H.; Khan, A. Q.; Malik, A., A Facile Synthesis of Quaternary Amino Sugars. *J. prakt. Chem* **1988**, 330, 1030-1032.
182. Hu, J.; Fox, M. A., A Convenient Trimethylsilylthioxy-Dehalogenation Reaction for the Preparation of Functionalized Thiols. *J. Org. Chem.* **1999**, 64, 4959-4961.

Vita

Joshua Robert Uzarski was born on September 29, 1980 in Grand Rapids, Michigan, to Robert and Krystyna Uzarski. He has two younger sisters, Veronica and Sarah, who are 2 and 6 years his junior respectively. Joshua attended Comstock Park High School in Comstock Park, Michigan where he graduated as class salutatorian in 1999. He attended Aquinas College in Grand Rapids, Michigan where he graduated in May 2003 with a Bachelor of Science degree. After meeting Dr. Morris, Joshua decided to attend Virginia Tech to pursue an advanced chemistry degree. He completed his Master of Science degree in June 2006 and plans to stick around to pursue a Ph.D.